A Low-Cost Computer Vision Approach for Objectively Evaluating Triple Jump Technique: Proof of Concept

Heather Grandy

Thesis submitted to the University of Ottawa
in partial Fulfillment of the requirements for the
Master of Applied Science in Biomedical Engineering

Department of Mechanical Engineering
Faculty of Engineering
Ottawa-Carleton Institute for Biomedical Engineering
University of Ottawa

Table of Contents

List of Tables

List of Figures

List of Equations

Acknowledgements

I would like to express my gratitude to my supervisor, Dr. Ryan Graham, for welcoming me into his lab and giving me the freedom to pursue a thesis topic that sparked my interest. Your guidance has been invaluable throughout this journey, and I feel incredibly fortunate to have been part of such an innovative and inspiring lab environment.

A special thank you to my lab mates, Matt, Alex, Reza, Xiong, Victor, Kristen, Camille, Mohammad, Jessica, Annagh, Di, and Mike, as well as Dr. Allison Clouthier from the Movement Biomechanics and Analytics Lab for their camaraderie and support. I'd like to especially thank Matt, who has helped me in my transition back to academia since day one when I joined the lab as a summer Research Assistant in 2022. From helping with data collection for a class project to editing my conference abstract on short notice, and even meticulously reviewing my lengthy thesis, Matt's help has been instrumental in getting me to this point. I also want to thank Annabelle, our incredible summer 2024 lab co-op student, whose help with more tedious aspects of my analyses – particularly data labelling – saved me at least a month of work on my thesis.

To my track and field teammates and coaches at the Ottawa Lions, thank you for keeping me engaged in a sport I never thought I'd still be competing in at this stage of my life. Your energy and motivation kept me grounded through the challenges of grad school and reminded me why I love sport. You also inspired me to explore a track and field-related topic in my research!

To the friends I've made at uOttawa, especially my fellow MASc Biomedical Engineering classmates, Wendy and Sarah – your understanding of the ups and downs of thesis writing, coursework, and everything in between has been a source of comfort and solidarity. I'm grateful for your friendship and support and for organizing much-needed non-school-related activities to keep us all sane.

I also owe a huge thank you to my parents for supporting my decision to leave a stable career and embark on this academic journey, albeit with some skepticism! Your belief that I will always figure things out has made all the difference. And finally, to my husband, Thomas, thank you for your constant support, patience, and understanding, especially when I had to spend entire weekends working. Your love and encouragement kept me going, and I couldn't have done this without you.

Definition of Terms

2D	Two-dimensional
3D	Three-dimensional
CNN	Convolutional Neural Network
COM	Centre of mass
CPU	Central Processing Unit
CV	Computer Vision
GMP	Google MediaPipe
GPU	Graphics Processing Unit
HPE	Human pose estimation
IAAF	International Amateur Athletic Federation and International Association of Athletics Federations
ML	Machine learning
PAF	Part Affinity Fields

Abstract

The triple jump is a track and field event comprising an approach run followed by three phases – hop, step, and jump – culminating in a sand pit landing. Typically, triple jump technique is evaluated subjectively by coaches, with quantitative assessments often relying on high-cost multi-camera systems. To address this limitation, a low-cost framework was developed for objectively analyzing triple jump technique in real-world settings using a single iPhone 12 camera and the open-source human pose estimation software, Google MediaPipe pose (GMP pose). Data were collected from 30 participants (15 male, 15 female) performing six triple jumps each across four different track and field facilities, resulting in 154 usable videos for analysis. Participants were categorized by skill level based on their personal best triple jump distance.

Central to the framework is the use of homography transformations, which enabled the conversion from GMP pose data to real-world coordinates to calculate triple jump performance metrics, including horizontal and vertical centre of mass velocities, last stride velocity, effective distance, phase distances and phase ratios. Additional performance metrics, including ground contact times, flight times, and knee angles, were derived from the video recordings and GMP pose data. Validation of the pose estimations and homography transformations was done primarily through subjective visual assessments using a custom Python tool, with reprojection error serving as an additional quantitative measure of relative homography performance.

The performance metric results showed that more skilled participants exhibited superior step phases compared to their less skilled counterparts and demonstrated performance trends similar to elite jumpers from World Athletics reports, particularly in the reduction of horizontal and vertical velocity across jump phases, albeit at lower velocities. Moreover, participants' phase ratios were consistent with elite-level jumpers. Comparisons with World Athletics data provided a reference to validate the triple jump performance metrics, showing promising alignment.

This study demonstrates the potential of an affordable, single-camera markerless motion capture system to analyze triple jump technique in real-world settings. Although the system shows promise, much of the process remains manual, limiting its scalability for broader use. Despite its current limitations, the proposed framework offers a novel perspective on the feasibility of affordable, single-camera markerless motion capture systems in real-world environments, providing a foundation for further development.

Chapter 1: Introduction

Triple jump is a complex track and field event that demands exceptional acceleration, velocity preservation, and precise timing to execute the hop, step, and jump phases [1], [2] to achieve the farthest possible horizontal jump distance [3]. Identifying the movement patterns required to improve triple jump performance can be challenging, warranting the need for quantitative feedback mechanisms. Various biomechanical analyses and simulations employed to evaluate the triple jump technique have been predominantly focused on elite athletes competing at or near the Olympic level [2], [3], [4], [5]. This narrow focus fails to adequately represent the broader spectrum of triple jumpers, limiting the applicability of findings for most athletes. Moreover, existing triple jump analyses appear to rely on costly hardware and proprietary software, with usage primarily observed at world championships organized by the World Athletics, formerly International Amateur Athletic Federation and International Association of Athletics Federations (IAAF), sport governing body [6], [7], [8], [9].

It is recognized that there is diversity in technique amongst triple jumpers, and even elite athletes demonstrate technique inconsistencies across jump trials in competition [5]. The consensus suggests the most effective technique may vary according to an athlete's individual biomechanics, physique, skills, and preferences [5]. This recognition highlights the inherent variability among triple jumpers and underscores the importance of experimentation and continuous refinement as athletes strive to optimize their jump performance. Using subjective coaching feedback and collecting quantitative measures, athletes can garner the personalized approach to technique development that they need. Thanks to technological advancements in the field of computer vision (CV) and machine learning (ML), tools for developing such measures are increasingly available. Specifically, advancements have catalyzed the use of markerless motion capture for biomechanical applications [10].

Motion capture methods are broadly classified as marker-based, markerless, and inertial-based. Marker-based motion capture involves placing a set of active or passive markers at strategic anatomical locations on a human participant, along with the use of high-resolution, synchronized infra-red cameras [10], [11]. Active markers emit light, whereas passive markers reflect infra-red light back to the cameras [11]. In contrast, markerless motion capture methods extract participant movement information without the need for physical markers, relying instead

on human pose estimation (HPE) algorithms, which have emerged from advancements in CV [10]. Markerless motion capture HPE architectures often leverage "Convolutional Neural Networks (CNNs) to extract features of an image and decoder networks to determine 2D key point body part locations in the image space [12]." Inertial measurement units (IMUs) are small wearable devices equipped with an accelerometer, gyroscope, and sometimes a magnetometer [13]. The data generated by these sensors can be utilized to perform motion analysis with demonstrable success in sporting applications [14], [15], [16]. While IMUs offer a portable, low-cost option in biomechanics research, they necessitate hardware placement on athletes, adding complexity for coaches [13]. A video-based approach using cameras, however, aligns with existing coaching practices. Based on the researcher's experience as a triple jump coach and athlete, filming triple jumps in practice and competition settings using a smartphone camera is already standard, making single-camera video-based methods more practical for coaching applications.

Despite being considered the "gold standard" in biomechanics research, marker-based motion capture has several limitations [17], [18]. Firstly, the indoor laboratory environment typically used in marker-based motion capture studies can introduce unknown influences on a participant's movement, thus deviating from natural conditions [10], [12]. Although marker-based motion capture can be conducted outside an indoor laboratory setting, the markers, typically placed on the skin, introduce additional movement that violates the rigid body assumption [10], [12], [19], [20]. Moreover, setup time is extensive, and marker placements may vary between researchers [10]. Due to these limitations and the desire to evaluate movement patterns without obstructions, markerless motion capture presents an attractive alternative [10], [18], [21]. Additional advantages of markerless motion capture over marker-based methods include reduced study setup times, the ability to capture participants in their natural environments more easily, and the potential for more cost-effective setups. However, this approach also presents a variety of challenges, including demanding computational requirements, often necessitating high-performance computers with Graphics Processing Units (GPUs) to be used [22]. Moreover, achieving accurate measurements typically entails the use of multiple cameras, which adds complexity when implementing markerless motion capture outside of controlled laboratory environments. Many commercial solutions still require the use of multiple cameras and proprietary software purchase [22]. Consequently, the advantage of capturing

participants in their natural surroundings can become impractical and expensive. Further, much of the existing literature focuses on validating markerless motion capture technologies against the marker-based "gold standard," leading to predominant use in controlled settings [23]. While markerless motion capture is extensively researched and applied in fields like smart surveillance and virtual reality, its practical adoption in real-world settings remains limited [18], [24], [25].

To fully leverage the benefits of markerless motion capture in real-world environments, challenges hindering its widespread adoption must be addressed. Open-source markerless motion capture solutions using low-cost cameras have the potential to make motion capture accessible to clinicians and coaches alike without the need for costly equipment [24]. Ideally, markerless systems should seamlessly operate with a single camera. However, the single-camera approach has several limitations, such as depth ambiguities, high-dimensional representation of human pose, self occlusion, and unconstrained lighting [25]. While single-camera dual lens systems, such as stereo cameras, do exist, they are inaccessible to most coaches and athletes due to both their cost and specialized knowledge needed for effective operation [26]. One solution to address these issues in sports analyses scenarios is the implementation of homography techniques [27], [28], [29]. Homography is a "projective transformation between two planes, or alternatively, a mapping between two planar projections of an image [30]." Employing homography methods becomes necessary when dealing with images taken from different angles as objects in the scene may appear distorted; for example, objects closer to the camera appear larger than those further away. In practical terms, homography allows the relation of points in one image to their corresponding points in another image, even when these images were taken from different angles. This is a powerful technique that, when combined with markerless motion capture solutions, can enable biomechanical analyses in uncontrolled environments.

Leveraging homography techniques with a single camera setup and open-source markerless motion capture software presents an innovative avenue for conducting athletic performance assessments. This study provides a blueprint for employing a low-cost markerless motion capture system for triple jump analyses "in the wild." The proposed methodology holds promise for democratizing biomechanical insights by offering an affordable approach, compared to alternative multi-camera motion capture setups, accessible to athletes of all skill levels and addresses critical limitations in the current use of markerless motion capture in uncontrolled

settings. This study aimed to develop an end-to-end framework for a single-camera markerless system for evaluating triple jump technique. The solution was validated primarily using subjective visual assessments of pose detection performance, as well as triple jump performance metrics compared to elite athletes included in World Athletics reports [6], [7], [8], [9].

Chapter 2: Literature Review

2.1 Triple Jump Background

Men's triple jump has been an Olympic event since the first modern Games in Athens in 1896 [31]. Initially, the event involved two hops on the same foot followed by a jump, but this was changed to the hop, step, jump technique in 1908 [32]. The men's world record was set in 1995 by Jonathan Edwards of the United Kingdom with a jump of 18.29 metres [33]. The men's Canadian record stands at 17.29 metres, set by Edrick Floreal in 1989 [34]. It took ninety years for women to be permitted to triple jump at the Olympics, with the inaugural event held at the 1996 Games in Atlanta [32]. Yulimar Rojas of Venezuela holds the women's triple jump world record with her jump of 15.74 metres achieved in 2022 [33]. The Canadian record was set by Caroline Ehrhardt at 14.03 metres in 2023 [34].

Despite Canada's recent success in numerous track and field events including earning medals at the 2024 Paris Olympic Games in the men's 100-metre relay, the women's pole vault, the men and women's hammer throw, the men's 800-metres, as well as several notable near-podium finishes, there have been no Canadian Olympic triple jumpers since 1988 [35], [36], [37]. Only four Canadian men have ever competed in the triple jump at the Olympics – J. Garfield MacDonald and Calvin Bricker in 1908, with Bricker also competing in 1912, Sammy Richardson in 1936, and most recently, Edrick Floreal at the 1988 Games [37]. No Canadian woman has ever met the Olympic qualifying standards for the event [37]. The absence of a Canadian triple jumper at the Olympics for over 30 years highlights an intriguing phenomenon, given the country's success in other track and field events. While this work does not aim to uncover the reasons behind this disparity, it was partially motivated by this fact.

The components of triple jump, as outlined in Table 2.1 and visually depicted in Figure 2.1, include the approach run, hop, step, and jump phases. Athletes must begin their hop phase on or before a wooden board on the jump runway; if they take-off beyond the board, this is considered a foul and the jump is not measured [38]. In Figure 2.1, observe the athlete's initial take-off foot is clearly before the red marking on the board, indicating a valid jump.

Table 2.1: Triple jump phases. Descriptions obtained from [3], [5].

Triple Jump Component	Description
Approach Run	Athletes begin the triple jump by running; they can choose where they start their run.
Hop (first phase)	Athletes take-off on one foot at a predetermined board and land on the same foot.
Step (second phase)	After landing the hop, athletes step onto the opposite foot.
Jump (third phase)	After landing the step, athletes complete their jump in a sand pit.

Figure 2.1: The men's first place triple jump of 17.26m by Girat A. at the 2009 IAAF World Championships in Athletics in Berlin. Image obtained from [39].

In triple jump competitions, each athlete is initially permitted three jumps [38]. After these three rounds, the top eight competitors, based on their best distance, are allowed three additional jumps, resulting in a total of six rounds [38]. The athlete with the longest triple jump from any of the six attempts is declared the winner [38]. During the competition, triple jump officials carefully watch the board to record any fouls [40]. At elite meets, cameras are generally used to film the board, allowing for instant replays if an athlete wishes to challenge a foul. For outdoor events, a wind gauge is required and the wind speed during each jump must be recorded for the jump to be valid [40]. A wind speed below 2.0 metres per second is considered legal. If an athlete jumps under illegal wind conditions, their results count for the competition but are not eligible for official rankings or records [40]. Indoor events do not require a wind gauge, simplifying the setup.

As athletes perform the triple jump, they may choose to use a single-arm or double-arm technique at each phase. Consequently, triple jump is often broadly categorized into single-arm and double-arm techniques, depicted in Figure 2.2. The optimal arm movement in the triple jump is a subject of ongoing scrutiny within the track and field community, with debate focusing on whether employing a single- or double-arm movement yields further triple jump distances [5], [41]. The single-arm technique involves the arms moving asymmetrically as one does when running, while the double-arm technique involves a symmetrical shoulder flexion during takeoff, starting from an extended position [41]. The debate delves into biomechanical principles and

efficiency of movement, requiring athletes and coaches to navigate this nuanced topic. This work does not explore the impact of arm technique on jump performance, but it is included for completeness given its relevance in the triple jump technique discourse.

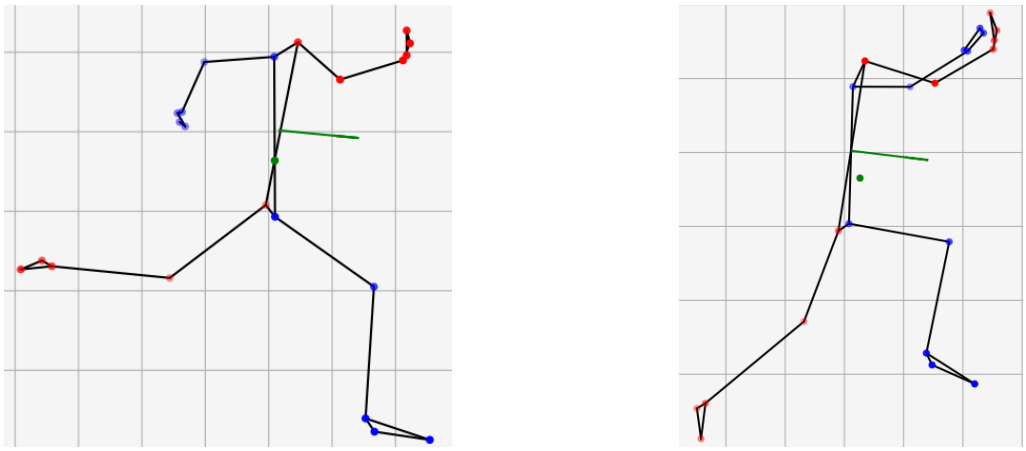

(a) (b)

Figure 2.2: Visual depiction of (a) single-arm technique and (b) double-arm technique. Blue dots indicate left body landmarks, and red dots indicate right body landmarks. The green dot indicates the estimated centre of mass, and the green line depicts the direction of travel.

Beyond single-arm and double-arm categories, various biomechanical factors and jump attributes are discussed as important measures of performance, including final stride velocity which reflects the initial take-off velocity and influences momentum carried into the jump sequence; phase ratios, which refer to the distances of each phase represented as percentages of the total distance [42]; horizontal and vertical velocity trade-offs which provide insight into how athletes manage energy transfer throughout the jump; and take-off angles which influence the horizontal and vertical trajectory of the jump. By exploring these biomechanical factors and performance metrics, it is possible to gain a deeper understanding of the intricacies of the triple jump technique.

Diverse approaches for conducting biomechanical assessments of the triple jump technique exist in the literature. Particularly noteworthy is a 1992 publication by Dr. James G. Hay, who performed an impressive in-depth analysis of triple jump biomechanics, including the development of a theoretical model, presented in Figure 2.3, to “describe biomechanical factors that determine the distance of a triple jump,” where each factor is determined by the factors below it [5]. Hay’s model played a pivotal role in triple jump research and serves as the basis for many subsequent studies.

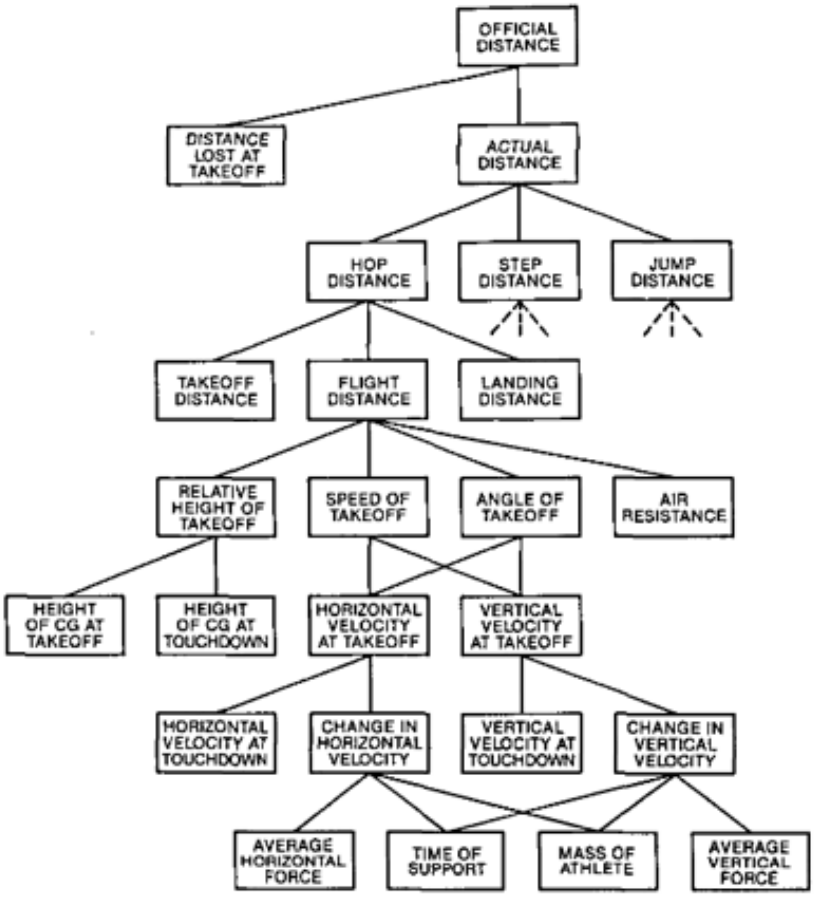

Figure 2.3: Theoretical model of biomechanical factors influencing the distance of a triple jump, developed by James G. Hay and included in his publication, "The biomechanics of the triple jump: A review," *Journal of Sports Sciences*, Vol 10 Issue 4 © Taylor & Francis 23 Sep 1991, reprinted by permission of Informa UK Limited, trading as Taylor & Francis [5]. The abbreviation CG (Centre of Gravity) is used in the diagram. All biomechanical factors under hop distance also apply to step distance and jump distance but are omitted for simplicity.

The primary metric used to assess triple jump performance is the jump distance: a further distance is a better jump. Athletes select a take-off board location from a predetermined set of options, commonly spanning distances of seven, nine, eleven, and thirteen metres. The triple jump is measured from the chosen board to the athlete's nearest landing mark in the sand pit [38], [40]. At a competition, athletes must specify to the officials their desired take-off board before initiating a jump and may change their board at any point throughout the competition. If an athlete takes off from behind their selected board, the jump is still measured from that board. However, if the take-off point is beyond the board, the jump is not measured and is classified as a foul, as previously mentioned. Hay's definitions for official distance, distance lost at take-off, and actual distance are provided in Table 2.2 below [5].

Table 2.2: Triple jump take-off performance measures [5].

Performance Measure	Description
Official distance	Official distance is measured by meet officials and is recorded in competition results. It is the measurement from the edge of the board to the landing location in the sand pit.
Distance lost at take-off	Refers to the distance between the athlete's toe position at first take-off and the edge of the board. Ideally, this distance is zero, though this is challenging to achieve.
Actual distance	Refers to the distance from where the athlete's toe position at first take-off to their landing location in the sand pit. In competitions, this distance is not recorded since part of the challenge of the event is to take off as close to the edge of the board as possible. For a valid jump, the actual distance is the official distance plus the distance lost at take-off.

While numerous factors evidently influence triple jump distance, it is generally agreed that phase ratios, approach run speed, and effectively managing horizontal and vertical velocity trade-offs are amongst the most important aspects of triple jump technique and are further explored in subsections 2.1.1 – 2.1.4 [5], [43]. Despite some consensus on these factors, ongoing discussions persist regarding the relative significance of each element.

2.1.1 Phase Ratios

Phase ratios refer to the distances of each phase represented as percentages of the total distance [42]. Athletes can be classified as hop-dominant, jump-dominant, or balanced [42]. Hop or jump dominance is determined if the corresponding "phase percentage is at least 2% greater than the next largest phase percentage [42]." Extensive research has been conducted on the influence of phase ratios on triple jump performance and the identification of an optimal phase ratio. Although work published by Yu and Hay demonstrated that "there is no single optimum phase ratio for all triple jumpers [44]," there is a theoretical economic distribution for each phase of 36-37% for the hop, 29-30% for the step, and 33-34% for the jump phase [42], [44], [45].

Researchers have tested these theoretical distributions; most notably, Allen et al. developed a computer simulation to determine the optimal triple jump phase ratio [42]. For the single subject in their study, they found a hop-dominated technique with phase ratios of 35.7%, 30.8%, and 33.6% was optimal [42]. These theoretical results can be validated against actual elite triple jump performances. World Athletics published phase ratios for men and women's triple jump at the Athletics World Championships in 2017 and 2018, summarized in Table 2.3 below [6], [7], [8], [9].

Table 2.3: Mean phase ratios and standard deviations (SD) from elite male and female triple jumpers compared to theoretical economic phase distributions. Phase ratios were summarized across all athletes included in the 2017 and 2018 World Athletics reports [6], [7], [8], [9]. Theoretical economic distributions obtained from [42], [44], [45].

Phase	Female Mean Percentage (%) (SD)	Male Mean Percentage (%) (SD)	Theoretical Economic Distribution (%)
Hop	36.1 (1.30)	35.8 (1.40)	36-37
Step	29.0 (1.89)	29.9 (1.90)	29-30
Jump	34.9 (1.76)	34.3 (2.10)	33-34

2.1.2 Speed at Take-off and Last Step Length

In a 1986 triple jump study, Hay et al. found that when evaluating four performance factors – relative height at take-off, speed at take-off, angle of take-off, and loss due to air resistance – only the speed at take-off appeared to impact the triple jump distance [46]. Moreover, a triple jump simulation model created by Allen et al. found that jump distance improved with increased approach run velocities, assuming athletes possessed the strength and coordination required to manage such velocities [47]. The speed at take-off is considered by some researchers to be “the most critical kinematic factor” in triple jump [4], [46].

During the approach run, it is ideal for stride frequency to increase during the final four to eight steps to increase speed [48]. Athletes typically begin to lower their centre of gravity during these final steps in preparation for the hop phase [5]. Notably, it is believed that the length and frequency of the last one to two strides are critical to jump performance and that athletes should aim to reach their peak velocity during these strides [3], [48]. The maximum horizontal velocities at take-off achieved by male athletes at the 2017 and 2018 World Athletics competition were 9.84 m/s and 9.85 m/s, respectively, achieved at the hop take-off, as last stride velocity was not reported [8]. On the women’s side, maximum horizontal velocities achieved were 8.57 m/s in 2017, and 8.79 m/s in 2018 [9]. Interestingly, only one of these athletes with the highest horizontal velocity at hop take-off won their respective competition – the decorated American athlete Christian Taylor with 9.85 m/s at the 2017 World Athletics Championships [7]. Though definitive conclusions cannot be determined from such a small sample size, it implies that while horizontal velocity at take-off is an important aspect of the triple jump, this measure alone does not define jump distance and must be balanced with other technique considerations.

2.1.3 Horizontal and Vertical Velocity Trade-Offs

Unlike a sprinting event, athletes cannot only focus on running as fast as possible; they must manage their horizontal and vertical velocities throughout the triple jump. Minimizing horizontal velocity loss throughout the three take-off phases leads to a better result and is, therefore, an important consideration when assessing triple jump performance [3], [43]. However, an "increase in horizontal velocity component results in reduced vertical velocity component and vice versa," requiring athletes to find an optimal balance [43], [47]. Both Yu and Allen et al. remarked that generally, as vertical velocity increases, a proportionally greater loss of horizontal velocity occurs in their respective publications [47], [49]. In this regard, horizontal velocity is "gained during the approach and lost primarily due to ground contact during each of the three take-off phases," which results in a decrease in horizontal velocity observed at each phase [3].

To further demonstrate the horizontal and vertical velocity trade-offs, data from the World Athletics triple jump reports were once again summarized [6], [7], [8], [9]. The average horizontal and vertical velocities achieved at each take-off point for both men and women are presented in Table 2.4 and Table 2.5, respectively.

Table 2.4: Mean horizontal velocities and standard deviations (SD) in metres per second (m/s) achieved at each take-off point in the triple jump for elite men and women. Horizontal velocities for each phase were summarized across all athletes included in the 2017 and 2018 World Athletics reports [6], [7], [8], [9].

Phase	Female Mean Horizontal Velocity (m/s) (SD)	Male Mean Horizontal Velocity (m/s) (SD)
Hop	8.15 (0.31)	9.34 (0.32)
Step	7.44 (0.28)	8.15 (0.44)
Jump	6.23 (0.36)	6.80 (0.56)

Table 2.5: Mean vertical velocities and standard deviations (SD) in metres per second (m/s) achieved at each take-off point in the triple jump for elite men and women. Vertical velocities for each phase were summarized across all athletes included in the 2017 and 2018 World Athletics reports [6], [7], [8], [9].

Phase	Female Mean Vertical Velocity (m/s) (SD)	Male Mean Vertical Velocity (m/s) (SD)
Hop	2.58 (0.21)	2.77 (0.27)
Step	2.02 (0.25)	2.37 (0.39)
Jump	2.68 (0.22)	2.87 (0.46)

Evidently, achieving optimal horizontal and vertical velocity throughout the approach run and three jump phases is a challenging task and are important metrics to evaluate to inform the triple jump technique.

2.1.4 Additional Triple Jump Performance Metrics

Flight time refers to the duration during which athletes remain airborne in a triple jump, indicating the interval between ground contacts [2]. While prolonged flight times often correlate with improved jump distances, the balance between horizontal and vertical components must be considered. For instance, an athlete may achieve considerable flight time but expend excessive energy in vertical motion. Consequently, while the first phase may feature an impressive flight time, sustaining the jump amidst significant vertical movement becomes challenging. Flight times of elite male and female athletes at the 2017 and 2018 World Athletics championships are presented in Table 2.6 [6], [7], [8], [9].

Table 2.6: Mean flight times and standard deviations (SD) in seconds (s) at each phase for elite male and female triple jumpers. Flight times for each phase were summarized across all athletes included in the 2017 and 2018 World Athletics reports [6], [7], [8], [9].

Phase	**Female Mean Flight Time (s) (SD)**	**Male Mean Flight Time (s) (SD)**
Hop	0.51 (0.03)	0.53 (0.04)
Step	0.37 (0.04)	0.46 (0.06)
Jump	0.64 (0.04)	0.69 (0.06)

Ground contact times refer to the support phases during triple jump where one foot is planted on the ground [2]. Athletes aim to minimize the time spent on the ground since as horizontal velocity decreases, the duration of support phases increases [43]. In other words, lower velocities are related to longer ground contact times, both of which have been shown to lead to a shorter jump distance [2]. Ground contact times of elite male and female athletes at the 2017 and 2018 World Athletics championships are presented in Table 2.7 [6], [7], [8], [9].

Table 2.7: Mean ground contact times and standard deviations (SD) in seconds (s) at each phase for elite male and female triple jumpers. Ground contact times for each phase were summarized across all athletes included in the 2017 and 2018 World Athletics reports [6], [7], [8], [9].

Phase	Female Mean Ground Contact Time (s) (SD)	Male Mean Ground Contact Time (s) (SD)
Hop	0.13 (0.01)	0.12 (0.01)
Step	0.16 (0.01)	0.16 (0.02)
Jump	0.17 (0.02)	0.18 (0.02)

Knee angles at each take-off are also often considered in triple jump performance assessments. While definitive optimal angle ranges could not be found in the literature, examining results from published reports by World Athletics provided a useful range for comparison. These reports define the knee angle as the angle between the thigh and lower leg, "considered to be 180 degrees in the standing anatomical position," and measuring it at its minimum during the contact of each triple jump phase [6], [7], [8], [9]. Further, the constraints of human biomechanics prevent the consideration of physically implausible knee angles, assisting the determination of realistic boundaries. This is helpful as the relationship between knee angles and performance is not as clear compared to other performance metrics. Minimum knee angles of the contact limb of elite male and female athletes at the 2017 and 2018 World Athletics championships are presented in Table 2.8 [6], [7], [8], [9].

Table 2.8: Mean minimum contact limb knee angles (angle between the thigh and lower leg considered to be 180 degrees in the anatomical standing position) and standard deviations (SD) in degrees (°) at each phase for elite male and female triple jumpers. Minimum knee angles for each phase were summarized across all athletes included in the 2017 and 2018 World Athletics reports [6], [7], [8], [9].

Phase	Female Mean Minimum Knee Angle (°) (SD)	Male Mean Minimum Knee Angle (°) (SD)
Hop	138.6 (8.83)	136.3 (8.92)
Step	133.6 (7.05)	128.0 (7.40)
Jump	135.5 (9.03)	127.9 (7.46)

Take-off angles of the trunk at each phase impact the jump distance, with larger initial take-off angles resulting in a higher flight trajectory of the body's centre of mass (COM), consequently leading to a lengthened flight time during the third phase [43]. Conversely, increasing the take-off angle may prolong braking time, potentially resulting in reduced horizontal velocity from one take-off phase to the next [3], [50]. Such velocity reduction can adversely affect the overall jump distance, emphasizing the challenge of attaining the optimal

take-off angle, particularly during the initial phase, to maximize performance across the entire jump. Take-off angles of the trunk at each phase were not computed due to challenges in accurately capturing these values; however, their critical impact on performance must be considered. For example, while an extended flight time may produce a better performance, an excessively high vertical component of the take-off angle could lead to unnecessary energy expenditure in the vertical direction at the expense of horizontal velocity [2]. Therefore, the take-off angle remains an important performance metric for a comprehensive understand of the triple jump technique.

Finally, *single-arm versus double-arm movement* is widely discussed in the context of triple jump performance. At the elite level, the adoption of the double arm technique is prevalent amongst male athletes, while the single-arm technique is predominantly used by female jumpers [51]. The current male world record holder employed a double-arm technique for his 18.29 metre jump [52], while the female world record holder leapt to 15.74 metres using a single-arm technique [53]. Evidently, the debate between single and double arm technique persists. There is limited research on the impact of arm technique on jump performance beyond work published by Allen et al. and Panoutsakopoulos et al. [41], [51]. Notably, Allen et al. found possible benefits of the double arm technique including "cushioning the stance leg during impact, raising the COM of the body at take-off, and facilitating an increase in kinetic energy at take-off [41]." Athlete preferences are also a factor when considering whether single-arm or double-arm technique is optimal.

2.1.5 Triple Jump Performance Metrics Summary

The distance achieved in triple jump is influenced by a complex interplay of a variety of factors and a subset of these factors was explored. Athletes and coaches must strategically manage these variables to optimize their technique. Objectively measuring jump performance metrics may provide useful feedback to athletes as current feedback mechanisms are largely limited to subjective observations.

Basic elements of triple jump technique are stable; however, various factors such as mental state, stress, fatigue, wind, and temperature, have an impact on technique and performance [43]. While these factors are beyond the scope of this thesis, it is necessary to acknowledge their potential effect on athlete performance.

2.2 Markerless Motion Capture in Biomechanical Analyses

Markerless motion capture holds promise for advancing biomechanical analyses. There is potential to quickly and reliably capture larger numbers of participants and collect natural movement data outside of controlled laboratory environments. However, there are significant challenges that need to be addressed before low-cost and accessible markerless motion capture systems are available to the general population, including coaching staff.

The performance of markerless motion capture against "gold standard" marker-based approaches in multi-camera scenarios has produced encouraging results [18]. Theia3D (Theia Markerless, Kingston, Canada) proprietary markerless software is widely used in research and has demonstrated considerable success in numerous studies when validating its performance in computing kinematic variables and joint angles against marker-based motion capture systems both "in the wild" and in controlled settings for clinical and sports applications [54], [55], [56], [57]. Though Theia3D software can produce results nearly comparable to marker-based approaches, it "requires a minimum of six cameras for tracking," making it difficult to employ in many real-world scenarios [58]. The open-source software, OpenPose (Carnegie Mellon, Pittsburgh, United States), is another markerless motion capture solution commonly employed in biomechanics research and has also produced promising results in validation studies [59], [60], [61], [62].

While many studies have demonstrated success in utilizing markerless motion capture solutions with multi-camera configurations, it is critical to note the limitations in real-world settings. Cronin et al. assessed the feasibility of OpenPose in assessing long jump take-off metrics during the 2017 World Athletics Championships [23]. The authors found very poor agreement between data from two calibrated cameras and manually digitized data labelled by an experienced individual using SIMI Motion software (Simi Reality Motion Systems GmbH, Germany) [23]. Beyond the anticipated challenge of placing cameras in ideal locations during competition, the highly variable OpenPose results hindered the identification of specific limitations of the markerless approach [23]. These findings suggest usage of open-source markerless systems to perform analyses in real competition scenarios requires significant improvements before it can be usable, though the authors only tested the OpenPose software.

Cronin et al. concluded that manual alternatives currently demonstrate more reliable results when the environment is unconstrained [23].

An important consideration with open-source markerless motion capture software is that these solutions are often developed using public training datasets, which comprise a small number of healthy adult participants engaged in basic movements like walking and standing [24]. Open-source markerless motion capture software is often trained on these datasets and may not perform as well for clinical populations and sports analyses, where subjects may present with atypical gait patterns and perform more complex movements, respectively, which are unfamiliar to the HPE algorithms [24], [63]. Other challenges currently being researched include variations in human visual appearance and physique, lighting conditions, partial obstructions, high pose dimensionality, and loss of 3D information when observing poses in two-dimensional (2D) images [64].

Despite the aforementioned obstacles, markerless motion capture may offer advantages over marker-based methods, depending on the research objective. Markerless motion capture enables easier and broader participant inclusion, and so long as an acceptable level of accuracy is achieved, it may outweigh the benefits of highly precise marker-based methods. However, the context is crucial – in clinical settings where results can influence a patient's treatment plan, for example, the highest possible accuracy is likely desirable. In contrast, for sports assessments where the goal is to augment coaching feedback, the lower accuracy of markerless motion capture systems may be sufficient. Moreover, certain analyses are infeasible within a laboratory setting, including assessing triple jump technique, which requires substantial space and specialized equipment. In such cases, choosing a less accurate analysis provided by a markerless system, but still within acceptable limits, may be preferable to not conducting the analysis at all. Furthermore, with ongoing advancements in CV and HPE, it is anticipated that markerless motion capture solutions will continue to improve. These developments, along with current research examples, are discussed in subsection 2.2.1.

2.2.1 Existing Open-Source Markerless Motion Capture Solutions

While various open-source markerless motion capture software solutions exist, two were chosen for evaluation – OpenPose and Google MediaPipe (GMP) – based on their accessibility, processing capabilities, and suitability for the desired analyses. Proprietary markerless software

were excluded from consideration as they do not meet the research objective of building an accessible and low-cost solution. Both OpenPose and GMP software present promising avenues for sports analytics single-camera markerless systems.

OpenPose is a popular open-source pose estimation software that has been employed for a variety of biomechanics research purposes [59], [60], [61], [62], [65]. OpenPose was trained on the publicly available COCO [66] dataset and has a 25-keypoint model to detect human body part landmarks in 2D, as shown in Figure 2.4 [23].

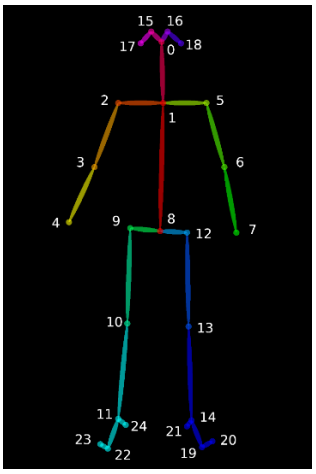

0 – Nose
1 – Neck
2 – Right shoulder
3 – Right elbow
4 – Right wrist
5 – Left shoulder
6 – Left elbow
7 – Left wrist
8 – Mid hip
9 – Right hip
10 – Right knee
11 – Right Ankle
12 – Left hip
13 – Left knee
14 – Left ankle
15 – Right eye
16 – Left eye
17 – Right ear
18 – Left ear
19 – Left big toe
20 – Left small toe
21 – Left heel
22 – Right big toe
23 – Right small toe
24 – Right heel
25 – Background

Figure 2.4: OpenPose 25-keypoint 2D pose model. Image from [67] and keypoint mappings from [68].

The pose estimation approach used in OpenPose leverages Part Affinity Fields (PAF), a technique used to determine which detected body parts belong to each person in an image [69]. PAFs establish connections between body parts, allowing the system to accurately associate limb segments with the correct person, even in complex and crowded scenes [69]. Users can interact with OpenPose through a command-line interface for basic scenarios and can optionally use the Python or C++ Application Programming Interfaces for solutions requiring more customization [68]. To save pose data, OpenPose supports exporting outputs to JSON files, enabling subsequent analyses [68].

The ability to easily extract pose data from OpenPose software has facilitated its widespread use in various research applications, as previously mentioned [59], [60], [61], [62]. However, there are several notable drawbacks. While OpenPose is capable of multi-person detection, it does not assign a consistent identifier to a person across video frames, requiring researchers to develop custom logic to handle this [23]. Moreover, the OpenPose solution is most

performant when using a device equipped with one or multiple GPUs, however, it is possible to run the software on a CPU-based device [68].

To assess the feasibility of OpenPose for triple jump analyses, attempts to process a subset of videos on a CPU-based device were made. Unfortunately, the processing speed was prohibitively slow, requiring nearly two hours for a single video with a length of approximately 15 seconds. Performance improved significantly when using a GPU-equipped device, but this approach was not ideal as the triple jump technique evaluation system should operate on hardware readily accessible to the general public. Additionally, the OpenPose license restricts use to non-commercial research purposes and prohibits distribution or commercialization, which could limit the potential for future productization of the proposed solution [70]. These limitations prompted the exploration of alternative solutions, bringing GMP into consideration.

Google MediaPipe (GMP) is a more recent open-source project and consists of a set of tasks for various ML applications including CV, text, audio, and generative Artificial Intelligence (AI) [71]. One of the vision-based tasks, Google MediaPipe pose landmark detection (GMP pose), can detect 33 body landmark locations in images or videos, and was investigated for use [72]. The pose landmarker model used to detect landmark locations is provided in Figure 2.5 [72].

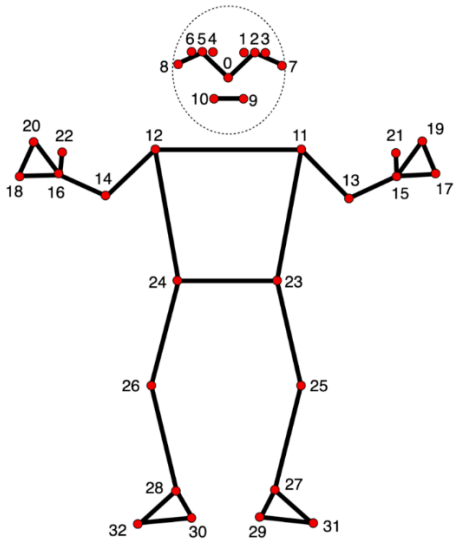

0 – Nose
1 – Left eye (inner)
2 – Left eye
3 – Left eye (outer)
4 – Right eye (inner)
5 – Right eye
6 – Right eye (outer)
7 – Left ear
8 – Right ear
9 – Mouth (left)
10 – Mouth (right)
11 – Left shoulder
12 – Right shoulder
13 – Left elbow
14 – Right elbow
15 – Left wrist
16 – Right wrist
17 – Left pinky
18 – Right pinky
19 – Left index
20 – Right index
21 – Left thumb
22 – Right thumb
23 – Left hip
24 – Right hip
25 – Left knee
26 – Right knee
27 – Left ankle
28 – Right ankle
29 – Left heel
30 – Right heel
31 – Left foot index
32 – Right foot index

Figure 2.5: Google MediaPipe pose landmarker model, capable of detecting 33 body landmark keypoints. Image and keypoint mappings obtained from [72].

Currently, GMP pose is only capable of single-subject pose estimation and can be used effectively on CPU-based devices. The GMP pose task leverages the BlazePose model developed by Bazarevsky et al. from Google Research [73]. The BlazePose model has a CNN architecture to perform pose estimation and has been validated against OpenPose on the COCO dataset [73]. Bazarevsky et al. compared OpenPose and BlazePose to a human-annotated baseline dataset and found that although OpenPose produced slightly better performance, BlazePose was superior for yoga and fitness scenarios [73]. Moreover, BlazePose was "found to be 25-75 times faster on a single mid-tier phone CPU compared to OpenPose on a 20-core desktop CPU," demonstrating its suitability for real-time use cases [73].

The GMP pose model returns [x, y, z] coordinates, visibility, and presence values for each keypoint for each frame. The x and y coordinates are "local to the region of interest and range from [0.0, 255.0] [74]." The z-coordinate "represents the distance relative to the plane of the subject's hips, which is the origin of the z-axis [74]." The z-coordinate is a 3D depth estimation in the BlazePose model architecture, which incorporates the Generative 3D Human Shape and Articulated Pose (GHUM) Model developed by Google Research [75]. The visibility result is a value between 0.0 and 1.0 to indicate that the landmark keypoint is "located within the frame and not occluded by another bigger body part or object [74]." The presence value has the same range as visibility and represents the "probability that a keypoint is located within the frame [74]."

Though GMP pose has fewer published validation studies, it offers several advantages over OpenPose:

- GMP pose was designed with fitness applications in mind and included subjects performing fitness exercises in the training dataset [74].
- GMP pose produces both 2D pixel coordinates, and 3D "world space" coordinates, with an origin at the subject's hip centre [71], [76]. In single-camera setups, OpenPose is limited to providing 2D pixel coordinates, as generating 3D keypoint values requires the use of multiple stereo cameras [77].
- GMP pose includes a lightweight model optimized for mobile usage (iOS and Android) and supports various programming languages including Python, C++, and JavaScript [78]. These features can facilitate the future development of mobile applications.

- GMP has more permissive licensing than OpenPose, enabling its use in potential future development of mobile applications.
- GMP pose demands fewer computational resources than OpenPose and can be used on CPU-based devices [22], [73].
- Google is actively developing the MediaPipe project including updating documentation, providing code usage examples, and fostering a community of users. No major features have been released in the OpenPose project since November 2020; it is unclear if there will be updates in the future [68].

In their 2022 literature review on healthcare applications with single camera markerless motion capture setups, Scott et al. observed that OpenPose and DeepLabCut are computationally expensive and unlikely to provide real-time results on most devices [22]. They suggest Google MediaPipe as a potential alternative to address this issue but note that no studies used it in their review [22]. A 2024 study that investigated the use of open-source markerless software for classifying Pilates poses compared the performance of OpenPose and GMP pose [78]. They found that although OpenPose had a higher recognition accuracy, GMP pose used fewer computational resources and was faster while still achieving reasonably good recognition rates [78]. Given its computational advantages, this underscores the necessity for further research with GMP and highlights its suitability for real-time sports analytics scenarios, making it a suitable choice to evaluate triple jump technique.

2.2.2 Single Camera Setups with Markerless Motion Capture

Single camera setups introduce additional complexities but could facilitate the deployment of markerless technologies in sports settings without requiring expertise in CV [24]. Research in this area has primarily focused on estimating sagittal plane kinematics in a controlled environment, successfully identifying joint angles in comparison to manually-labelled or marker-based methods [18], [24]. In their 2023 publication, Wade et al. note that existing research often does not consider “occluded joint centre locations on the far side of the body” although this information is provided by HPE algorithms [24]. Scott et al. also recommend that future research should focus on improving the accuracy of out of plane movements, reiterating a current limitation of single camera markerless systems [22].

While single-camera markerless systems present limitations, they offer reduced setup times and avoid the need for potentially intrusive markers [22]. However, these systems generally demonstrate reduced accuracy compared to 3D marker-based motion capture [79]. Some researchers argue that true 3D HPE with a single camera is not yet feasible, although "2.75D" estimates can be achieved in specific scenarios, such as track and field, where simplifying assumptions around the direction of movement are applicable [27]. However, single-camera markerless "may still provide greater reliability compared to subjective or self-reported measures [80]." Further, single-camera markerless systems enable motion analysis in scenarios and environments that would not be possible with more complex setups [22], including evaluating triple jump technique. These lower cost systems are also more accessible, requiring fewer resources and less expertise, enabling more frequent data collection for significantly more participants [79], [80]. Facilitating data collection for a greater number of participants is particularly critical as "a recent review of 30 years of publications within the Journal of Applied Biomechanics found that 84% of studies used convenience samples of less than 30 subjects [18]." Expanding the application of markerless motion capture assessments beyond laboratory settings is essential for their practical utility. While challenges remain, further investigation into single-camera markerless systems is warranted. Markerless motion capture, particularly with single-camera setups, offers a promising avenue for democratizing biomechanics research in sports coaching scenarios and beyond, provided that acceptable performance standards can be met.

2.2.3 Advancements in Markerless Motion Capture

Research in the area of CV have facilitated notable improvements in HPE algorithms, leading to the development of both open-source and proprietary markerless motion capture software. The availability of public datasets that can be used to train models with complex architectures is critical to advancements in this field. Table 2.9 summarizes popular public datasets that have been used to develop HPE algorithms: ImageNet [81], Human3.6M [82], HumanEva-I and II [83], and COCO [66].

Table 2.9: Publicly available datasets often used for training computer vision models.

Dataset	Description
ImageNet	Database of 3.2 million annotated images designed for use in "visual object recognition, image classification, and automatic object clustering [81]."
Human3.6M	One of the largest public motion capture datasets, consisting of 3.6 million human poses and corresponding images captured by a high-speed motion capture system; contains 11 participants in 17 scenarios [82].
HumanEva-I and II	Contains subjects performing a set of predefined actions, recorded using synchronized 3D motion capture and multi-view video [83]. The HumanEva-I dataset has four subjects performing a set of six predefined actions with three repetitions; the HumanEva-II dataset contains "two subjects performing an extended sequence of actions [83]."
COCO	Common Objects in Context or COCO is a "large-scale object detection, segmentation, and captioning dataset [66]."

While these publicly available datasets have contributed to significant progress in CV algorithm development, the range of participants and movements are limited. Drazan et al. highlighted the importance of training markerless motion capture "on datasets that are close matches to the intended use case [18]." This is particularly important in clinical and sports settings where participants may not always come from a healthy population or perform "typical" movements, respectively. Solutions including DeepLabCut, which facilitates training a neural network from a labelled dataset, have been developed to address these shortcomings [84]. For example, Yamamoto et al. leveraged DeepLabCut to enhance their single-camera markerless analysis of golf swings, yielding a useful system for coaching golf [85].

In addition to more widely available training data, models have become more efficient. Previously, it was not possible to perform CV tasks within a reasonable timeframe without GPUs. Now, open-source HPE solutions such as Google MediaPipe can be run on most CPU-based systems, further reducing the barrier to these technologies [71].

Evidently, both marker-based and markerless motion capture techniques possess inherent limitations, the selection of an appropriate approach must align with research objectives. In the context of this study aimed at enhancing accessibility of triple jump performance analyses, markerless motion capture is the preferred choice, leading to the selection of GMP software for the proposed framework.

2.3 Homography Background

A significant challenge with a single-camera markerless motion capture setup in an uncontrolled environment is establishing a real-world coordinate system for the participant's movement. While it is possible to calculate certain metrics, such as relative joint angles, using pixel space coordinates generated by open-source markerless software, this approach has limitations when applied to calculating performance metrics in the real world. For example, when evaluating triple jump technique, horizontal and vertical velocities, as well as distance metrics, are not meaningful in pixel space. This necessitates a solution for translating the participant's pose data in pixel space to real-world space. One solution to this problem is the implementation of homography techniques. A homography is a "projective transformation between two planes or, alternatively, a mapping between two planar projections of an image [30]," as depicted in Luo et al.'s diagram shown in Figure 2.6 [86]. Homography relates points in one image to their corresponding points in another image when the images were taken from different angles [30], [86].

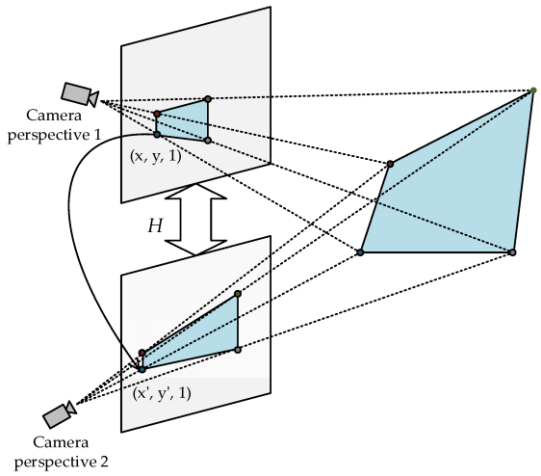

Figure 2.6: Homography estimation is a projective transformation between two images taken from different perspectives. Diagram obtained from [86] under the Creative Commons CC BY 4.0 license.

Homography techniques are useful in the development of a single-camera markerless system, as they provide an approach to transform pixel coordinates to real-world coordinates using known dimensions. Applying homography involves a multi-step process outlined in Figure 2.7.

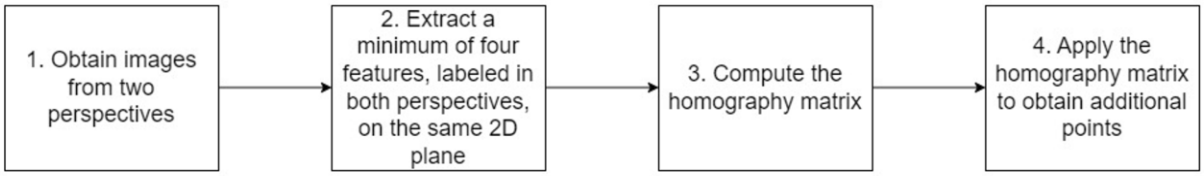

Figure 2.7: High-level steps for utilizing homography techniques. Diagram steps adapted from [86].

For the first step, two perspectives can be obtained either by using two images or video frames of the same scene taken at different angles, or one image or video frame and a "reference model [28]." The former case requires multiple camera perspectives to be available. In contrast, the reference model approach is applicable when only a single camera was used, but the facility has known feature dimensions that can be modeled from an overhead view. For example, Bjering developed an ice rink model in their 2019 paper using the established feature dimensions of a hockey rink to enable homography transformations [28].

Next, four pairs of corresponding points on the same 2D plane between the two perspectives must be labelled, although having more than four pairs is advantageous [28], [86], [87]. Automated feature-extraction approaches have been used to identify corresponding points and can be broadly classified into feature-based or deep-learning based methods [86]. For feature-based methods, a variety of algorithms can be used including Scale Invariant Feature Transform (SIFT) and Speeded Up Robust Features (SURF), which enable the identification of key points in images by identifying distinct patterns like edges and corners, whereas deep learning methods leverage CNNs to obtain features and perform feature matching between the two perspectives [86]. While these approaches are not restricted to extracting features on a single plane, the homography transformation is effective only if all features exist on the same plane. Alternatively, features can be manually labelled, as is often required in the reference model scenario [88].

Regardless of how the points for homography are determined, the third step is to compute the homography matrix. To compute the mapping between two perspectives, the homography matrix H must be computed as shown in Equation 2.1 [86],

$$H = \begin{bmatrix} h_{11} & h_{12} & h_{13} \\ h_{21} & h_{22} & h_{23} \\ h_{31} & h_{32} & h_{33} \end{bmatrix} \qquad \text{(Eq. 2.1)}$$

where $[h_{11}, h_{12}, h_{21}, h_{22}]$ represents the affine transformation, $[h_{13}, h_{23}]$ represents the translation and transformation, and $[h_{31}, h_{32}]$ represents the perspective transform between images [86]. The last element, h_{33}, is normalized to 1 so that *H* has eight degrees of freedom [86]. To implement this technique, OpenCV provides a set of geometric image transformations and camera calibration functionalities, which can be used to determine the homography matrix and apply it to obtain the transformed data [89], [90]. The final step is to apply the homography matrix to obtain additional points in the desired coordinate space.

Once homography transformations are implemented, their validity must be assessed, which can be done quantitatively and qualitatively. Visually overlaying homography results provides one mechanism to assess its subjective accuracy. Specifically, reprojecting pose landmarks after applying homography transformations allows for a visual subjective assessment of the homography accuracy. For quantitative assessments, there is no standardized evaluation metric, however, reprojection error in 2D image space can be used [27]. Reprojection error can measure the effectiveness of the homography transformation by converting the homography-transformed 3D world coordinates back to pixel coordinates. Adapting reprojection error from Baumgartner et al., the squared sum of the differences between the known pixel coordinates labelled using the reference model and the reprojected pixel coordinates is computed across all frames for each video to obtain the overall reprojection error [27]. Despite being a quantitative measure, guidelines for an acceptable reprojection error are unclear as errors of measurement are not reported consistently in existing research [22].

To apply the homography approach described in Figure 2.7, "track and field reference models," which represent the facility's coordinates from an overhead view, can be developed. Similar to hockey rinks, track and field facilities have markings and objects such as wooden boards that, though not always standardized, can be easily measured. In this scenario, the first perspective consists of 2D videos, and the second perspective is the known dimensions of the track and field facility from an overhead view, created via manual measurements, and expressed as a series of x-y coordinates. By relating known points on these models to 2D videos captured from a different perspective, the homography transformation can be calculated. It is crucial to note that not all known points are equally useful; parallel lines, due to their collinearity, result in

the vanishing point effect where they appear to converge towards a single point, providing insufficient information for computing a homography transformation [27].

Evidently, homography estimations have demonstrable usefulness in a wide range of fields, including sports analytics. However, when combining homography techniques with pose data obtained from a single-camera markerless system, valid results are limited to those where the participant has a contact point with the ground. This is because homography relies on fixed relationships between points on a common plane to accurately map positions between perspectives. For instance, in hockey, the player's skate must be on the ice, and in triple jump, the athlete's foot must be on the track. Analyzing frames where the participant is not in contact with the ground would require estimating their position in space using different techniques, introducing additional complexity. Incorporating methods to analyze non-ground contact frames is beyond the current scope, though it is an interesting topic for future research.

2.3.1 Homography Applications in Sports Analytics

Employing homography techniques in sports analyses is useful as sports footage is often captured using a single camera that pans as athletes move, and sporting facilities have features of known dimensions. For instance, in hockey, a single camera commonly captures footage of the ice rink, panning as players move, and the rink's markings can be leveraged for homography computation [28], [88]. When the player has a contact point with the ice rink, pose data from HPE algorithms can be employed to determine the physical whereabouts of players in real-world space, enabling subsequent analyses. Beyond hockey, homography techniques have also proven effective in sports analyses for golf, soccer, weightlifting, and track and field [27], [29], [87], [91], [92].

There are two broad approaches for identifying suitable points for homography in sports analytics when feature-based and deep-learning based methods are not applicable, (1) manual labelling of features with known dimensions, and (2) automated selection of known reference objects as features. While automated approaches are preferred, they are not always feasible in practice. In 2021, Walters et al. developed a tool for manually annotating homographies from hockey broadcast videos [88]. The authors emphasized the need for ground truth labels for point correspondences between each frame of hockey broadcast videos and an overhead view of an ice rink [88]. Importantly, broadcast videos involve camera panning, tilting, and zooming; therefore,

each frame must be registered to obtain real-world locations of the players and puck, a process they refer to as "sports field localization [88]." The proposed tool allows users to select as many corresponding points as possible between a video frame and the ice rink model, noting that "the best points are located at the ends of lines on the playing surface [88]." Once at least four corresponding points are selected, the homography transformation is computed and the result is overlaid so users can visually validate the efficacy of their selected points [88]. The tool has enabled the development of a dataset containing 4,262 hockey broadcast homographies [88].

Researchers have also explored methods requiring less manual intervention by strategically placing known reference objects in video frames. For instance, in 2021, Pueo et al. employed homography transformations to facilitate measuring barbell velocity from videos of athletes performing back squats recorded by a single smartphone camera [87]. The researchers placed known reference marks on a multipower machine to facilitate automatic point detection for homography transformation [87]. This enabled mapping image pixels to real-world coordinates, and subsequently the calculation of barbell velocity [87]. Placing reference objects on sports fields, including ice rinks and track and field facilities, is often impractical due to the potential interference with athletes and the challenge of ensuring the objects are visible in all frames, particularly in larger sports venues. Moreover, analyses are often performed on broadcast video obtained from public sources, where there is no opportunity for researchers to strategically place reference objects in the field of view. Therefore, pursuing methods that do not rely on reference objects is valuable, as it better simulates real competition scenarios for sports such as track and field, hockey, and soccer, and is applicable to analyses captured from public broadcast videos. However, implementing such approaches entails several obstacles.

Limitations in applying homography techniques to assess track and field events in uncontrolled environments present ongoing challenges for researchers. Unlike ice hockey rinks, track markings largely consist of parallel lines indicating lane markings [27]. According to Baumgartner et al., homography cannot be computed from track and field broadcast footage alone without additional known points due to the collinearity of input data consisting only of lane demarcations [27]. However, in their 2018 conference publication, Yagi et al. presented a methodology for estimating stride length in the 100-metre dash from a broadcast video using a homography approach [29]. The authors obtained a panoramic view of the track, counted the

runner's steps and employed HPE to detect body landmarks, and estimated the homography matrix using a minimum of four corresponding points in the panoramic view and the video frame [29]. Using this approach, they calculated 20-metre interval times, step length, and step frequency of one runner in the 2009 World Athletics 100-metre final and had strong agreement with the results from the publicly available World Athletics report from that year [29]. Yagi et al. demonstrated that homography can be successfully employed in track and field from footage captured by a single camera, although their method could not be easily scaled to more than one runner and required significant manual intervention. Beyond these publications by Baumgartner et al. and Yagi et al., there is limited literature on the application of homography in track and field performance analyses.

Homography techniques in sports analytics have proven to be effective for analyzing single-camera footage, which is common in sports broadcasting. These methods are relatively simpler when the camera is stationary, as in weightlifting, but become more complex with panning cameras, such as those used in hockey and track and field. While automated approaches for determining points for homography are preferred, they are not always practical because reference objects cannot always be placed in sports facilities, and they must be visible in every frame. Manual approaches, while tedious, overcome this challenge, as demonstrated by Walters et al. [88]. Despite its challenges, homography remains a powerful tool in sports analytics which, when combined with HPE, enables the computation of performance assessments in real-world coordinate systems.

2.4 Summary

Triple jump technique assessments must consider a variety of performance metrics to be useful for feedback. Most coaches and athletes have access to smartphones, which they may use to capture videos of the triple jump both in practice and during competition. Therefore, exploring how triple jump analyses can be conducted using only video footage captured by a single camera that pans may enable the development of a quantitative feedback tool. To build a solution accessible to the general public, the open-source GMP pose landmark model was selected to perform HPE. Combining knowledge of triple jump, GMP pose, and a single camera, an accessible solution could be developed. To overcome the challenges of using a single-camera system in an unconstrained environment, homography techniques provided a solution to compute

real-world coordinates of participant body landmarks, enabling the subsequent calculation of relevant performance metrics. The approach in this study was influenced by the aim to create a low-cost and accessible system to evaluate triple jump technique. Although biomechanical feedback alone has not been shown to reliably guide optimal training modifications, observing changes in performance metrics over time can assist athletes and their coaches in identifying areas for improvement [93].

Chapter 3: Objectives

This study aimed to develop a proof-of-concept methodology for the quantitative analysis of triple jump technique in real-world settings using a low-cost system comprised of a single smartphone camera and open-source markerless motion capture. The triple jump performance metrics, selected according to literature and metrics included in World Athletics triple jump reports, included ground contact times, flight times, take-off knee angles, phase distances, phase ratios, horizontal and vertical take-off velocities, and last stride velocity. Participants in this work are athletes of varying ages, years of experience, and skill levels, defined by their personal best (greatest triple jump distance achieved). Data collection was performed at both outdoor and indoor track and field facilities.

For preliminary validation of the proposed approach, performance metrics were compared between the studied athletes and those published in the World Athletics triple jump reports, in addition to visual assessments of the resulting pose estimation and reprojection error after applying homography. It was anticipated that more skilled participants would have shorter ground contact times, longer flight times, longer jump distances, more consistent intra-trial phase ratios and take-off knee angles, as well as higher last stride, horizontal and vertical take-off velocities compared to the less skilled participants. Compared to elite athletes assessed in the World Athletics reports, the studied athletes were expected to have longer ground contact times, shorter flight times, and shorter jump distances. Since the relationship between knee angles and performance is less evident, the range of knee kinematics was expected to overlap with those of elite jumpers due to physical biomechanical constraints. Given that phase ratios are a relative measure, they were also expected to overlap with those of elite jumpers. Moreover, the studied athletes were expected to demonstrate lower velocity metrics compared to elite athletes.

The primary goal of this study was to assess the feasibility of a low-cost, single-camera markerless motion capture system in analyzing triple jump technique. While current literature primarily explores markerless motion capture in controlled settings, conducting studies in uncontrolled environments with a single camera is necessary to democratize the use of markerless technology beyond academic settings. By proposing an end-to-end framework for performing markerless motion capture “in the wild,” key challenges, limitations, and areas for improvement were identified and can provide valuable insights to inform future research.

Chapter 4: Methods

4.1 Participants

Thirty participants (15 female, 15 male; average age 19.0 $\pm$ 4.0 years) were recruited with assistance from the Ottawa Lions Track and Field Club (OTTC). The OTTC is a long-standing Canadian track and field institution with access to a network of athletes in the Ottawa region and beyond. Canadian track and field coaches in Ontario, Quebec, and Nova Scotia were sent study information via email. Some participants were known to the researcher; this was disclosed in the University of Ottawa ethics submission.

Eligible participants were those who trained regularly in track and field (at least twice per week), with a focus on jumping events, and did not report any neurological, cardiovascular, or muscular disorders or injuries that may impact their triple jump performance. Moreover, participants were not required to alter their training schedule to participate in the study. A summary of the participant characteristics, grouped by relevant age categories used by Athletics Canada, the national governing body for track and field in Canada, is presented in Table 4.1 [94].

Table 4.1 Participant description, categorized by select age groups used by Athletics Canada, indicated in the parentheses. The abbreviations F (female), M (male), SD (standard deviation) are used in the table.

Age groups (years)	Number of participants	Body mass (kilograms)	Height (centimetres)	Personal best (metres)
		Mean (SD)	Mean (SD)	Mean (SD)
Under 16	5 F	52.6 (5.41)	165.0 (3.00)	9.57 (1.10)
	4 M	64.6 (7.52)	175.0 (4.09)	12.7 (0.70)
Total	**9**			
16-19 (Under 20)	8 F	62.9 (5.85)	171.0 (5.74)	10.7 (0.70)
	6 M	74.8 (9.18)	181.0 (4.90)	13.6 (0.97)
Total	**14**			
20 and over (Open)	2 F	62.4 (1.60)	170.0 (2.47)	11.6 (0.62)
	5 M	72.7 (1.79)	181.0 (5.43)	13.6 (0.66)
Total	**7**			
Grand Total	**15 F**			
	15 M			

4.1.1 Consent

Prior to data collection, participants were provided with a paper copy of the consent form and research questionnaire in their preferred language (English or French). The study was approved by the University of Ottawa research ethics board (Ethics file number: H-04-23-9061). Research ethics certificate and consent forms in English are included in Appendix A, including the participant research assent and corresponding parental consent forms for participants under 13 years of age, per University of Ottawa ethical guidelines. The project overview and data collection protocol were verbally explained to ensure that participants understood the study and could ask questions before determining their willingness to participate. As part of the informed consent process, individuals were told they could withdraw from the study at any time during or after completing the protocol.

After the informed consent process was completed, participants completed a research questionnaire where they self-reported their height, weight, age, sex, and email, as well as their dominant leg for the triple jump and their personal best triple jump distance achieved in a competition. To confirm participant eligibility for the study, the questionnaire also asked them to specify their years of training for triple jump, weekly practice frequency, and any health conditions that may impact their ability to perform the triple jump. Participant emails were collected to enable the distribution of personalized biomechanical reports, as outlined in the research consent forms. Beyond the personalized biomechanical reports, no compensation was offered to the participants.

4.2 Procedure

4.2.1 Facilities

Data collection was conducted at four locations: (1) Terry Fox Athletic Facility (TFAF) in Ottawa, Ontario (10 participants), (2) Pavillon d'Éducation Physique et Sport (PEPS) at Laval University in Quebec City, Quebec (6 participants), (3) Gryphon Fieldhouse at the University of Guelph in Guelph, Ontario (2 participants), and (4) Toronto Track and Field Centre (TTFC) at York University in North York, Ontario (12 participants). Images of each facility are shown in Figure 4.1.

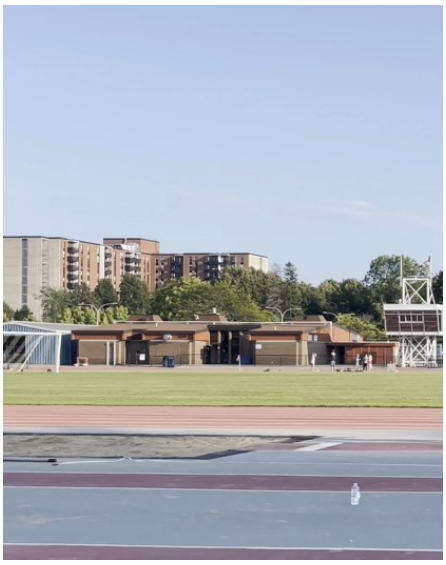

(a)

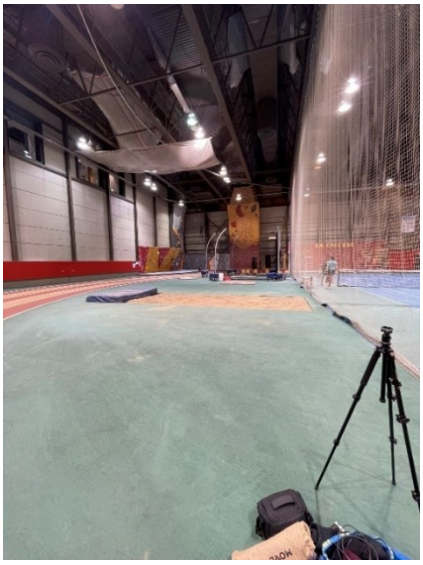

(b)

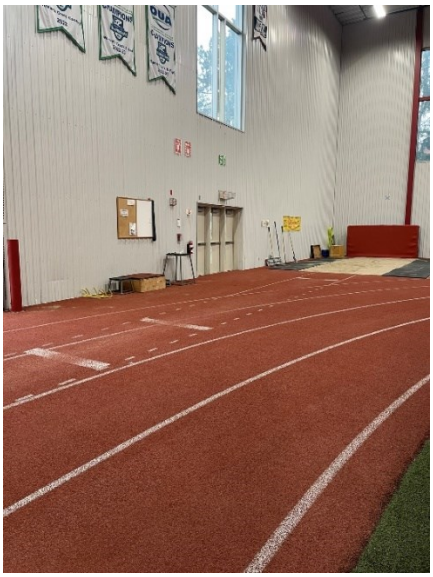

(c)

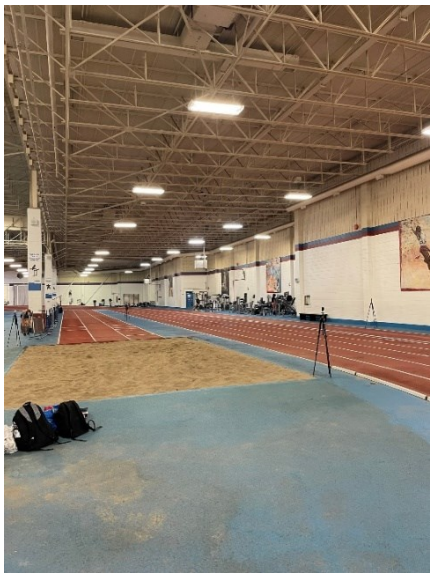

(d)

Figure 4.1: Track and field facilities used during data collection. Clockwise from top left – (a) Terry Fox Athletic Facility in Ottawa, Ontario; (b) Pavillon d'Éducation Physique et Sport at Laval University, Quebec City, Quebec; (c) Toronto Track and Field Centre at York University, North York, Ontario; (d) Gryphon Fieldhouse at the University of Guelph, Guelph, Ontario.

The TFAF is an outdoor facility, whereas the other three locations are indoor facilities, each with a designated area for horizontal jumps. At PEPs, the jumping area is located within tennis courts, which means the jumping runway includes tennis court markings, differing from a typical track and field facility. When not in use for jumping, the area is enclosed with a net, as seen in Figure 4.1. The Gryphon Fieldhouse has a more isolated jumping area and can only be filmed from one side as the sand pit is positioned along a wall. Lastly, the TTFC has a large horizontal jumps

area, however, one side is adjacent to a 200-metre track accessible to the public and other track and field clubs, while the other side is a throwing area. It is important to acknowledge that special considerations were needed during data collection to adapt to these facilities with varying layouts.

4.2.2 Equipment

To record each participant's jumps, a total of four tripods were used, one of which was part of the PIXEM 2 (MOVE 'N SEE, France) automated tracking system. The PIXEM 2 system included three external sensors, deemed micro-beacons, a PIXEM 2 robot with an iPhone mount, which was mounted to a tripod, and a silicon wristband equipped with a sensor worn by the participants [95]. An iPhone 12 (Apple, USA; 30 Hz; resolution 3840 × 2160) was mounted on the PIXEM 2 robot, which was inserted onto one of the tripods. The remaining three tripods were used to mount the three micro-beacons. The PIXEM 2 robot automatically adjusted the position of the iPhone by triangulating the location of the wristband using the three micro-beacons, ensuring that participants remained centred in the frame throughout their approach run and triple jump. The PIXEM 2 automated adjustments helped to minimize potential filming inconsistencies that could occur with manual recording. Due to equipment availability and researcher errors, the PIXEM 2 system was employed for nineteen of the thirty participants (9 female, 10 male). For the remaining participants, the iPhone was mounted on one of the tripods, and video capture, including video panning, was done manually. The absence of the PIXEM 2 system may have introduced minor variations in filming but it is not expected to have led to any significant issues.

A measuring tape was used to obtain comprehensive measurements of the jumping area at each track and field facility. This informed the development of hand-drawn diagrams that depicted the manually measured dimensions of the jump runway lines, sand pit, and take-off boards. The hand-drawn diagrams and corresponding measurements were used to develop a coordinate system for the jumping area of each facility, detailed in Section 4.3.6. No other equipment was required to conduct data collection. However, cones/pylons available at each facility were used to mark the appropriate take-off board if requested by the participant.

4.2.3 Participant Preparation

Participants were instructed to dress in comfortable athletic clothing and were informed that loose-fitting clothing may negatively impact study result accuracy. Prior to data collection, participants performed their preferred warm-up routine and signalled to the researcher when they were ready to begin their jumping trials. The warm-up time ranged from approximately 15 to 60 minutes, depending on the participant. Subsequently, they were directed to select a take-off board and an approach run distance that best aligned with their training program. Participants came from several different training groups led by different coaches and were not asked to alter their training programs, and thus data collection reflected a range of fatigue levels, with some participants having recently competed. This approach was intentionally chosen to minimize disruption to participants' routines.

Each participant was asked to perform six triple jump attempts to simulate a competition setting. This limit was also set based on an understanding of the event's physical demands, and the impracticality of requiring more than six jumps from all participants. Participants were encouraged to focus on completing each triple jump attempt, without concern for fouling. Since the data collection did not occur during an official track and field competition, avoiding fouls was not emphasized as it could lead to the exclusion of valuable data. A jumping trial, referred to as an attempt, that involved a foul but included the completion of all jump phases and a landing in the sand pit was deemed valid. For valid attempts, jump distance was always measured from the take-off board. An invalid attempt included failure to successfully complete all jump phases and land in the sand pit. Regardless of the jump's validity, a minimum rest period of five minutes was required between jumps, with additional time permitted if desired by the participant.

4.2.4 Jumping Protocol

Prior to data collection, the PIXEM 2 system was configured per the MOVE 'N SEE user guide [96]. The iPhone mount was attached to the PIXEM 2 robot and secured to a tripod set at a height of ~1.40-metres. The three micro-beacons were each placed on tripods set at a height of ~1.20-metres, as they needed to be at least one metre off the ground [96]. The tripod with the PIXEM 2 robot and iPhone was positioned near the sand pit, placed to capture the entire approach run and jump while accounting for the layout constraints of the facility. The distance between the PIXEM 2 micro-beacons was not a critical factor, provided it remained below 100

metres – well beyond the distance of any participant's approach run and triple jump. The micro-beacons were arranged in a triangular configuration, with micro-beacon two positioned to the left of micro-beacon one and micro-beacon three located farthest from the camera [96]. This setup is illustrated in Figure 4.2. For the eleven participants that did not use the PIXEM 2 system, the setup was simplified using only a single tripod set at a height of ~1.60-metres near the pit, with the iPhone mounted on it and the camera panning done manually. The height difference between the tripods in the PIXEM 2 and non-PIXEM 2 setup was to ensure the iPhone was at the same relative height in both configurations.

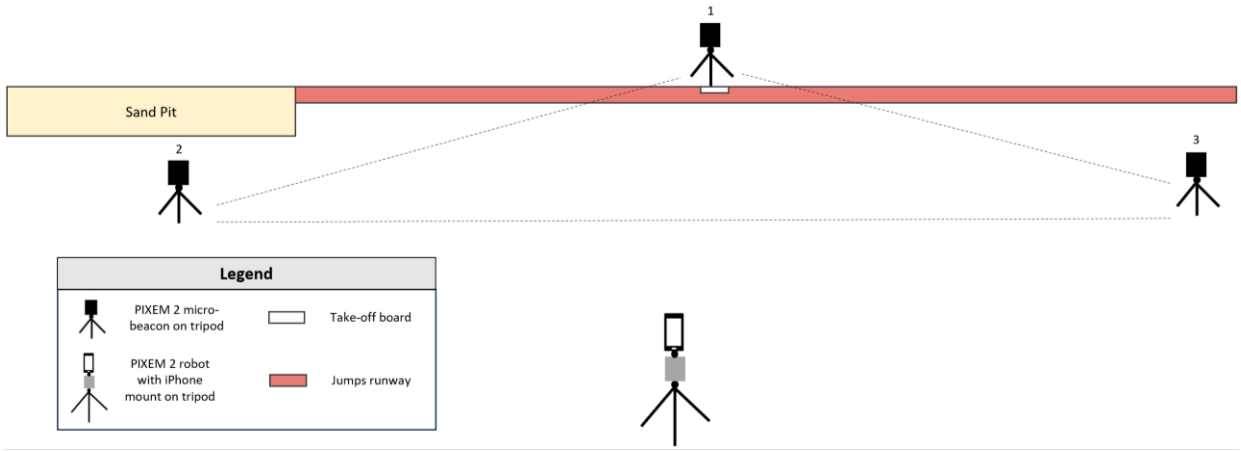

Figure 4.2: Experimental data collection setup using an iPhone 12 mounted to the PIXEM 2 tripod and robot, positioned to capture the sagittal view of each jump, and the three PIXEM 2 micro-beacons fixed on tripods.

The experimental setup shown in Figure 4.2 was either configured and tested before participants arrived or while they performed their warm-up routine, depending on facility availability. Once the setup was finalized and the participants were ready to begin, they wore the PIXEM 2 sensor wristband on the wrist closest to the camera to avoid occlusion. Before each jump, the researcher raised their arm to signal that the participant could start their triple jump attempt and carefully ensured that each video was recorded properly, regardless of whether the PIXEM 2 system was used. After each valid attempt, the jump distance was manually measured with a measuring tape and recorded by the researcher. Although video footage of non-valid jumps was retained, distances were not measured for these attempts. All video recordings were automatically saved to iCloud (Apple, USA). In total, 192 videos were collected, including retries of missed attempts requested by participants, resulting in some participants exceeding the expected six jump attempts.

4.3 Data Analysis

4.3.1 Software Architecture

Python served as the primary programming language used to implement the methodology, along with some use of Structured Query Language (SQL). The software architecture was carefully designed to prioritize efficiency, consistency, and code reusability. For example, classes were developed to enable consistent usage of specific data structures across multiple Python scripts. This design also supported the automation of processing steps, such as performance metric calculations, and tools to allow for visual evaluations of the pose detection results. Git was employed for local code source control, while GitHub provided a cloud-based platform for storing the private repository, ensuring code backups, and enabling potential future development efforts [97], [98]. Git and GitHub are widely used tools in software development, offering change tracking capabilities, security, and facilitating code collaboration. Details of the software architecture and Python script dependencies are included in Appendix B, and the visualization tool used for validation is described in Appendix C. Though the visualization tool was a component of the overall software architecture, it is presented in its own appendix because it operated independently from the other scripts. Note that additional supplemental scripts for data loading and aggregation are not included in these appendices.

4.3.2 Data Management

A relational data model and database were implemented to facilitate all data processing and analysis tasks for this study. This standardized approach to data management was necessitated by the open-source nature of GMP, which lacks a built-in storage solution. To efficiently manage GMP data and integrate it with other study data, a custom solution was required to avoid the inefficiencies of manual handling. Adopting a structured data management approach enabled the reuse of data inputs and outputs across Python and SQL scripts, thereby ensuring consistency and reducing development overhead. Employing a database management system was a prudent decision and offers scalability for potential future development needs. An entity-relationship diagram (ERD), a tool to aid in designing an effective data model, was developed during the planning stage of the database implementation and is available in Appendix D [99]. Appendix D also includes a description of the database tables. ERDs are a “visual

representation of how items in a database are related to each other" and are an important component of data management planning [100].

The database was implemented using SQLite, a file-based, open-source and lightweight relational database management system capable of meeting the study requirements while minimizing complexity [101]. The SQLite database engine is "the most used database engine in the world," with over 1 trillion SQLite databases in active use and is "built into all mobile phones [101]." The popularity and accessibility of SQLite made it a suitable choice for implementation, particularly if the proposed solution is developed into a mobile application in the future.

Importantly, relational databases, including SQLite, are not optimized for storing large bulk data, such as video files. Therefore, the videos were stored elsewhere and referenced in the database using file paths. All videos were downloaded in .MOV format to retain the highest possible resolution, moved to a OneDrive folder, and renamed using a consistent naming format to facilitate further analyses. As part of this process and to maintain participant privacy, each participant was assigned a unique participant ID – an integer value – used to organize all related study data. For example, videos for participant 11 were organized in a subfolder named raw_videos with the participant ID and attempt number specified in the filename: P11_1.MOV, P11_2.MOV, P11_3.MOV, and so on. A diagram of this folder structure is available in Appendix E. The jump distances and participant characteristics from the study questionnaire were entered into an Excel spreadsheet and then loaded into an SQLite table. Backups of all video files were stored in an Azure Blob storage account in the Canada Central region.

4.3.2.1 *Video Preparation*

To reduce file size and eliminate extraneous footage, videos were trimmed to capture the footage between the final four strides of the approach run and landing in the sand pit. A Python script utilizing the moviepy library was developed for this purpose [102]. This script allowed for the manual specification of start and end times to trim the videos accordingly. The resulting videos were stored in a designated folder named "trimmed_videos" according to the file structure described in Section 4.3.2 and illustrated in Appendix E.

4.3.3 Object Detection

The primary processing Python script was created to obtain and visualize participant pose results. This script contained logic to perform object detection to identify the participants in each video frame prior to performing pose detection, thereby improving the pose detection results. To do this, the GMP object detection task in Python was introduced to identify the bounding box pixel coordinates (x and y, coordinates, height, width) of participants in each frame [103]. The bounding box coordinates were used to effectively "zoom in" and crop video frames, focusing on the region containing the participant. These coordinates were stored in the SQLite database and overlaid on the trimmed videos to visually assess the object detection performance. The visual evaluation, enabled by functionality introduced into the primary processing Python script, involved determining whether the bounding box accurately encompassed the participant in each video frame. The GMP objection detection task alone was inadequate, warranting the development of custom code to improve performance, with all enhancements executed in the pixel coordinate space.

4.3.3.1 *Improving Object Detection Programmatically*

The GMP object detection task can detect multiple objects per frame; therefore, logic to identify the correct participant bounding box was required. The GMP object detector returns bounding boxes with the highest confidence score and does not assign unique identifiers to track individuals over multiple frames [103]. Setting the number of detected objects to five was effective in reliably capturing the participant. If the number was set below five, the GMP object detector risked missing the participant when multiple individuals were present in the frame, whereas increasing the number beyond five appeared to offer no additional benefit, based on visual observation. A systematic approach was introduced to calculate the percent overlap between bounding boxes across sequential frames to determine which of the five bounding boxes corresponded to the participant. A low percentage overlap indicated potential inaccuracies in bounding box detection. In such scenarios, the next bounding box was predicted by analyzing previous bounding box coordinates and predicting the subsequent position in the next frame. This involved introducing two functions to the main processing Python script to predict the next bounding box and calculate the bounding box percentage overlap between frames.

To predict the next bounding box, given a subset of previous bounding box coordinates for a video, the centre positions, widths and heights were extracted. Next, polynomial fitting was implemented to model the trend of centre positions, widths and heights. The trend line equation was then applied to estimate the coordinates of the next bounding box, ensuring it fit within the video frame boundaries. Once the next bounding box was predicted, the percentage overlap could be calculated. The polyfit function from the NumPy polyval library was used to implement this technique [104].

To calculate the bounding box percentage overlap, first the area of the predicted bounding box was computed using Equation 4.1.

$$predicted\ bounding\ box\ area = bounding\ box\ width \times bounding\ box\ height \quad \text{(Eq. 4.1)}$$

Next, the intersection of the predicted bounding box and the current bounding box was found. This included the x and y coordinates, as well as the width and height of the intersection. The area of the intersection was then calculated using Equation 4.2.

$$intersection\ area = \max(0, intersection\ width) \times \max(0, intersection\ height) \quad \text{(Eq. 4.2)}$$

Finally, the percentage overlap of the two bounding boxes was calculated using Equation 4.3:

$$percentage\ overlap = \frac{intersection\ area}{predicted\ bounding\ box\ area} \quad \text{(Eq. 4.3)}$$

By predicting the next bounding box and calculating the percentage overlap between the predicted and current bounding box, a quantitative metric was introduced to select the best bounding box for the participant in an automated fashion. For a given frame, the bounding box with the highest percentage overlap value was used to guide the GMP object detections. This limited instances where bounding boxes would erroneously shift focus to a background object instead of focusing on the participant.

4.3.3.2 *Overriding Object Detection Manually*

To further refine the object detection performance, a "bounding box override" capability was introduced in the Python script, allowing the bounding box to be manually drawn. When navigating frame-by-frame using the main processing script, the "A" key was pressed for frames with incorrect bounding box detections. Using OpenCV tooling, the correct bounding box was manually drawn on the frame [105]. Manually drawn bounding boxes replaced erroneous detections, and an "overridden flag" was added to the appropriate SQLite table to track frames where manual overrides were necessary. For more details on the bounding box manual override tool, refer to Appendix F. The combination of manual override functionality and programmatic bounding box smoothing notably enhanced the GMP object detection performance, as determined by visual assessment. At the end of the object detection step, bounding boxes for each video frame for all participants and the overridden flag, where applicable, were available in the SQLite database.

4.3.4 Pose Landmark Detection

The primary processing Python script utilized the participant bounding box coordinates extracted through the object detection approach described in Section 4.3.3. These coordinates were read from the SQLite database, and input into the GMP pose landmark detection model to generate pose landmark coordinates for each participant. For all 33 landmarks in the GMP pose model, two sets of pose coordinates were obtained for each video frame: 2D-pixel coordinates and 3D-GMP world coordinates [72]. Landmarks for both coordinate types were saved in the SQLite database. Visual assessments of GMP pose detection performance, conducted using the primary Python script, which overlaid the pose detection results in pixel coordinates on the videos and enabled frame-by-frame navigation, revealed opportunities for pose detection improvements. Consequently, further refinements were necessary, including skipping video frames with poor detections, and applying gap filling and smoothing between video frames, which are detailed in the following subsections.

4.3.4.1 *Skipping Frames*

In some video frames, the GMP pose landmark detections were incorrect. For example, the landmarks were all clustered closely together, or the lower limbs were detected as bent when

the subject's knees could be visually observed as straight. To address this, the main processing script was updated to allow poor-quality frames to be skipped, ensuring they would not negatively impact downstream processing or the quality of the triple jump performance metric results. During the frame-by-frame navigation enabled by the main Python processing script, the "X" key was pressed to indicate a "bad" frame. No data for these frames were stored in the SQLite database at this stage. Instead, missing frame data was addressed during the gap filling and landmark smoothing process.

4.3.4.2 *Gap Filling and Landmark Smoothing*

To mitigate the impact of missing landmark data on subsequent analyses, a Python script was developed to fill in and smooth missing pose data in both GMP pixel coordinates and 3D world coordinates space. After identifying frames with missing data, interpolation functions from SciPy estimated pose landmark values using pose data from adjacent frames. Specifically, the CubicSpline class from the SciPy interpolate library was used to smooth pose data [106]. This class fits piecewise cubic polynomials to the data, ensuring smooth transitions at the boundaries between polynomials [106]. Each segment of the spline is defined by Equation 4.4:

$$S_i(x) = a_i + b_i(x - x_i) + c_i(x - x_i)^2 + d_i(x - x_i)^3 \quad \text{(Eq. 4.4)}$$

where $S_i(x)$ represents the spline function in the interval $[x_i, x_{i+1}]$, and a_i, b_i, c_i, d_i are coefficients determined from the data. x_i and x_{i+1} are the x-coordinates of the data points that define the current interval of the spline.

Cubic spline interpolation was sufficient for small gaps in pose estimation. However, interpolating large gaps (more than four missing adjacent frames) provided unacceptable results, as determined by visual observation. In these scenarios, the data were discarded. To reduce missing data, GMP pose landmark detection must be improved (discussed in Section 7: Future Work).

The entire GMP object detection and pose landmark detection process with custom enhancements (Sections 4.3.3 and 4.3.4) is illustrated in Figure 4.3 below.

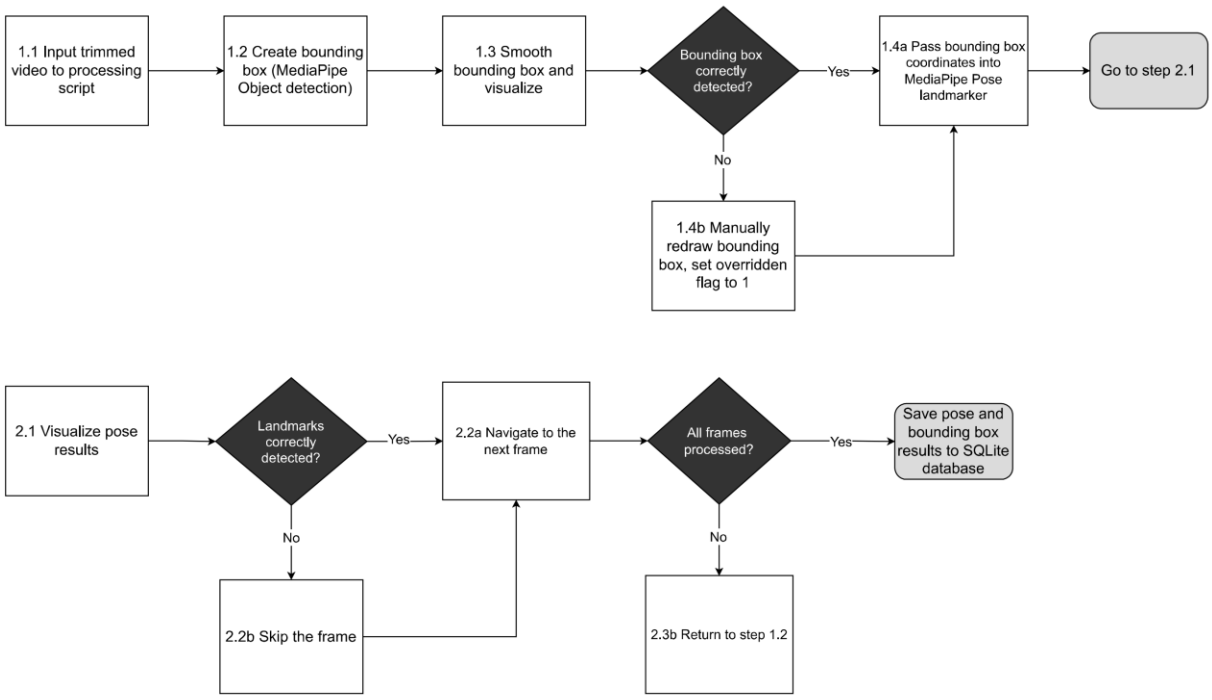

Figure 4.3: Flow diagram of data processing steps to obtain pose estimations: Google MediaPipe (GMP) objection detection, bounding box smoothing and optional manual override, GMP pose landmark detection, skipping frames, and saving the results to an SQLite database. Smoothing and gap filling was applied to the GMP pose data as a post-processing step.

4.3.5 Centre of Mass Estimation

The participant COM was required for velocity performance metric calculations, described in Section 4.4.3, and therefore was calculated in the main Python processing script for each frame. Estimates of relative body segment mass according to Dempster's anthropometric table were used to estimate COM [107]. GMP pose landmarks were mapped to segments in Dempster's table as accurately as possible, acknowledging that they are approximations. The segment mapping details are documented in Appendix G.

The COM equations below (Eq. 4.5 – 4.7), described as the COM of a multisegment system in Winter's Biomechanics and Motor Control of Human Movement book [107], were used for the calculation. The COM of the system has coordinates (x_0, y_0), where each coordinate needs to be calculated separately [107]. In the equation, $M\ denotes\ total\ mass, m$ denotes segment mass, x defines the x-coordinate of the segment, and y defines the y-coordinate of the segment.

$$M = m_1 + m_2 + \cdots + m_n \quad \text{(Eq. 4.5)}$$

$$x_0 = \frac{m_1 x_1 + m_2 x_2 + m_3 x_3}{M} \quad \text{(Eq. 4.6)}$$

$$y_0 = \frac{m_1 y_1 + m_2 y_2 + m_3 y_3}{M} \quad \text{(Eq. 4.7)}$$

Note: Equations from [107], and n represents the number of segments.

A Python script was developed to compute the participant COM at every frame since it is "continuously changing with time… and is, therefore, necessary to recalculate it after each interval of time [107]." This was achieved by implementing Equations 4.5 – 4.7 above, where the masses were obtained from Dempster's anthropometric table [107], and the positions from GMP 3D world coordinates. The resulting COMs were saved in the SQLite database to facilitate use in downstream calculations.

4.3.6 2D Track Templates

The hand-drawn diagrams described in Section 4.2.2 were used to generate facility models, referred to as 2D track templates. Measurements of the facility jump area were translated into a series of points with corresponding x and y coordinates to map the area onto a 2D plane. For each facility, each point was assigned a point ID, and the x and y coordinates were stored in an Excel spreadsheet, which was subsequently loaded into the SQLite database. The edge of the sandpit nearest to the iPhone during data collection was designated as the origin point (assigned point ID 0) for each facility, with all other points referenced relative to this origin.

To verify that the 2D track templates reasonably represented the facility jump areas, the coordinates were plotted using a Python script which leveraged matplotlib.pyplot [108] for visualization. The Gryphon Fieldhouse hand-drawn diagram, and an example of the corresponding points labeled in a video frame are shown in Figure 4.4. The hand-drawn diagrams and corresponding plots generated using Python representing the 2D track templates for all facilities are provided in Appendix H.

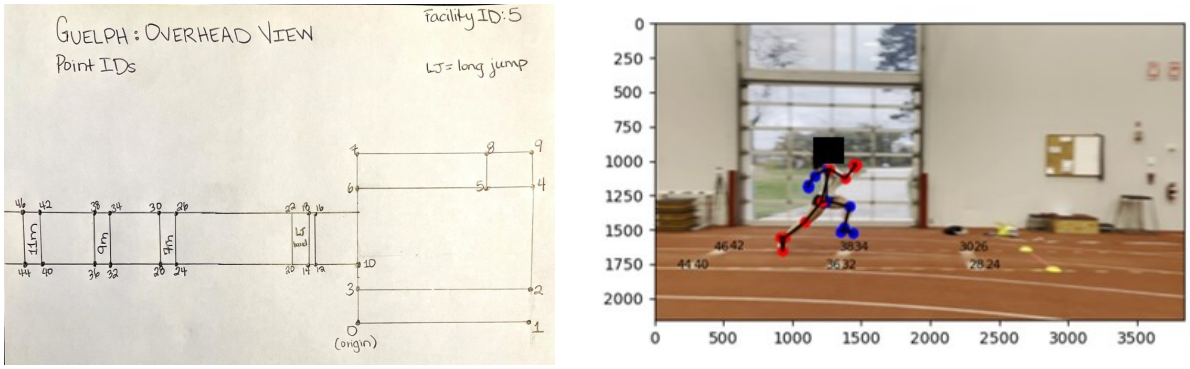

Figure 4.4: The hand-drawn 2D track template for Guelph (left) and the corresponding points labeled on a video frame (right) at the Gryphon Fieldhouse in Guelph, Ontario.

The 2D track template approach was inspired by the LensCalibrator GitHub project, which used coordinate systems to represent images as part of a process to perform camera calibration [109]. The approach also aligned with Bjering's use of "ice rink models" to compute homography matrices from hockey broadcast footage [28]. The term 2D track templates was coined in reference to similar methodologies used by Bjering and Walters et al. in their publications involving applications of homography in sports [28], [88].

4.3.7 Ground Contact Labelling

4.3.7.1 *Participant-Related Labels*

Independent from the main processing script described in Section 4.3.3, ground truth labels were required to discern frames when a participant's foot or feet are planted on the ground to facilitate subsequent homography calculations. As previously discussed, the proposed approach is only applicable to ground contact frames. Using the main Python processing script, the frame-by-frame navigation display was used to manually collect ground contact information into an Excel spreadsheet for each participant attempt. This information, summarized in Table 4.2, included: frame number (only frame numbers of ground contacts were recorded), foot, contact type, phase, switch, and foul. The switch label denoted instances where GMP pose detection erroneously swapped the sides of landmarks, resulting in left landmarks being positioned on the right side and vice versa. Manual identification of these errors from visual assessment was facilitated by the use of distinct colours to represent left and right landmarks. These switching errors are further discussed in future sections (Section 6.2: Limitations and Section 7: Future Work). The foul label was included to enable downstream distance-based

metrics to be computed. All manual labels were performed by the researcher and were loaded from the Excel spreadsheets into the SQLite database using a Python Script.

Table 4.2: Description of participant-related manual labels for video frames where the participant's foot or feet are in contact with the ground.

Attribute	Definition	Possible Values
Foot	Indicates the foot on the ground.	• L (Left) • R (Right) • B (Both)
Contact Type	Indicates the position of the foot on the ground.	• Heel • Toe • Full
Phase	Indicates the phase of the triple jump.	• 1 – Approach Run • 2 – Hop (First phase of the triple jump) • 3 – Step (Second phase of the triple jump) • 4 – Jump (Third phase of the triple jump) • 5 – Landing
Switch	Indicates whether GMP pose landmarks were identified at all, and/or whether the participants' left and right sides were identified correctly.	• 0 – No switch • 1 – Switch • N/A – Pose landmarks not detected
Foul	Indicates whether the athlete fouled their jump or not.	• 0 – No foul • 1 – Foul

4.3.7.2 *Facility-Related Labels*

Additional ground contact labels were required for the facilities, denoted key point labels. Key point labels represented the corresponding points in the 2D track templates and video frames in pixel coordinates. Inspired by the annotation tool developed in Python by Walters et al. [88], a custom Python script was developed to facilitate manual key point labelling in video frames, largely relying on OpenCV capabilities [105]. Since the proposed homography approach was only suitable for ground contacts, key point labels were done only for frames manually identified as a ground contact from the step described in Section 4.3.7.1.

The key point labelling Python script allowed the participant ID and attempt number to be specified via command-line arguments and opened the corresponding video in an OpenCV window to facilitate labelling [105]. The tool permitted backward and forward navigation between ground contact frames using the right and left arrow keys. The up and down arrow keys enabled the selection of an integer value, representing a point ID, in the appropriate 2D track

template. Functionality was included to permit clearing and redoing labels for a given frame, as well as the ability to quit the program without saving any labels. During labelling, the 2D track template was opened next to the OpenCV window for reference. Once the desired point ID was selected using the arrow keys, the corresponding point on the video frame was indicated using the left mouse click. Approximately six to eight points per ground contact frame were chosen to ensure a buffer beyond the four-point minimum required for homography transformations [28] [86], [87]. Key point labels were saved to the SQLite database. All key point labels were completed manually by the researcher and a student research assistant. Additional details on the key point labelling script, including a detailed user guide, are available in Appendix I.

4.3.8 Homography Transformation

4.3.8.1 *Determine Contact Foot Position*

The goal of the homography transformation was to transform points from the 3D GMP world coordinate system, with an origin at the participant's hip centre, to the 3D real-world coordinate system. This was accomplished through the development of a Python script. The 2D track templates and manual key point labels for ground contact frames were used as input to calculate the homography matrix. This was achieved using the OpenCV Python function findHomography(), which "finds a perspective transformation between two planes [90]." Next, the homography matrix was applied to the GMP pose 3D world coordinates of the ground contact foot (landmarks 29, 31 for the left foot, and 30, 32 for the right foot) to produce the 2D foot position in coordinates relative to the 2D track template origin using the OpenCV Python function perspectiveTransform() [89]. Since all analyzed frames were ground contacts, an implicit z-value of zero could be assumed, allowing the estimation of the 3D foot position in real-world space on the plane where the z-value is zero. The foot was selected as the anchor point for homography because it was the only body segment in contact with the known 2D plane between the 2D track templates and the manual key point labels. The validity of the 3D foot position was evaluated through visual inspection by plotting the foot position and corresponding distances using matplotlib.pyplot [108]. By comparing these plots with the video footage, it was clear that the estimated foot positions were reasonably accurate. For example, a participant using the 7-metre take-off board for their triple jump had a foot position close to 7-metres at the instant of hop take-off, as expected.

Determining the 3D foot position in real-world space using homography enabled the calculation of distance-based triple jump metrics. While the foot position served as the anchor point, mapping the remaining GMP pose landmarks to real-world space was essential for calculating other performance metrics. Note that although all landmarks were saved in the SQLite database, those representing the face (landmarks 0-10) were excluded from the analyses as they were not relevant for performance metric calculations.

4.3.8.2 *Transform Landmarks Using Contact Foot as Anchor*

Using the 3D real-world foot position as an anchor point, the translation, rotation, and scale factor were estimated to construct the transformation matrix necessary for mapping the remaining GMP pose 3D world landmarks to 3D real-world coordinates [110], [111]. An "initial guess" of each component of the transformation matrix was required. The 3D real-world coordinates of the foot midpoints were used as anchor points to derive the translation. For the rotation component, 3D GMP pose world coordinates and 3D real-world foot coordinates were converted into direction vectors within their respective coordinate systems. The axis of rotation between these vectors was computed, serving as the "initial guess" for the rotation between the two coordinate systems. Lastly, the scale factor "initial guess" was set to one as the GMP pose foot data proved unreliable for scaling, resulting in unrealistic participant sizes. The transformation matrix was represented using homogeneous coordinates to consolidate the transformation into a single matrix multiplication, an approach selected for its computational convenience [111].

The transformation matrix based on the "initial guesses" was used as a starting point to determine the remaining GMP pose landmarks in 3D real-world space. While using the contact foot as an anchor point allowed for proper alignment of rotation and direction, it failed to account for an additional degree of freedom. This could produce scenarios where, for example, the computed real-world coordinates were upside down. To resolve this issue, an optimization approach was introduced to refine the transformation matrix estimate.

4.3.8.3 *Optimize Landmark Transformation*

After generating an "initial guess" for the transformation matrix, an optimization function was configured, which required a quantitative metric to guide improvements. Reprojection error

was selected as the metric to be minimized. Reprojection involves mapping 3D real-world coordinates onto a 2D image plane by incorporating information about the physical camera (camera matrix, lens distortions, position in space, and angle), and computing where the 3D points in real-world space would appear in a virtual image in pixel coordinates [27]. These pixel coordinates were then compared to the GMP pose pixel coordinates to obtain the reprojection error. Specifically, the reprojection error for each point was computed as the Euclidean distance between the pixel coordinates detected by GMP (x_m, y_m), where x_m and y_m denote the x and y pixel coordinates of a pose landmark as determined by GMP pose detection results. The reprojected pixel coordinates after the homography transformation were defined by (x_r, y_r), where x_r and y_r indicate the x and y pixel coordinates of a pose landmark after applying the homography transformation to GMP pose world landmarks and reprojecting the results back to pixel coordinate space. This computation was facilitated by reading the appropriate values from the SQLite database. The reprojection error equation is shown in Equation 4.8.

$$reprojection\ error = \sqrt{(x_m - x_r)^2 + (y_m - y_r)^2} \quad \text{(Eq. 4.8)}$$

The problem was formulated as an objective function that aimed to minimize the reprojection error by optimizing the rotation and scale components of the transformation matrix, while translation remained fixed.

The camera matrix and lens distortion values were required to compute the reprojection error and were calculated by performing camera calibration. Performing camera calibration involved estimating the parameters of a camera model to approximate the physical camera and was an essential step to ensure accurate homography estimations [112]. To calculate the camera parameters, the OpenCV Python tutorial for camera calibration was adapted [113]. First, an image of a checkerboard of known dimensions was printed on a sheet of paper and filmed from different angles with the same iPhone 12 and video settings used in data collection. Next, a Python script was developed to compute the camera matrix and lens distortions and save the outputs in NumPy's NPY format, a "simple format for saving numpy arrays to disk with the full information about them [114]." These files were saved as blobs in the SQLite database. The camera matrix and lens distortion values were read from the table in the main homography script.

The optimization function was implemented using the SciPy minimize function from the optimize library [115]. After trial and error done by visual observation, the Constrained Optimization by Linear Approximation (COBYLA) algorithm was selected as the type of solver to be used by the SciPy minimize function [115]. After the minimization function ran, an optimized transformation matrix resulted. This transformation matrix was then used to transform the remaining GMP 3D world coordinates into 3D real-world space, enabling the downstream calculation of triple jump performance metrics. The homography transformations were validated using visual observation and reprojection error. Visual observation was facilitated using the visualization tool presented in Appendix B. It enabled visualization of the pose landmarks after the optimized homography transformation using frame-by-frame navigation, for ground contact frames. Figure 4.5 depicts the homography transformation process required to obtain the 3D foot position, and the subsequent steps for transforming additional GMP pose landmarks into 3D real-world space.

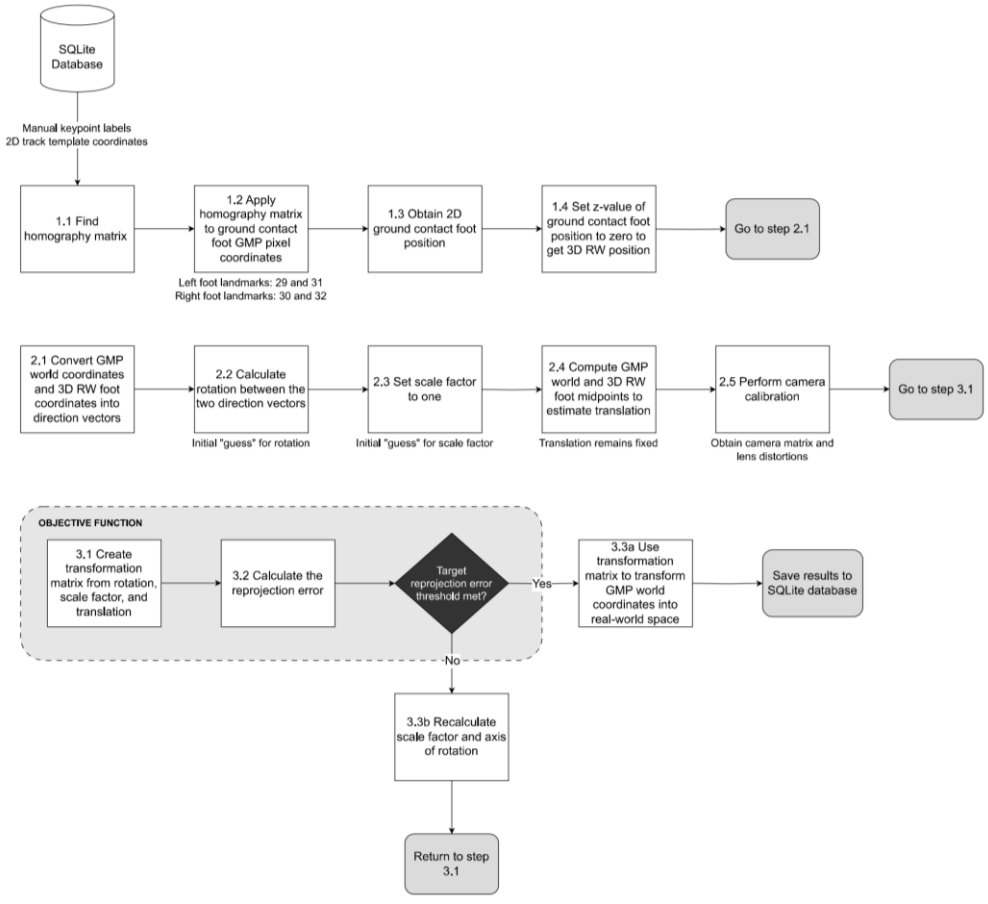

Figure 4.5: Homography transformation process diagram. The abbreviations GMP (Google MediaPipe) and RW (real-world) are used in the figure.

4.4 Performance Metrics Calculations

The computed performance metrics were split into three categories, as shown in Table 4.3 below. Performance metrics were calculated for each participant for each of their valid jumps. The selected performance metrics were largely influenced by those included in the 2017 and 2018 IAAF World Athletics Championships triple jump reports [6], [7], [8], [9]. A select number of these metrics were used based on data quality and feasibility.

Table 4.3: Summary of triple jump performance metrics by category.

Performance Metrics Category	Description of Category	Included Metrics
A: Video-based	Metrics requiring video data and participant-related manual labels	• Flight time for each phase (seconds) • Ground contact time for each phase (seconds)
B: MediaPipe-based	Metrics requiring the items in "A," as well as MediaPipe pose landmarks after performing smoothing	• Minimum knee angles at take-off for each phase (degrees)
C: Homography-based	Metrics requiring the items in "A" and "B," as well as measured distances, and manual key point labels (2D track templates required)	• Hop, step, and jump phase distances (metres) • Phase ratios (percentage) • Last step length (metres) • Take-off loss or foul distance (metres) • Effective distance (metres) • Horizontal COM velocity at take-off for each phase (metres/second) • Vertical COM velocity at take-off for each phase (metres/second) • Change in vertical and horizontal COM velocity between phases (metres/second)

The categories were selected based on the inputs required after the data analysis, as described in Table 4.3 and visualized in Figure 4.6.

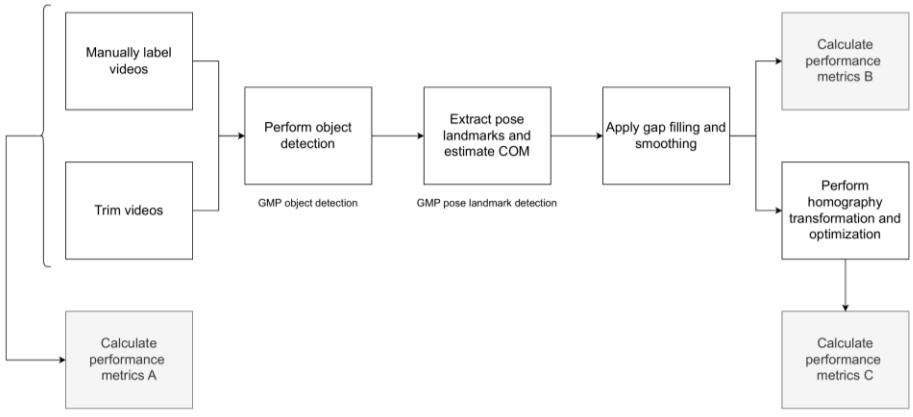

Figure 4.6: Diagram of methodology overview for data processing and performance metric calculations. The abbreviations GMP (Google MediaPipe) and COM (centre of mass) are used in the figure.

4.4.1 Category A Performance Metrics: Video-based

Ground contact time and flight time for each phase, measured in seconds, were computed from the participant-related labels previously described in Section 4.3.7.1 and Table 4.2. Ground contact time was measured by counting the number of frames labelled as a ground contact time for each phase and dividing by the frame rate. Therefore, for a given phase, p, the ground contact time in seconds was calculated by determining the ground contact frames (Equation 4.9) and using the video frame rate to convert to the result to seconds (Equation 4.10).

$$ground\ contact\ frames_p = last\ frame_p - first\ frame_p + 1 \quad \text{(Eq. 4.9)}$$

$$ground\ contact\ time_p = \frac{ground\ contact\ frames_p}{video\ frame\ rate} \quad \text{(Eq. 4.10)}$$

where $first\ frame_p$ is the first frame of phase p, $last\ frame_p$ is the last frame of phase p. Similarly, flight time for each phase was calculated by counting the number of frames between ground contacts for each phase and dividing by the frame rate. For a given phase, p, the flight time was computed using Equations 4.11 and 4.12.

$$flight\ time\ frames_p = first\ occurrence_{p+1} - last\ occurrence_p - 1 \quad \text{(Eq. 4.11)}$$

$$flight\ time_p = \frac{flight\ time\ frames_p}{video\ frame\ rate} \quad \text{(Eq. 4.12)}$$

Where $last\ occurrence_p$ is the last occurrence of phase p, and $first\ occurrence_{p+1}$ is the first occurrence of the next phase $p + 1$.

4.4.2 Category B Performance Metrics: MediaPipe-based

The minimum knee angle of the contact limb for each phase was estimated using GMP pose 3D world landmarks for the right knee (landmarks 24, 26, 28) or the left knee (landmarks 23, 25, 27), depending on the contact limb. A Python function was developed to accept x, y, z coordinates for any three landmarks. The final equation for computing an angle from GMP pose world landmarks is shown in Equation 4.13 [116]. A step-by-step guide for the function inputs, intermediate steps, and final equation is included in Appendix J, and was adapted from [116].

$$knee\ angle = arccos\left(\frac{(x_1 - x_2)(x_3 - x_2) + (y_1 - y_2)(y_3 - y_2) + (z_1 - z_2)(z_3 - z_2)}{\sqrt{(x_1 - x_2)^2 + (y_1 - y_2)^2 + (z_1 - z_2)^2} \cdot \sqrt{(x_3 - x_2)^2 + (y_3 - y_2)^2 + (z_3 - z_2)^2}}\right) \times \left(\frac{180}{\pi}\right) \quad \text{(Eq. 4.13)}$$

For each video containing a valid jump, the knee angle in degrees was computed for each contact frame and phase. From the computed angles, the minimum value for the appropriate limb for each phase was selected as the minimum knee angle.

4.4.3 Category C Performance Metrics: Homography-based

All performance metrics in Category C used the 3D real-world foot landmark coordinates obtained from the homography transformation step described in the first part of Section 4.3.7. The foot landmark allowed distance metrics to be calculated, but this landmark alone was insufficient to compute velocity-based metrics, necessitating the optimization step described to determine the rotation and scale factor, allowing the computation of the remaining landmarks and COM in real-world space.

For homography-based metrics, a Python function was developed that accepted foot landmarks of the contact foot – landmarks (32, 30) for the right foot, and (29, 31) for the left foot – for each valid attempt. From these landmarks, only the toe x-position was used (32 for the right toe, and 31 for the left toe). The Python function also accepted the distance measured manually during data collection, the take-off board distance, and whether the jump was a foul as inputs; these values were all read from the SQLite database. As previously mentioned, all valid jumps were included, regardless of whether a foul occurred. Equations 4.14 – 4.21 present the formulas for last step length, phase distances, phase ratios, take-off loss or fault distance, and effective distance.

Last step length:

$$last\ step\ length = |\ contact\ toe_{x1} -\ contact\ toe_{x0}| \quad \text{(Eq. 4.14)}$$

where $contact\ toe_{x0}$ is the x-coordinate of contact toe at the last step of the approach run, and $contact\ toe_{x1}$ represents the x-coordinate of contact toe at the hop take-off.

Take-off loss or foul distance:

$$take\text{-}off\ loss\ or\ foul\ distance = \left|take\text{-}off\ board\ distance - \ contact_{toe_{x1}}\right| \quad \text{(Eq. 4.15)}$$

where the take-off board and foul information is obtained from data collection information.

Effective distance:

If the jump was not a foul, the effective distance is:

$$effective\ distance = \ |official\ distance + take\text{-}off\ loss| \quad \text{(Eq. 4.16)}$$

If the jump was a foul, the effective distance is:

$$effective\ distance = \ |official\ distance - fault\ distance| \quad \text{(Eq. 4.17)}$$

Hop distance:

$$hop\ distance = |\ contact\ toe_{x2} - \ contact\ toe_{x1}| \quad \text{(Eq. 4.18)}$$

where $contact\ toe_{x2}$ is the x-coordinate of contact toe at the end of the hop phase and the beginning of the step phase.

Step distance:

$$step\ distance = |\ contact\ toe_{x3} - \ contact\ toe_{x2}| \quad \text{(Eq. 4.19)}$$

where $contact\ toe_{x3}$ is the x-coordinate of the contact toe at the end of the step phase, and the beginning of the jump phase

Jump distance:

$$jump\ distance = effective\ distance - hop\ distance - step\ distance \quad \text{(Eq. 4.20)}$$

Real-world coordinates for the jump phase landing were not used because the sand pit introduced additional complexity, resulting in poor pose landmarks estimated by GMP pose. Calculations

using incorrect pose landmarks would not produce useful metrics; therefore, the effective distance was deemed to be more suitable for computing the jump distance.

Phase ratios:

$$phase\ ratio_p = \frac{distance_p}{effective\ distance} \quad \text{(Eq. 4.21)}$$

where $distance_p$ is the phase distance, with the possible phase values of hop, step, or jump

Horizontal and vertical COM velocity: The velocities were calculated by considering the last full foot ground contacts before each jump phase take-off. Limitations of this approach are discussed in Section 6: Discussion and Section 7: Future Work. To compute the velocities, differences in the COM coordinates in 3D real-world space between the final consecutive full ground contact frames for each phase were considered (Equations 4.22 and 4.23). The COM data for each frame had been previously calculated and saved in the SQLite database, as described in Section 4.3.5.

$$\Delta\ COM_x = COM_x(i) - \ COM_x(i-1) \quad \text{(Eq. 4.22)}$$

$$\Delta\ COM_z = COM_z(i) - \ COM_z(i-1) \quad \text{(Eq. 4.23)}$$

$\Delta\ COM_x$ and $\Delta\ COM_z$ represent the difference in the COM's x (horizontal), and z (vertical) coordinates between the last consecutive full ground contact frames. These differences were calculated for each phase. Next, the difference in frame numbers between the ground contact frames was calculated using Equation 4.24, and subsequently, the difference in time was computed by dividing by the frame rate, as shown in Equation 4.25.

$$\Delta\ frame\ numbers = frame\ number(i) - \ frame\ number\ (i-1) \quad \text{(Eq. 4.24)}$$

$$\Delta\ t = \frac{\Delta\ frame\ numbers}{frame\ rate} \quad \text{(Eq. 4.25)}$$

Where $\Delta\ frame\ numbers$ represents the difference in frame numbers between consecutive frames, Δt represents the time difference between consecutive frames, and the frame rate is the video frame rate. Finally, the horizontal and vertical COM velocity was estimated using Equations 4.26 and 4.27.

$$horizontal\ COM\ velocity = \frac{\Delta COM_x}{\Delta t} \quad \text{(Eq. 4.26)}$$

$$vertical\ COM\ velocity = \frac{\Delta COM_y}{\Delta t} \quad \text{(Eq. 4.27)}$$

Change in horizontal and vertical COM velocity: The change in horizontal and vertical COM velocity was calculated between the hop and step phases, and the step and jump phases using Equations 4.28 and 4.29.

$$\Delta\ horizontal\ COM\ velocity_{hop\text{-}step} = step\ COM_x - hop\ COM_x \quad \text{(Eq. 4.28)}$$

$$\Delta\ horizontal\ COM\ velocity_{step\text{-}jump} = jump\ COM_x - step\ COM_x \quad \text{(Eq. 4.29)}$$

Where $\Delta\ horizontal\ COM\ velocity_{hop\text{-}step}$ represents the change in horizontal velocity between the hop and step phases, and $\Delta\ horizontal\ COM\ velocity_{step\text{-}jump}$ represents the change in horizontal velocity between the step and jump phases.

$$\Delta\ vertical\ COM\ velocity_{hop\text{-}step} = step\ COM_z - hop\ COM_z \quad \text{(Eq. 4.30)}$$

$$\Delta\ vertical\ COM\ velocity_{step\text{-}jump} = jump\ COM_z - step\ COM_z \quad \text{(Eq. 4.31)}$$

Where $\Delta\ vertical\ COM\ velocity_{hop\text{-}step}$ represents the change in vertical velocity between the hop and step phases, and $\Delta\ vertical\ COM\ velocity_{step\text{-}jump}$ represents the change in vertical velocity between the step and jump phases.

4.4.4 Performance Metrics Summary

The triple jump performance metrics are summarized in Table 4.4 below.

Table 4.4: Summary of triple jump performance metrics, the units they are measured in, and their definitions. Performance metrics and definitions adapted from [6], [7], [8], [9]. Units are as follows, metres (m), metres per second (m/s), percent (%), change in metres per second (Δ m/s), seconds (s), and degrees (°).

Performance Metric	**Units**	**Definition**
Official distance	m	The official distance measured during data collection.
Ground contact time	s	The time spent in contact with the ground during the support phases of the hop, step, and jump (calculated for each phase).
Flight time	s	The time spent in the air during the flight phase of the hop, step, and jump (calculated for each phase).
Knee angle	°	The angle between the thigh and lower leg; considered to be 180 degrees in standing position. Measured when it reached its minimum during ground contact of the hop, step, and jump.
Last step length	m	The length of the last approach step before the take-off board. Measured from the contact toe to the next contact toe.
Take-off loss / foul distance	m	The distance from the contact toe to the front edge of the take-off board. Considered as foul distance if the jump is a foul.
Effective distance	m	If the jump was not a foul, it is the take-off loss, plus the official distance. If the jump was a foul, the foul distance is subtracted from the official distance.
Phase distances	m	The length of the hop, step, and jump. Distances are measured from the contact toe in each phase to the next contact toe.
Phase ratios	%	The percentage length of the hop, step, and jump relative to the effective distance.
Horizontal velocity	m/s	The participant's horizontal (anteroposterior direction) COM velocity in their final ground contacts before the take-off of the hop, step, and jump (calculated for each phase).
Change in horizontal velocity	Δ m/s	The difference between the horizontal velocity of the hop and step, and of the step and jump.
Vertical velocity	m/s	The participant's vertical COM velocity in their final ground contacts before the take-off of the hop, step, and jump (calculated for each phase).
Change in vertical velocity	Δ m/s	The difference between the vertical velocity of the hop and step, and of the step and jump.

4.4.5 Participant Skill Levels

To group participants by skill level, their personal best triple jump distance was used. This approach is a relative measure of skill level considering only athletes participating in the study. Skill level was grouped by sex and split into thirds, or five athletes per group for males and females. The bottom third were considered as novices, the middle third intermediate, and the top third advanced. Two participants did not have a personal best as they were new to triple jump; they were assigned to the novice skill level category. The personal best ranges defining these categories are presented in Table 4.5.

Table 4.5: Novice, intermediate, and advanced skill level triple jump distance ranges for male and female participants. Categories were defined by athlete personal bests and separated into ranges relative to all participants. The n/a value represents participants who had not yet competed in a triple jump competition and, therefore, did not have a personal best.

Sex	Novice Range (Minimum, Maximum)	Intermediate Range (Minimum, Maximum)	Advanced Range (Minimum, Maximum)
Female	(n/a, 9.83) metres	(10.19, 10.85) metres	(11.11, 12.06) metres
Male	(n/a, 12.89) metres	(12.91, 13.23) metres	(13.96, 14.86) metres

4.5 Statistics

Statistics were computed for quantitative metrics. For the homography transformation, this involved computing the median, 25th percentile, 75th percentile, and 95th percentile reprojection error for each facility, as well as the statistics across all locations. The same set of reprojection error statistics was computed for both the videos recorded with the PIXEM 2 system and those recorded without it. These calculations were facilitated by the SQLite database. Since acceptable values for reprojection error could not be found in the literature, this error metric instead provided insight into whether there were notable differences between facilities, and whether the PIXEM 2 system impacted reprojection error.

Triple jump performance metric results were aggregated using SQL and Python scripts. All performance metric results were grouped by sex and skill level and calculated for each jump phase. All performance metrics were summarized in tables, grouped by sex and skill level. The mean and standard deviation for each homography-based performance metric were computed for each sex and skill level using an SQL script. The same summary tables were employed for performance metrics involving COM velocity. Additionally, COM velocity data were displayed as line charts to better observe trends and facilitate comparisons among participants of different skill levels.

To mitigate the impact of poor GMP pose detections, unreasonably good performance metric values were excluded using the World Athletics report data as a reference point. Outliers were identified using Equation 4.32, and the number of excluded values was tracked to assess the extent of data removal.

$$outlier = World\ Athletics\ average\ metric\ value + 2 \times World\ Athletics\ standard\ deviation\ metric\ value \quad \text{(Eq. 4.32)}$$

All reported triple jump performance metrics were compared to aggregated data from the 2017 and 2018 World Athletics triple jump reports [6], [7], [8], [9]. Relevant performance metrics from these reports were manually copied to an Excel spreadsheet. Excel functions were used to compute the mean and standard deviations for each reported performance metric for both males and females. Data were aggregated across all athletes for each sex to obtain a single average and standard deviation for each performance metric. For example, the average hop length for female athletes was calculated by averaging hop length results from all female jumpers in both 2017 and 2018. The same results were considered when computing the associated standard deviation. Summarizing the performance metrics from the World Athletics reports was critical as it offered a frame of reference for the study participant results. By hypothesizing how the study participants might compare to athletes in the World Athletics reports, a frame of reference is established, allowing for informed assumptions about the results.

Chapter 5: Results

5.1 Video Processing Results

In total, 31,456 frames from 154 videos were included in the analysis from the 192 recordings. The breakdown of the 38 excluded videos is shown in Table 5.1.

Table 5.1: Reasons for exclusion of videos from analyses, and number of impacted videos per reason.

Reason for Exclusion	Number of Impacted Videos
Invalid jumps	17
Pose detection errors	11
Researcher errors	6
Unusable footage	4
Total	38

Invalid jumps included incomplete jumps and incorrect execution of triple jump phases. Pose detection errors involved six videos where GMP pose detection failed to detect any landmarks for ground contact frames in each triple jump phase. Further, five videos had erroneous GMP pose detections at multiple ground contact frames, preventing the calculation of any performance metrics. Importantly, an additional subset of videos could not be used for certain performance metrics due to GMP pose detection errors (presented in Section 5.4.1). Table 5.1 only specifies videos that were completely unusable due to substantial GMP pose detection errors. Researcher errors consisted of failure to manually measure the jump distance in a valid attempt or an error in configuring the PIXEM 2 system that led to missing the video capture of a jump attempt. Unusable footage refers to videos where non-participants blocked the participant for multiple frames despite efforts to avoid these scenarios. The occluded frames prevented GMP pose landmark detection from producing pose estimates. One participant had no usable videos due to a combination of the aforementioned issues; approximately 80% of the videos collected were used in the analyses.

5.2 MediaPipe Pose Landmarks Validation

The validation of GMP object detection and pose landmark results was done qualitatively for every frame of every video using both the main Python processing script and the visualization tool described in Appendix B. Of the 31,456 frames analyzed across all videos, 6,340 frames, or approximately 20% of all frames, required manual redrawing of bounding

boxes. After applying landmark gap filling and smoothing, all frames were assessed qualitatively again using the custom visualization script, enabling the GMP pixel and GMP world coordinates to be visualized. Figure 5.1 shows the GMP pixel coordinates overlaid on a participant's video, with the participant's head redacted, while Figure 5.2 displays GMP world coordinates for the same frames. The landmarks in Figure 5.1 are intentionally enlarged to preserve the privacy of the participant. Both figures present the coordinates for a subset of frames, beginning the: last step before take-off, the hop phase take-off, the step phase take-off, and the jump phase take-off. Importantly, note that the x and y axes in Figure 5.2 do not change since the GMP world coordinates are relative to the participant's hip centre and provide no ability to discern whether the participant is moving forward.

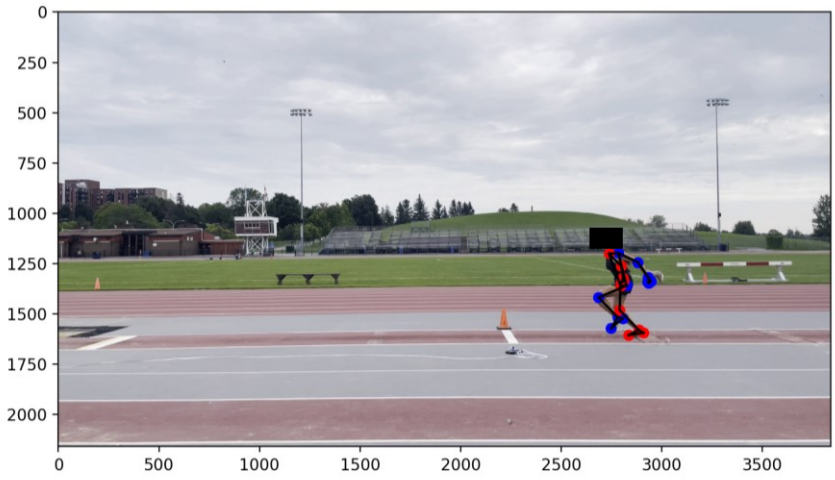

(a) Beginning the last step before take-off

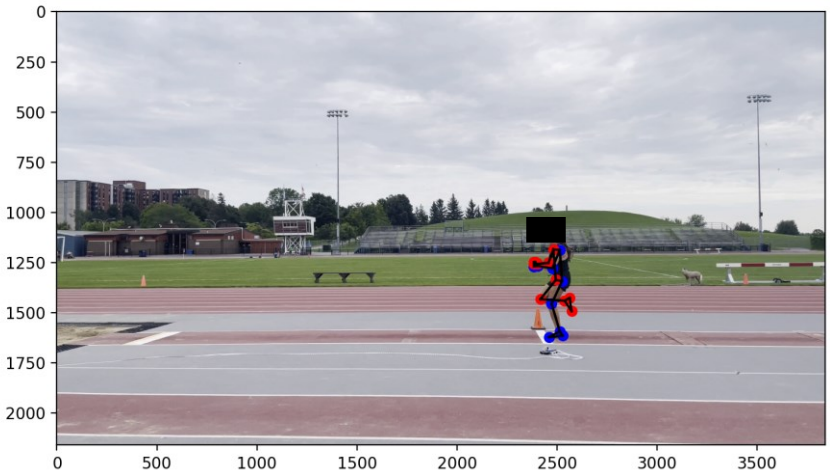

(b) Beginning the hop phase take-off

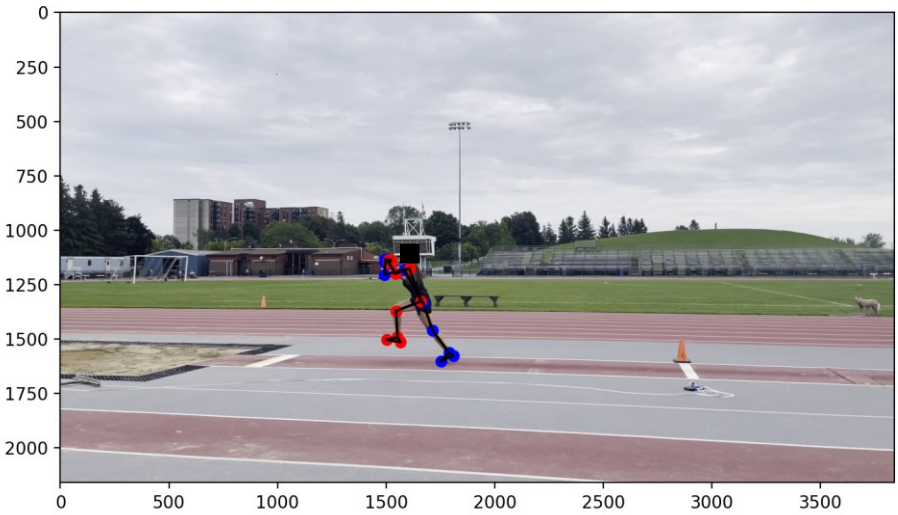

(c) Beginning the step phase take-off

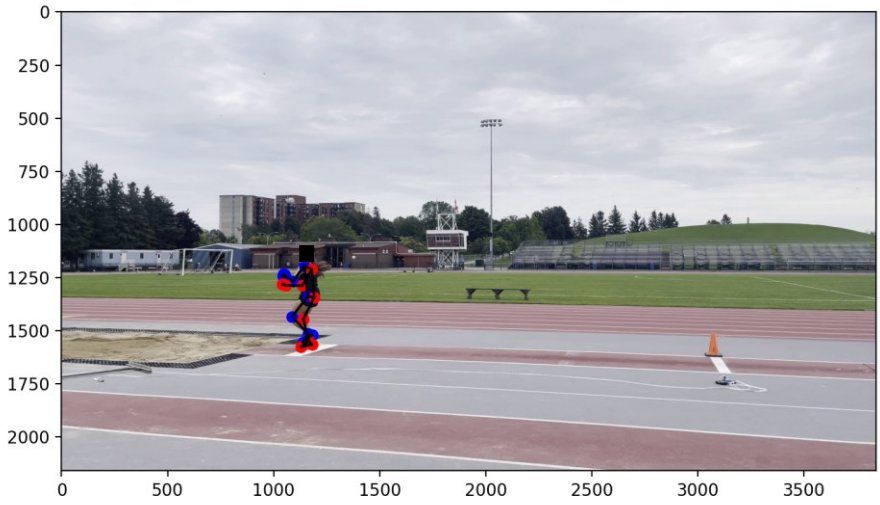

(d) Beginning the jump phase take-off

Figure 5.1: Google MediaPipe pose 2D pixel coordinates overlaid on a participant video for a subset of ground contact frames. Red circles represent right limb landmarks, and blue circles represent left limb landmarks. Plot units are in pixels. Landmarks are enlarged and the participant's head is redacted to preserve participant privacy.

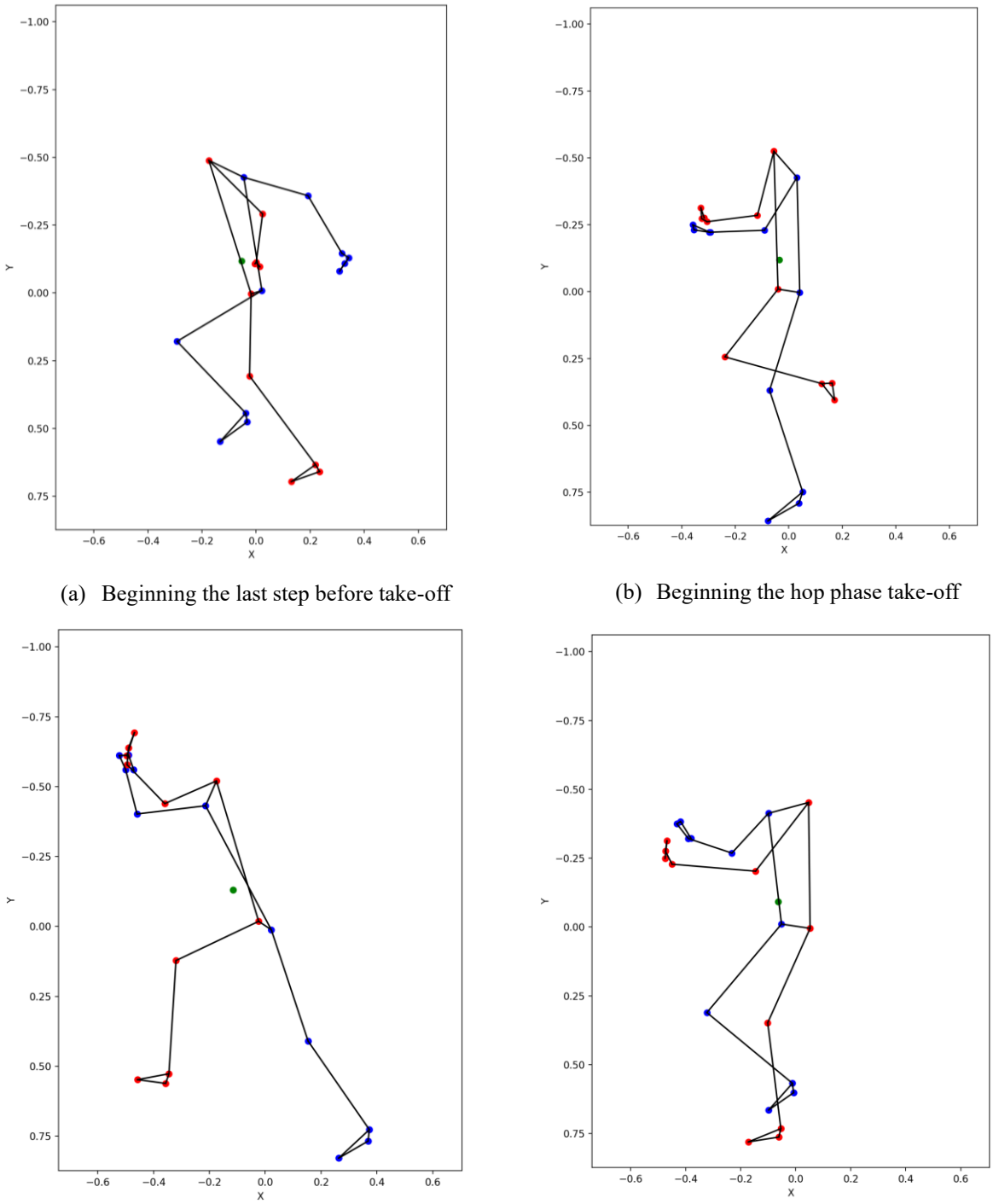

(a) Beginning the last step before take-off

(b) Beginning the hop phase take-off

(c) Beginning the step phase take-off

(d) Beginning the jump phase take-off

Figure 5.2: Google MediaPipe pose 3D world coordinates for a subset of ground contact frames. Red dots represent right limb landmarks, and blue dots represent left limb landmarks. Plots are unitless as Google MediaPipe pose does not provide any units for their world coordinates. The green dot represents the participant's estimated centre of mass.

5.3 Homography Validation

5.3.1 Qualitative Homography Validation

All ground contact frames of participant videos were assessed visually to validate the pose landmarks in real-world coordinates following the homography transformation using the visualization tool described in Appendix B. This visualization tool enabled the display of reprojected landmarks in pixel space overlaid on the original video, and the simultaneous display of 3D real-world coordinates after homography transformation. Figure 5.3 presents an example of the 3D real-world coordinates plotted at select ground contact frames – beginning the: last step before take-off, the hop phase take-off, the step phase take-off, and the jump phase take-off. The participant in the figure used the 7-metre take-off board for their triple jump attempt.

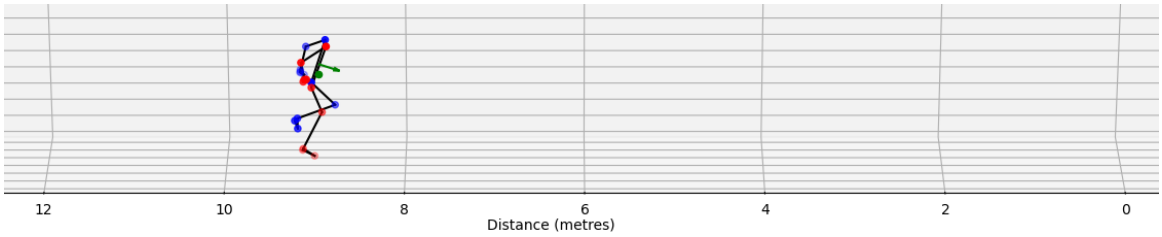

(a) Beginning the last step before take-off

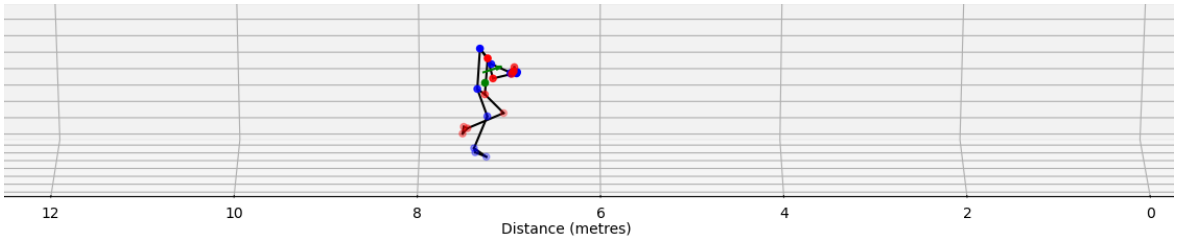

(b) Beginning the hop phase take-off

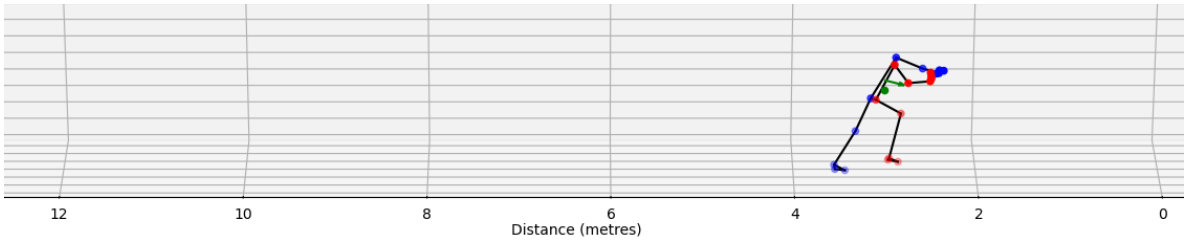

(c) Beginning the step phase take-off

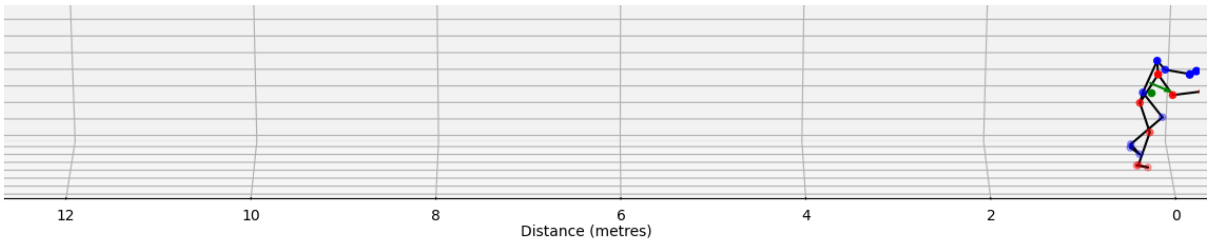

(d) Beginning the jump phase take-off

Figure 5.3: Real-world pose landmark coordinates plotted for validation, showing take-off points for all triple jump phases. This participant jumped from the 7-metre board, and 0-metres represents the edge of the sand pit. Red dots represent right limb landmarks, and blue dots represent left limb landmarks. The green line indicates the direction of travel, and the green dot denotes the participant's estimated centre of mass.

5.3.2 Quantitative Homography Validation

The median reprojection error in pixels following the homography transformation was 99.9 across all facilities, considering only ground contact frames. The overall 25th percentile was 60.5, the 75th percentile was 201.3, and the 95th percentile was 4120.1. The reprojection error statistics per facility are presented in Table 5.2 to investigate whether there were any notable differences between data collection locations.

Table 5.2: Median, 25th, 75th, and 95th percentile of the reprojection error in pixels from the homography transformation per facility, and across all facilities.

Facility	Median Reprojection Error	25th Percentile	75th Percentile	95th Percentile
Terry Fox Athletic Facility	103.0	61.3	179.4	1518.8
Pavillon d'Education Physique et Sport	181.9	99.0	489.4	9135.2
Gryphon Fieldhouse	235.2	165.1	310.6	706.9
Toronto Track and Field Centre	68.3	51.6	111.2	649.9
All facilities	99.9	60.5	201.3	4120.1

From Table 5.2, the TTFC location demonstrated the lowest median reprojection error of all facilities, followed by TFAF, PEPS, and Gryphon Fieldhouse, in order of increasing error. PEPS had the highest 95th percentile reprojection error, suggesting that some frames had very high reprojection errors, leading to extreme outliers. This is likely due to a high number of incorrect pose detections, which impacted the homography transformation, and therefore the reprojection error.

Table 5.3 summarizes the reprojection error statistics for videos recorded with the PIXEM 2 automatic tracking system compared to those recorded without it.

Table 5.3: Median, 25th, 75th, and 95th percentile of the reprojection error in pixels from the homography transformation for videos filmed with and without the PIXEM 2 automatic tracking system.

Equipment Used	Median Reprojection Error	25th Percentile	75th Percentile	95th Percentile
PIXEM 2 System	85.6	56.4	196.8	8615.6
No PIXEM 2 System	120.5	74.5	206.9	1084.8

The PIXEM 2 system produced lower reprojection errors across all metrics, apart from the 95th percentile. This finding may indicate that a small subset of the data had extremely large reprojection errors, likely attributable to a high number of incorrect pose detections, as previously mentioned. It is important to note that the PIXEM 2 system was used to record videos for nineteen participants, whereas videos were manually recorded (no PIXEM 2 system) for eleven participants. The imbalance in participants in each category could skew reprojection error results.

5.4 Performance Metrics Results

5.4.1 Additional Video Exclusions

Video-based and MediaPipe-based metrics were calculated for all videos. Due to limitations of the GMP pose detection (discussed in Section 5.1), homography-based metrics could not be calculated for all videos. Poor GMP pose foot detection resulted in inaccurate homography transformations, leading to unreasonable values for some performance metrics. Table 5.4 presents videos excluded for each homography-based performance metric.

Table 5.4: Excluded videos for homography-based performance metrics due to poor Google MediaPipe pose detections. The counts may represent the same video that was excluded across multiple performance metrics.

Performance Metric	Number of Excluded Videos	Percentage of Total Videos
Last step length	10	6.5%
Take-off loss or foul distance	5	3.2%
Effective distance	6	3.9%
Phase ratios	10	6.5%
Hop horizontal COM velocity	25	16.2%
Step horizontal COM velocity	32	20.8%
Jump horizontal COM velocity	65	42.2%
Hop vertical COM velocity	9	5.8%
Step vertical COM velocity	4	2.6%
Jump vertical COM velocity	4	2.6%

The videos listed in Table 5.4 were programmatically excluded from the aggregations to prevent incorrect data from affecting the overall results. This was achieved using the approach outlined in Section 4.5: Statistics, where performance metric values exceeding the average plus two times the standard deviation of the World Athletics report data were removed.

5.4.2 Category A Performance Metrics: Video-Based

Table 5.5 and Table 5.6 present the mean ground contact time per triple jump phase and mean flight time per triple jump phase, respectively. The World Athletics metrics are also summarized in both tables for comparison purposes.

Table 5.5: Mean and standard deviation (SD) of ground contact times in seconds for the hop, step, and jump phases, grouped by sex and skill level. World Athletics data summarized from [6], [7], [8], [9].

Sex	Mean Ground Contact Time in Seconds (SD)				
	Phase	Novice	Intermediate	Advanced	World Athletics
Female	Hop	0.15 (0.01)	0.16 (0.00)	0.15 (0.01)	0.13 (0.01)
	Step	0.20 (0.01)	0.19 (0.02)	0.19 (0.02)	0.16 (0.01)
	Jump	0.20 (0.02)	0.21 (0.02)	0.18 (0.01)	0.17 (0.02)
Male	Hop	0.15 (0.01)	0.14 (0.01)	0.16 (0.02)	0.12 (0.01)
	Step	0.19 (0.01)	0.18 (0.01)	0.18 (0.02)	0.16 (0.02)
	Jump	0.20 (0.01)	0.19 (0.01)	0.20 (0.02)	0.18 (0.02)

In the study results, both the female and male participants generally demonstrated longer ground contact times compared to the world-class jumpers. Regardless of skill level, the ground contact length for participants increased at each jump phase, which reflects trends in the World Athletics report data.

Table 5.6: Mean and standard deviation (SD) of flight times in seconds for the hop, step, and jump phases, grouped by sex and skill level. World Athletics data summarized from [6], [7], [8], [9].

Sex	Mean Flight Time in Seconds (SD)				
	Phase	**Novice**	**Intermediate**	**Advanced**	**World Athletics**
Female	Hop	0.39 (0.05)	0.42 (0.02)	0.42 (0.03)	0.51 (0.03)
	Step	0.20 (0.09)	0.25 (0.06)	0.30 (0.05)	0.37 (0.04)
	Jump	0.48 (0.04)	0.48 (0.03)	0.51 (0.04)	0.64 (0.04)
Male	Hop	0.43 (0.04)	0.46 (0.02)	0.44 (0.06)	0.53 (0.04)
	Step	0.30 (0.02)	0.28 (0.07)	0.38 (0.07)	0.46 (0.06)
	Jump	0.56 (0.03)	0.60 (0.04)	0.62 (0.02)	0.69 (0.06)

Both male and female participants across all skill levels exhibited shorter flight times compared to elite triple jumpers. However, like World Athletics athletes, all participants followed the same trend, with the jump phase having the longest flight time and the step phase the shortest.

It is evident that female participants generally had longer ground contact times and shorter flight times across all jump phases compared to male participants. This is particularly noticeable in jump phase flight time, where male participants demonstrated much longer flight times than the female participants. Further, advanced and intermediate male participants exhibited longer flight times for the step and flight phases compared to the novice male participants. The results are mixed for females, with some novice participants demonstrating ground contact and flight times similar to those of advanced participants.

5.4.3 Category B Performance Metrics: MediaPipe-Based

The minimum knee angles of the contact limb at each triple jump phase are summarized by participant sex and skill level in Table 5.7. The participant results are also compared to the World Athletics report data.

Table 5.7: Mean and standard deviation (SD) of minimum knee angles in degrees for the hop, step, and jump phases, grouped by sex and skill level. The knee angle is defined as the angle between the thigh and lower leg, measured as 180° in a standing position [6], [7], [8], [9]. World Athletics data summarized from [6], [7], [8], [9].

Sex	Mean Minimum Knee Angle in Degrees (SD)				
	Phase	Novice	Intermediate	Advanced	World Athletics
Female	Hop	156.1 (30.1)	163.0 (4.8)	157.8 (6.1)	138.6 (8.8)
	Step	159.8 (9.3)	153.3 (14.4)	161.0 (5.7)	133.6 (7.1)
	Jump	153.3 (8.2)	165.6 (7.5)	165.4 (5.1)	135.5 (9.0)
Male	Hop	140.4 (29.9)	137.8 (27.2)	144.0 (7.4)	136.3 (8.9)
	Step	154.1 (17.5)	153.6 (12.5)	154.1 (2.5)	128.0 (7.4)
	Jump	152.8 (16.1)	162.3 (10.0)	159.6 (5.6)	127.9 (7.5)

The female participants demonstrated larger angles compared to the elite female jumpers, indicating greater leg extension at the contact point of each phase. The male study participants exhibited similar knee angles in the hop phase, and larger knee angles in the step and jump phases compared to the elite male jumpers. Among the study participants, there is no discernible pattern in minimum knee angle across different skill levels.

5.4.4 Category C Performance Metrics: Homography-Based

The mean and standard deviation of the last step length in metres are summarized in Table 5.8, the take-off loss or foul distance in Table 5.9, measured and effective distance in Table 5.10, triple jump phase distances in Table 5.11, and phase ratios in Table 5.12. Results are grouped by participant sex and skill level. The relevant distances from World Athletics report data are also included in each table for comparison purposes.

Table 5.8: Mean and standard deviation (SD) of last step length in metres, grouped by sex and skill level. World Athletics data summarized from [6], [7], [8], [9].

Sex	Mean Last Step Length in Metres (SD)			
	Novice	Intermediate	Advanced	World Athletics
Female	1.99 (0.29)	2.33 (0.64)	1.98 (0.09)	2.16 (0.12)
Male	1.83 (0.31)	2.36 (0.71)	2.15 (0.41)	2.27 (0.12)

The novice and advanced female participants had very similar last step lengths, both of which were shorter than those of the intermediate participants. Similarly, the intermediate male

participants had the longest mean last step length across skill levels. Advanced male participants had larger last step lengths than their novice counterparts, on average. The intermediate female participants were closest to the elite female athletes in the World Athletics reports, though the latter exhibited longer mean last step lengths. The novice and advanced females demonstrated shorter last step lengths than the elite females. Similarly, the intermediate male athletes had a longer mean last step length compared to the male athletes in the World athletics data. In contrast, the novice and advanced males had shorter last step lengths than the elite males.

Table 5.9: Mean and standard deviation (SD) of take-off losses and fault distances in metres, grouped by sex, and skill level. World Athletics data summarized from [6], [7], [8], [9].

Sex	**Mean Take-off Losses and Foul Distances in Metres (SD)**				
	Distance Metric	**Novice**	**Intermediate**	**Advanced**	**World Athletics**
Female	Take-off loss	0.38 (0.23)	0.31 (0.12)	0.16 (0.06)	0.08 (0.07)
	Foul distance	0.39 (0.25)	0.36 (0.24)	0.14 (0.11)	n/a
Male	Take-off loss	0.46 (0.62)	0.50 (0.28)	0.51 (0.39)	0.09 (0.08)
	Foul distance	0.14 (0.10)	0.44 (0.43)	0.14 (0.10)	n/a

Novice female participants exhibited the greatest mean take-off losses and fault distances. These distances were reduced for intermediate female participants, and even further reduced for advanced female participants. A trend in take-off loss and foul distance for male participants across each skill level was less apparent. Comparing study participant and World Athletics data for mean take-off loss distance is unfair given the World Athletics reports were generated from triple jump data collected during a competition. Study participants were instructed to focus on completing each triple jump attempt, and not to focus on whether the jumps were fouls, so it is expected that take-off loss distances would be greater than those in the World Athletics reports. Given there was no disincentive to foul, and the study jumps occurred in a non-competition scenario, these values were primarily used to compute accurate effective distances and are included for completeness. Foul distances are not available in the World Athletics reports as data for fouled jumps were not included.

Table 5.10: Mean and standard deviation (SD) of measured distance and mean effective distance in metres, grouped by sex and skill level. World Athletics data summarized from [6], [7], [8], [9].

Sex	Mean Distance Metrics in Metres (SD)				
	Distance Metric	**Novice**	**Intermediate**	**Advanced**	**World Athletics**
Female	Measured distance	8.88 (0.73)	9.68 (0.47)	10.26 (0.85)	14.17 (0.34)
	Effective distance	9.03 (0.59)	9.84 (0.49)	10.27 (0.80)	14.26 (0.33)
Male	Measured distance	11.07 (0.89)	11.96 (0.48)	13.10 (0.59)	16.82 (0.56)
	Effective distance	11.34 (1.10)	12.37 (0.47)	12.80 (1.64)	16.90 (0.54)

For both sexes, the mean measured and effective distance increased with skill level. The male and female jump distance results from the World Athletics reports were both substantially further than the study participants. This is expected as the athletes included in these reports are among the best in the world and were competing at a track and field World Championships. The study participants varied in age and experience and were not competing during data collection, which likely influenced their jump distances.

Table 5.11: Mean and standard deviation (SD) of phase distances in metres for the hop, step, and jump, grouped by sex and skill level. World Athletics data summarized from [6], [7], [8], [9].

Sex	Mean Phase Distances in Metres (SD)				
	Phase	**Novice**	**Intermediate**	**Advanced**	**World Athletics**
Female	Hop	3.44 (0.61)	3.85 (0.39)	3.75 (0.26)	5.15 (0.22)
	Step	2.31 (0.73)	2.66 (0.39)	3.01 (0.29)	4.13 (0.25)
	Jump	3.28 (0.46)	3.22 (0.78)	3.51 (0.36)	4.98 (0.32)
Male	Hop	4.08 (0.47)	4.87 (0.37)	4.95 (0.36)	6.06 (0.22)
	Step	3.23 (0.42)	3.33 (0.50)	4.17 (0.21)	5.06 (0.37)
	Jump	3.88 (0.47)	4.16 (0.45)	4.04 (0.37)	5.80 (0.43)

The mean phase distances generally improved with participant skill level. Notably, the mean jump phase distance for novice female participants was greater than that of intermediate females. However, the larger standard deviation among intermediate females shows that some participants in this skill group achieved greater jump phase distances compared to the novice group. Similarly, the mean hop phase distance for intermediate female participants was further than that of the advanced females. For males, intermediate participants exhibited larger mean

distances across all phases compared to novice participants. Moreover, advanced male participants had further mean hop and step phase distances compared to intermediate participants, but shorter jump phase distances.

The phase distances from male and female athletes in the World Athletics reports are much greater than those observed by study participants. The elite athletes included in these reports jumped greater distances greater than those seen in the study, therefore, these results are expected. A more relevant comparison metric is the phase ratios, a relative measure of triple jump distance distribution, shown in Table 5.12.

Table 5.12: Mean and standard deviation (SD) of phase ratios in percentages for the hop, step, and jump phases, grouped by sex and skill level. World Athletics data summarized from [6], [7], [8], [9].

Sex	Mean Phase Ratios Percentages (SD)				
	Phase	**Novice**	**Intermediate**	**Advanced**	**World Athletics**
Female	Hop	38.3 (7.39)	39.1 (3.10)	36.6 (1.83)	36.1 (1.30)
	Step	25.4 (6.75)	29.1 (8.75)	29.3 (1.28)	29.0 (1.89)
	Jump	36.3 (4.06)	32.7 (8.04)	34.1 (1.47)	34.9 (1.76)
Male	Hop	36.3 (4.46)	39.4 (3.23)	37.6 (2.18)	35.8 (1.40)
	Step	28.5 (2.27)	26.9 (3.92)	31.7 (1.72)	29.9 (1.90)
	Jump	35.2 (4.18)	33.6 (2.97)	30.7 (2.43)	34.2 (2.10)

Female participants across all skill levels had similar hop phase ratios, with intermediate participants having the highest hop ratio. The step phase ratios of female participants were also similar between skill levels, with advanced participants slightly edging out intermediate participants with a mean ratio of 29.3±1.28%. Novice female participants exhibited the largest jump phase ratio and smallest step phase ratio. Notably, advanced females demonstrated the lowest standard deviations across all phases, implying higher levels of jump phase distribution consistency compared to novice and intermediate participants. For female participants of all skill levels, the phase ratios are similar to those produced by the female jumpers included in the World Athletics reports for all phases [6], [9].

There is similarity in phase ratios between the male study participants and the male jumpers included in the World Athletics reports [7], [8]. The hop phase ratio is slightly higher amongst male participants compared to the elite male athletes. Moreover, the step phase ratio of

novice and intermediate male participants is lower compared to the elite male jumpers, while the advanced participants demonstrate a slightly higher ratio for their step phase. This suggests the novice and intermediate male participants have relatively weaker step phases compared to the male athletes in the World Athletics report data and instead incorporate a larger hop phase in their triple jump technique.

Mean horizontal velocities for each triple jump phase are shown in Table 5.13 and mean vertical velocities for each phase are shown in Table 5.14. Both velocity metrics are measured in metres per second. The mean horizontal and vertical COM velocities at each phase are also visualized in Figures 5.4 – 5.7. Results are grouped by participant sex and skill level. It is important to reiterate that within the proposed framework, the horizontal and vertical COM velocities were calculated based on full foot ground contacts at each phase, whereas the World Athletics reports used the toe-off points during take-offs. Consequently, the reported participants' COM velocities are likely lower than if they were measured at the toe-off point. Nonetheless, using the World Athletics results as reference still offers valuable insight into trends for these performance metrics.

Table 5.13: Mean and standard deviation (SD) of horizontal COM velocities in metres per second for the hop, step, and jump phases, grouped by sex and skill level. World Athletics data summarized from [6], [7], [8], [9].

Sex	**Mean Horizontal COM Velocities in Metres per Second (SD)**				
	Phase	**Novice**	**Intermediate**	**Advanced**	**World Athletics**
Female	Hop	6.54 (1.02)	6.81 (1.05)	6.64 (1.04)	8.15 (0.31)
	Step	4.78 (2.49)	5.34 (1.86)	5.86 (1.37)	7.44 (0.28)
	Jump	4.24 (2.32)	4.30 (2.08)	3.85 (1.85)	6.23 (0.36)
Male	Hop	7.21 (0.871)	7.80 (1.33)	7.14 (1.89)	9.34 (0.32)
	Step	5.94 (2.02)	6.00 (2.07)	6.89 (1.39)	8.15 (0.44)
	Jump	5.11 (1.76)	5.42 (1.62)	5.27 (1.51)	6.80 (0.56)

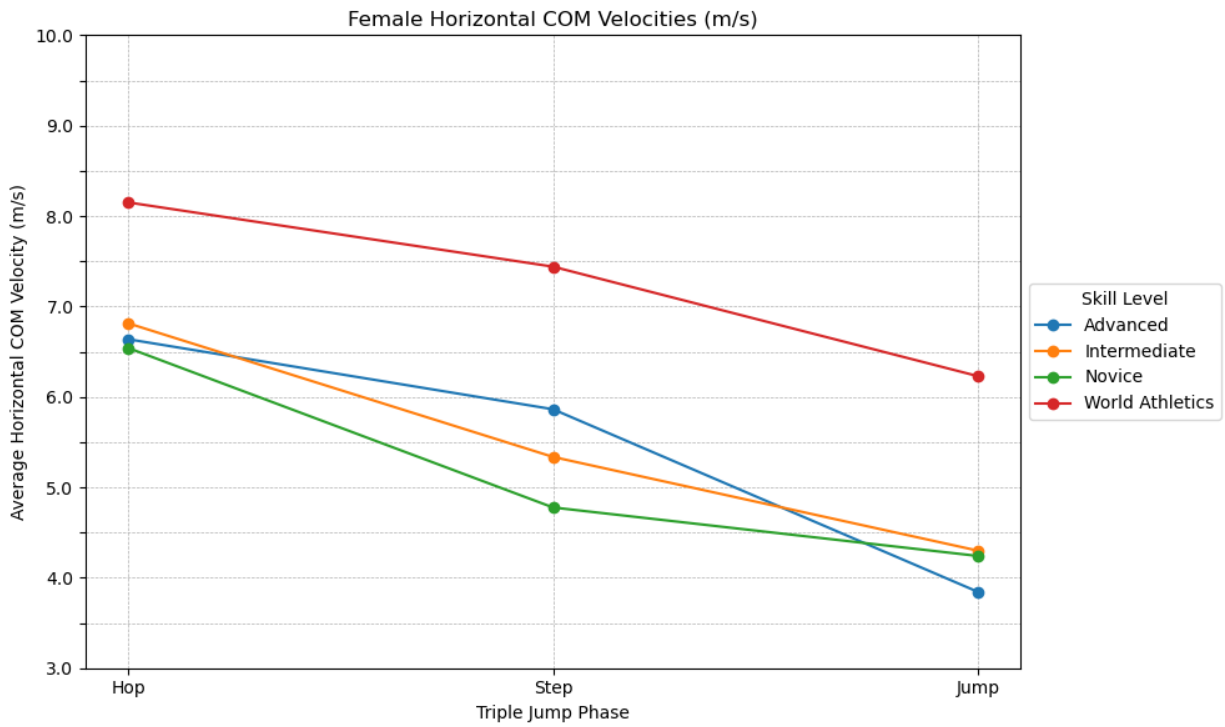

Figure 5.4: Horizontal COM velocities in metres per second (m/s) for the hop, step, and jump phases for female participants, grouped by skill level. World Athletics data summarized from [6], [9].

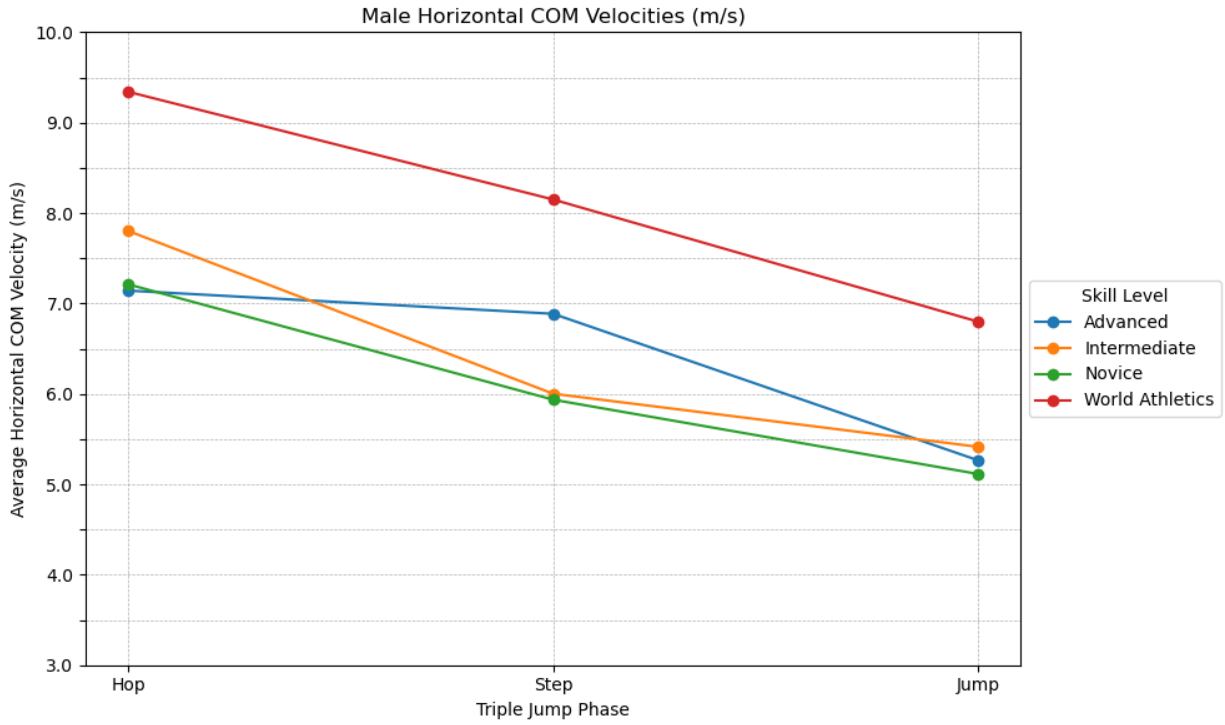

Figure 5.5: Horizontal COM velocities in metres per second (m/s) for the hop, step, and jump phases for male participants, grouped by skill level. World Athletics data summarized from [7], [8].

Table 5.14: Mean and standard deviation (SD) of COM vertical velocities in metres per second for the hop, step, and jump phases, grouped by sex and skill level. World Athletics data summarized from [6], [7], [8], [9].

Sex	Mean Vertical COM Velocities in Metres per Second (SD)				
	Phase	**Novice**	**Intermediate**	**Advanced**	**World Athletics**
Female	Hop	0.64 (0.66)	1.80 (2.40)	0.78 (0.49)	2.58 (0.21)
	Step	0.91 (0.56)	1.09 (0.74)	0.40 (0.34)	2.02 (0.25)
	Jump	0.93 (0.57)	0.83 (0.54)	0.78 (0.54)	2.68 (0.22)
Male	Hop	1.10 (0.901)	1.08 (0.73)	1.01 (0.70)	2.77 (0.27)
	Step	1.05 (1.20)	1.08 (0.75)	0.632 (0.54)	2.37 (0.39)
	Jump	0.80 (0.64)	1.21 (0.69)	1.09 (0.79)	2.87 (0.46)

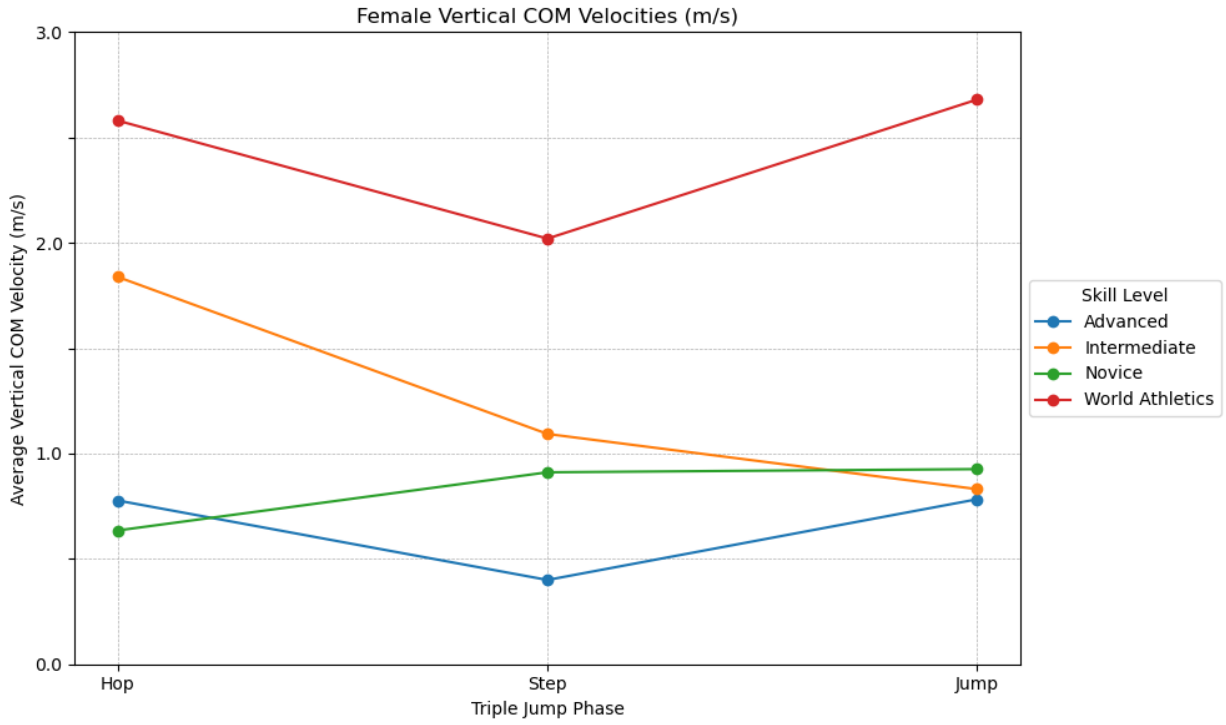

Figure 5.6: Vertical COM velocities in metres per second (m/s) for the hop, step, and jump phases for female participants, grouped by skill level. World Athletics data summarized from [6], [9].

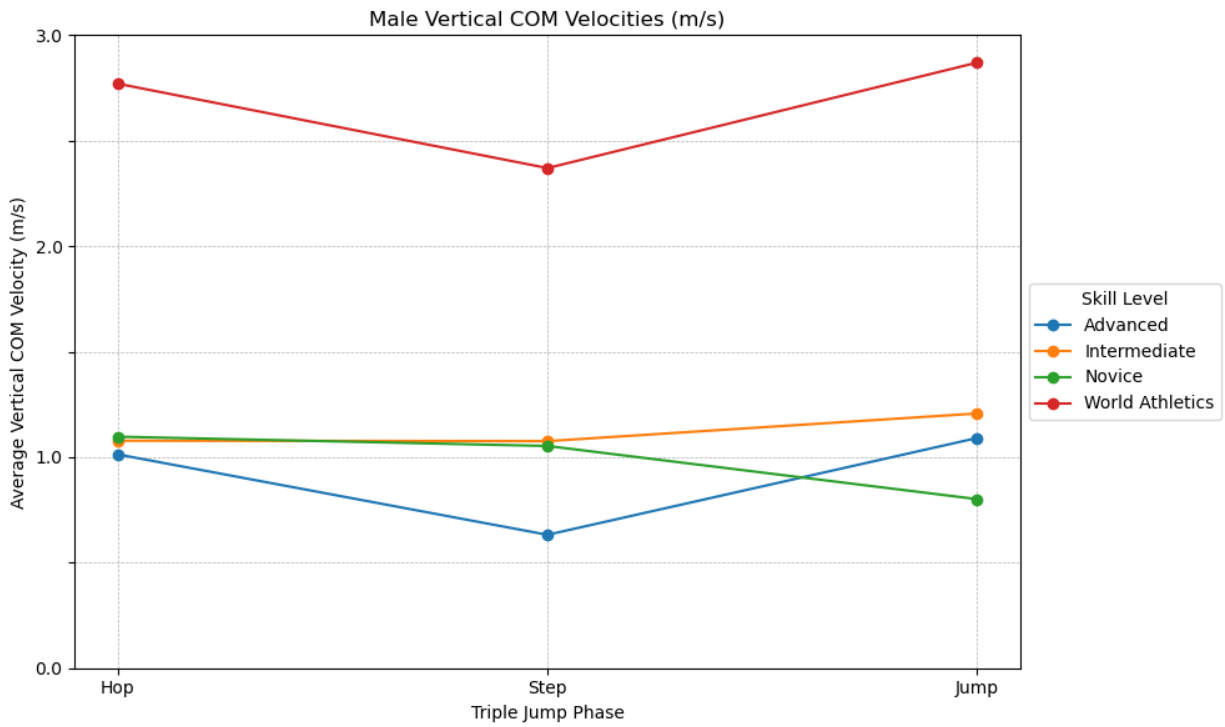

Figure 5.7: Vertical COM velocities in metres per second (m/s) for the hop, step, and jump phases for male participants, grouped by skill level. World Athletics data summarized from [7], [8].

From Tables 5.13 and 5.14, as well as Figures 5.4 – 5.7, it is evident that all participants exhibited a decrease in horizontal COM velocity trend similar to the World Athletics athletes, albeit with lower velocities. Novice participants of both sexes generally had slightly lower velocities than those of higher skill levels, with the biggest difference noticeable in the step phase. Advanced participants had demonstrably higher horizontal COM velocity during the step phase compared to the novice and intermediate participants. For both males and females, the World Athletics athletes exhibited a relatively smoother decrease in horizontal COM velocity at each phase and maintained higher velocities throughout the entire triple jump compared to the study participants.

While World Athletics athletes exhibited higher vertical COM velocities at each phase, the overall trend most closely resembled that demonstrated by the advanced study participants of both sexes. This observed trend shows a slight decrease in vertical COM velocity at the step phase, and an increase at the jump phase. In contrast, novice females increased their vertical COM velocity at the step phase and maintained it into the jump phase, whereas the vertical COM velocity decreased at each phase with the intermediate females. For the male participants, the

novice participants demonstrated a slightly decreasing vertical COM velocity as they progressed through the triple jump phases. The intermediate male participants instead demonstrated a slight increase in vertical COM velocity throughout each triple jump phase.

Following the computation of horizontal and vertical COM velocities at each phase, Tables 5.15 and 5.16 present the corresponding changes in these velocities. The World Athletics values are again included for reference.

Table 5.15: Changes in mean horizontal COM velocities in metres per second between the hop and step phases, and the step and jump phases. World Athletics data summarized from [6], [7], [8], [9].

Sex	Change in Mean Horizontal COM Velocities in Metres per Second				
	Phase	**Novice**	**Intermediate**	**Advanced**	**World Athletics**
Female	Hop-Step	-1.76	-1.48	-0.77	-0.71
	Step-Jump	-0.54	-1.04	-2.02	-1.21
Male	Hop-Step	-1.28	-1.80	-0.26	-1.19
	Step-Jump	-0.82	-0.59	-1.62	-1.35

Table 5.16: Changes in mean vertical COM velocities in metres per second between the hop and step phases, and the step and jump phases. World Athletics data summarized from [6], [7], [8], [9].

Sex	Change in Mean Vertical COM Velocities in Metres per Second				
	Phase	**Novice**	**Intermediate**	**Advanced**	**World Athletics**
Female	Hop-Step	0.28	-0.75	-0.38	-0.56
	Step-Jump	0.02	-0.26	0.38	0.66
Male	Hop-Step	-0.04	-0.001	-0.38	-0.40
	Step-Jump	-0.25	0.13	0.46	0.50

All participants demonstrated a decrease in horizontal COM velocity between the hop to step phase, and the step to jump phase. Both the male and female advanced participants exhibited a larger decrease between the step to jump phase compared to the hop to step phase. This aligns with the trend observed in the World Athletics report data. Notably, the novice and intermediate participants of both sexes demonstrated smaller decreases in horizontal COM velocity between the step to jump phase when compared to the hop to step phase.

The intermediate male participants, as well as the advanced male and female participants, exhibited a pattern similar to the World Athletics athletes, with a decrease in vertical COM velocity from the hop to step phase, followed by an increase from the step to jump phase. Conversely, the novice male participants saw a decrease in vertical COM velocity throughout the jump phases, while novice female participants showed an increase, both deviating from the trend observed in elite athletes.

Chapter 6: Discussion

6.1 Relevance and Interpretation

6.1.1 Video Processing

It was expected that not all participants would complete six valid jumps, as this number was chosen to simulate a competition scenario while balancing the physical demands of triple jump with the athletes' training programs. The loss of only 17 videos of 192 due to invalid jumps – less than 10% of the acquired data – is considered a positive outcome. Additionally, six videos were unusable due to researcher-controlled errors, an anticipated and reasonable outcome, especially given the manual measuring task involved in the data collection process. Filming participants without obstruction proved challenging, as is often the case at track and field facilities, where an unobstructed view of an athlete during a jump is not always guaranteed. The loss of only four videos due to non-participant obstruction did not create significant issues. Furthermore, given the uncertainty of GMP's performance in varied environments, it was expected that some footage would be unusable due to poor pose detections. Therefore, being able to retain approximately 80% of the data, including multiple attempts per participant, allowed for comprehensive analyses, and enabled the study objectives to be met.

6.1.2 Google MediaPipe Pose Landmark Detection

Analyzing GMP object and pose detection results frame-by-frame for each video using a custom Python script allowed for qualitative assessments of GMP, providing insights into the effectiveness of the open-source HPE solution. Although subjective, it could be clearly determined through visual observation whether GMP object detection identified an accurate bounding box for the participant, and whether the GMP pose detections were reasonably accurate. For example, it was evident when the GMP landmarks overlaid on the video did not match the limb position of the participant or when landmark switching occurred, with right and left landmarks being swapped. While accurate bounding box detections greatly improve pose detection results, they did not fully eliminate inaccuracies. Conclusive findings cannot be drawn from visual assessments alone, but anecdotal evidence was gathered that may inform future studies using GMP solutions.

The key aspects to consider for improving GMP object and pose detection include presence of background items or people, participant clothing contrast to the background scene, lighting conditions, and video blur. These factors are significant to performance, given the tendency of GMP object detection to misidentify background objects and people as participants as seen with items including chairs, boxes, benches, hurdles, and even individuals standing in the background. If these items or people overlapped with the participant in the 2D image, it was nearly impossible to isolate the participant in a bounding box. Moreover, GMP pose also seemed to be more effective when the participant's clothing strongly contrasted with the background. For example, a participant wearing a red shirt and black shorts jumping at a facility with a red track exhibited slightly worse GMP pose detection performance compared to a participant dressed in black at the same location. In one scenario, a person in the background wearing all black was more likely to be identified during the GMP object detection step than the participant in the red shirt. As a result, the bounding box had to be manually redrawn before the automatic detection correctly tracked the participant.

Lighting conditions were another factor affecting the accuracy of GMP pose detection results. Videos recorded at the indoor TTFC facility in North York had the lowest median reprojection error, followed by those recorded at the outdoor TFAF facility in Ottawa. However, some video frames from both locations showed poor pose detection results without clear cause. Notably, TFAF videos recorded during the day appeared to produce better results than those recorded at night, based on subjective assessments. One participant's videos recorded at night were completely unusable as no GMP pose landmarks were detected, perhaps due to the glare from the stadium lights. Indoor facilities posed different challenges, with dim lighting across all three locations leading to both the best and worst reprojection errors. It is hypothesized that the higher volume of videos at TTFC helped mitigate the effects of dim lighting. Moreover, indoor facilities provide the benefit of consistent lighting, eliminating variations due to weather or time of day.

The most significant factor believed to impact GMP pose detection quality is the extent to which the participant appeared blurry in a given frame, which is likely correlated with lighting conditions. For instance, a subjective evaluation showed that a video recorded on a bright, sunny day, had fewer blurry frames compared to one recorded at the same facility at night. From the

qualitative visual assessments, it appeared that many pose detection errors occurred when the participant's limb was blurred, making it challenging for GMP pose to identify the appropriate landmark positions. As smartphone cameras continue to improve, this issue could be mitigated by using a more recent model with a higher-quality camera, with further improvements expected in the future.

6.1.3 Homography Transformation

The accuracy of the homography transformation results was largely influenced by the performance of GMP pose detection, particularly the accuracy of foot landmark detection as the foot served as the anchor point for the transformation. Based on qualitative visual assessments, it was noted that if the GMP pose detection results were reasonably accurate, so was the homography transformation. Therefore, to improve the performance of the homography transformation, it is recommended that the GMP pose detection performance should first be improved, discussed further in Section 7: Future Work.

It is worth noting that the 2D track template and manual key point labelling approach for homography appeared to be effective. Since the key point labels were relative to the facility, they were unaffected by GMP pose detection results. This suggests that homography techniques could be appropriate for similar sports performance analyses in uncontrolled environments. However, to reduce the need for human intervention and expedite the development process, it is recommended that an automated approach to labelling, as discussed in Section 7: Future Work, is explored.

The reprojection error, which served as a quantitative measure to investigate homography transformation performance, showcased surprising insights. The TTFC location had the lowest median reprojection error, despite the facility constraints and dim lighting. The second lowest median reprojection error was seen at the TFAF. Videos recorded during the daytime at this outdoor facility appeared to enable good GMP pose detection performance, but the error likely increased due to the videos recorded at night, noted as having poor performance during the subjective assessments. Next, PEPS showcased a median reprojection error nearly double that observed at TFAF, and the Gryphon Fieldhouse was much higher than all other locations. It is hypothesized that since the majority of participants were recorded at the TTFC (12 participants)

and TFAF (10 participants), this may have positively impacted the summary reprojection error statistics for these facilities.

Regarding the impact of using the PIXEM 2 automatic tracking system versus manually recording videos, the median, 25th percentile, and 75th percentile reprojection errors were lower with the PIXEM 2 system. However, this could either be due to the PIXEM 2 producing consistently higher quality videos or simply because a larger number of videos were recorded with the system. The latter seems more likely, as the TFAF location had the second-lowest reprojection error among all facilities, even though only one of ten participants from this location used the PIXEM 2 system. These findings suggest that reprojection error may decrease as the dataset size – here, the number of videos – increases, though this relationship cannot be definitively confirmed. Based on both the quantitative data and subjective visual assessments, it appears that while the PIXEM 2 automated tracking system offers advantages in ensuring consistent video capture as it is less susceptible to human error, it is not essential within the proposed framework; manually recorded videos are shown to be sufficiently reliable.

6.1.4 Performance Metrics

The performance metrics were computed as a means to demonstrate that the proposed framework produces reasonable results. The metrics were compared to the 2017 and 2018 World Athletics report data to provide a benchmark for elite athlete performance, and a frame of reference for the study results [6], [7], [8], [9]. The aggregated performance metrics revealed trends that provided valuable insights into triple jump performance. It is believed that within the proposed framework, aggregated performance metrics provide greater value than reviewing individual performance metric values.

When interpreting the performance metrics results, it is essential to consider the number of excluded videos for each metric. While most performance metrics included over 90% of the valid videos, the horizontal COM velocities at each phase presented challenges. In particular, only 57.8% of the videos were included in the horizontal COM velocity at the jump phase compared to the 83.8% and 79.2% included for the horizontal COM velocity of the hop and step phases, respectively. This reduction in usable data likely results from the participant's increasing angle relative to the camera as they perform each triple jump phase. Further, COM velocity

calculations rely on GMP pose landmark mappings to body segments in Dempster's anthropometric table [107], which are approximations, the accuracy of the GMP pose detections, and the subsequent homography transformation. Given the multi-step process for velocity calculations, minor errors at any step can lead to significant inaccuracies. For example, if the GMP pose foot landmark detection slightly overestimates or underestimates foot size between consecutive ground contact frames, combined with the iPhone 12 camera's low frame rate (30 Hz), it can produce grossly inaccurate velocity measurements. Enhancing the accuracy of GMP pose foot landmark detection is therefore a key focus area, essential for achieving more precise performance metrics. This is further discussed in Section 7: Future Work.

6.1.4.1 *Category A Performance Metrics: Video-Based*

Ground contact time and *flight time* were limited by the frame rate of the iPhone video camera (30 Hz). Nonetheless, compared to the World Athletics report data, the participants generally had longer ground contact times and shorter flight times compared to elite athletes of the same sex. This finding is encouraging as shorter ground contact times and longer flight times are associated with further triple jump distances, and elite athletes included in the World Athletics reports jump significantly farther than study participants. Notably, the study participants, especially those of the advanced skill level, had only slightly longer ground contact times than the elite jumpers, but relatively shorter flight times. This underscores the complexity of the triple jump, where multiple performance metrics must be considered collectively to holistically assess performance. The computed ground contact and flight times are realistic, given the World Athletics data as reference, albeit with low precision.

6.1.4.2 *Category B Performance Metrics: MediaPipe-Based*

Minimum knee angles of the contact limb at each phase also exhibited promising results as the ranges approached or overlapped those of elite triple jumpers. Since the relationship between triple jump performance and minimum knee angles is not evident, an overlapping range was hypothesized. Unexpectedly, the female participants generally demonstrated larger minimum angles compared to the male participants. It is not clear why this occurred, though it should be noted that the male participant's minimum knee angles were closer to the elite athlete knee angles than the female participants.

Several factors should be considered to explain the observed differences. The low frame rate of the iPhone camera (30 Hz) likely reduces the precision of the minimum knee angles compared to the World Athletics reports, potentially leading to inaccuracies in the knee angle measurements in this study. Additionally, the World Athletics reports did not use the GMP pose landmarker model for calculating minimum knee angles, which may contribute to discrepancies when comparing the results. Nonetheless, GMP pose was able to produce reasonable knee angle results, indicating its suitability for computing joint angles. Future research should explore the accuracy of the joint angle calculations, validated against the "gold standard," marker-based motion capture (discussed in Section 7: Future Work).

6.1.4.3 *Category C Performance Metrics: Homography-Based*

The *last step lengths* of the participants across all skill levels were generally comparable to those measured from elite jumpers, with all being close to 2-metres. While this may initially seem counter-intuitive, this result is plausible. From the researcher's experience as a triple jump coach and athlete, it is common for novice athletes to overstride as they try to reach the take-off board, thereby lengthening their last step. The intermediate and advanced participants, having more experience, are likely to have been coached to shorten their final stride. Additionally, stride length is influenced by an individual's height, and because most novice participants were younger and shorter than their intermediate and advanced counterparts, a 2-metre last step would be relatively longer for them. Further, it is reasonable to assume that many elite triple jumpers are tall, so a 2-metre last step would be a relatively shorter stride compared to the study participants. This finding may indicate the importance of shortening the last step before take-off to improve jump distance.

The *take-off loss* or *foul distance* is less noteworthy for discussion since the participant jumps were not measured during a competition. Due to the nature of data collection, participants were instructed to not concern themselves with fouls. Instead, their main objective was to complete the entire triple jump on each attempt. This likely contributed to the larger take-off loss distances observed among participants compared to those of World Athletics athletes. Additionally, foul distances were not reported in the World Athletics data, limiting comparative analysis. It would be valuable to apply the proposed methodology in a competition setting to

explore whether elite athletes are generally more effective at minimizing take-off loss than non-elite athletes.

The *hop, step, and jump phase distances,* as well as *effective and measured distances* revealed notable differences between jumpers of varying skill levels, particularly among male participants. The advanced male participants, for instance, demonstrated a mean hop phase distance of 4.95±0.36 metres, compared to 4.08±0.47 metres for novice males. The results align with expectations, as participants with longer effective and measured distances, due to higher skill levels, naturally achieved longer phase distances. Among female participants, the differences were less pronounced, particularly in the hop phase, where novice females achieved 3.44±0.61 metres, and intermediate females 3.85±0.39 metres, which was further than the advanced female mean hop phase distance at 3.75±0.26 metres. However, male and female advanced participants exhibited further step and jump phases compared to their novice and intermediate counterparts, with the step phase being particularly strong. This is understandable, as in the researcher's experience as a triple jump coach and athlete, the step phase is typically the most challenging for beginners but tends to improve with training and experience.

While it is unsurprising that the effective and measured distances, as well as phase distances, are substantially lower than those of elite jumpers in the World Athletics reports, this comparison highlights the vast difference in performance levels. Given the obvious disparity in raw distances, such comparisons are less meaningful; instead, the focus should shift to the phase ratios, which offer more nuanced insights.

Triple jump *phase ratios* across both male and female participants and all skill levels were generally consistent with those observed in elite athletes. In fact, the phase ratios aligned with both the World Athletics reports and the theoretical economic distributions from the literature (36-37% for the hop, 29-30% for the step, and 33-34% for the jump phase) [42], [45]. Notably, female participants across all skill levels exhibited higher average hop phase ratios than elite jumpers. For the step phase, intermediate and advanced participants closely matched the elite women, while novice females had the lowest step phase ratio. Interestingly, novice females showed the highest jump phase ratio, whereas intermediate and advanced females had slightly lower jump phase ratios compared to the elite women. Among the female participants, the phase ratios of the advanced group most closely resembled those of elite female jumpers, suggesting a

greater similarity in technique as skill increases. This finding also indicates that novice female athletes in the study exhibited relatively weaker step phases, compensating with larger hop and jump phases, a pattern commonly observed subjectively in beginners.

Similarly, male participants showed a higher average hop phase ratio than their elite counterparts. The step phase ratio was lower for novice and intermediate males, but higher for advanced males compared to the World Athletics male athletes. Novice males exhibited a larger jump phase ratio than elite male jumpers, while intermediate and advanced males had smaller jump phase ratios. The intermediate male participants displayed the highest hop phase ratio, likely compensating for their lower step phase ratio. Surprisingly, advanced male athletes had the lowest jump phase ratio, but the highest step phase ratio, even surpassing that of World Athletics jumpers. This anomaly could be attributed to two male participants with particularly strong step phases, which may have skewed the data. Unlike the female athletes, where advanced participants closely matched elite trends, the male participants did not consistently align with World Athletics data within a skill level group.

In summary, since phase ratios are a relative measure, they were expected to align closely with established values. The phase ratio results show a promising similarity to the phase ratios observed in the World Athletics data and those documented in previous literature. The alignment of the computed phase ratios with established benchmarks supports the validity of the study's methodology for evaluating this triple jump performance metric.

For all velocity metrics, due to the difference in measurement methodology compared to World Athletics data, the values themselves should not be compared directly. Instead, the patterns observed in the results can be compared and used to inform triple jump technique evaluation as well as potential future work in this area.

Horizontal COM velocity at each phase exhibited by the study participants was lower than that of elite athletes in the World Athletics reports, as expected. It is promising to observe that participants of both sexes across all skill levels had a similar trend to the elite athletes in that their horizontal COM velocity decreased at each phase, aligning with what has been noted in prior research [3]. Within the participant skill levels, the advanced group for both sexes exhibited larger horizontal COM velocities in the step phase compared to their intermediate and novice counterparts. The differences in horizontal COM velocities at the hop and jump phases were less

significant among skill levels. This suggests that within the study participants, minimizing horizontal velocity loss from the hop to step phase was one technique component that led to further jump distances, separating the advanced participants from the novice and intermediate. From the World Athletics reports, the male and female elite athletes both demonstrated a nearly linear decreasing trend in horizontal COM velocity across all phases. Unexpectedly, the novice male participants produced a trend line most similar to the elite athletes, though at much lower velocities. The reason for this is unclear and is not believed to be significant.

It is critical to acknowledge the challenges in computing the horizontal COM velocities, as many videos were excluded from these calculations due to unreasonable velocity results. As previously discussed, to improve the precision of these values, the primary focus should be on improving the GMP pose landmark detection results, discussed in more depth in Section 7: Future Work. Despite the issues in obtaining the horizontal COM velocity metrics for all participants, the overall trends observed are promising as they largely align with expected patterns. This further reinforces the utility of the performance metrics at an aggregated level rather than for any individual triple jump attempt.

Changes in horizontal COM velocity showed a decreasing trend within World Athletics athletes, with greater loss of horizontal COM velocity in the step to jump phases compared to the hop to step phases. Interestingly, advanced study participants of both sexes exhibited a similar trend, though with a steeper decline. Meanwhile, novice and intermediate participants of both sexes surprisingly exhibited smaller decreases in horizontal COM velocity in the step to jump phases compared to the hop to step phases. It is hypothesized that given these participants have relatively weaker step phases compared to the advanced participants and World Athletics athletes, they are able to maintain a relatively higher horizontal COM velocity. This suggests that while a decrease in horizontal COM velocity is inevitable and minimizing the loss may be associated with further jump distances, a strong step phase was an important factor to achieve greater jump distances within the study participants.

Vertical COM velocity at each phase revealed intriguing patterns. Although the vertical COM velocities of study participants were lower than those of the World Athletics athletes, the trend line for advanced participants most closely mirrored that of the elite jumpers. Both the advanced participants and the elite athletes experienced a drop in vertical COM velocity at the

step phase take-off but managed to increase it during the jump phase take-off. In contrast, intermediate female participants and novice male participants showed a decline in vertical COM velocity throughout the triple jump phases. Meanwhile, novice female participants and intermediate male participants increased their vertical COM velocity at each jump phase. These results suggest that a drop in vertical COM velocity at the step phase take-off is acceptable, provided that it is increased at the jump phase take-off. Further, it can be inferred that minimizing horizontal COM velocity loss while effectively managing vertical COM velocity is essential in maximizing the triple jump distance, as demonstrated by World Athletics elite athletes.

Changes in vertical COM velocity were most similar among advanced participants of both sexes, intermediate male athletes, and World Athletics athletes, all of whom displayed a decrease from the hop to step phase followed by an increase from the step to jump phase. The World Athletics athletes generally exhibited a more pronounced decrease and subsequent increase in vertical COM velocity compared to study participants. In contrast, the vertical COM velocity changes in novice participants and intermediate female participants were less consistent and deviated from the pattern observed by World Athletics athletes. These results suggest that more experienced participants athletes are better at managing their vertical COM velocities, more closely resembling the trends shown by elite athletes, though at lower velocities.

6.2 Limitations

The proposed methodology for a single-camera markerless motion capture system to assess triple jump technique has several limitations. These limitations are classified into participant-related, environment-related, software-related, and methodology-related categories. Each of these categories presented challenges that impacted the accuracy and reliability of the results.

6.2.1 Participant-Related

Participants were asked to perform six triple jumps; however, not all jumps were guaranteed to be successful, resulting in fewer than six valid jumps for some participants. Requesting additional jumps from athletes would deviate from the established study guidelines, implemented to simulate a competition and based on an understanding of the physical demands

of triple jump. Moreover, the study protocol did not require athletes to modify their training schedules prior to participating, leading to variations in fatigue levels. Consequently, some athletes jumped with minimal fatigue, while others had competed the day of or the day before data collection. The impact of fatigue on jump technique and performance was not explored. In relation to this, athletes were not guaranteed to be in the same phase of their training cycle, potentially affecting their performance. Future studies wishing to control for fatigue and differences in training cycles should conduct multiple trials throughout a season to further validate the presented methodology and findings.

6.2.2 Environment-Related

Data collection took place in different facilities and on different days, introducing environmental variability. At the outdoor TFAF location in Ottawa, weather conditions, such as varying sun and cloud cover, appeared to affect the GMP pose landmark results. Clear, sunny days with minimal cloud cover seemed to produce more reliable results, based on visual observation. Additionally, fluctuating wind conditions can have a notable impact on jump performance. Unlike sanctioned track and field competitions where wind gauges are used to ensure fair conditions, this study did not consider the impact of wind on performance.

Indoor facilities posed different challenges, including suboptimal lighting conditions that impacted video quality. Moreover, camera placement was significantly restricted in all three indoor locations due to facility layout constraints. The available camera locations were not always ideal for capturing footage. Another common limitation across all facilities was the presence of non-participants in the background or foreground of videos. Due to the inability to close facilities during data collection, efforts were made to minimize the impact of these individuals on the results. Despite these efforts, some video frames were unusable due to partial or complete obstruction by non-participants.

6.2.3 Software-Related

Several software-related limitations related to GMP pose detection behaviours were present in this study, including the items listed below. Table 6.1 provides one example of each software-related limitation.

1. *Right-left switching*, where GMP pose detection incorrectly identified the right side of the body as the left side, resulting in all landmarks being switched to the incorrect side.
2. Some videos exhibited *poor GMP pose landmark detections for foot landmarks*. While this was inconsequential for non-ground contact frames in the current context, if the foot landmarks were inaccurate even after data processing, the homography transformation was also inaccurate.
3. *Background people and objects* presented challenges in GMP pose detection as the detections would erroneously shift to these people or objects. In frames where a background object appeared to overlap with the participant, the GMP object detection could not separate the two, and therefore the GMP pose detections were negatively impacted.

Table 6.1: Examples of Google MediaPipe pose and object detection limitations. Participant heads and some body segments are redacted to preserve privacy.

Software Limitation	Example Description	Example Image
1. Right-left switching	Participant limb sides were detected on opposite sides in their last stride, which resulted in an inaccurate homography transformation, producing a last step length result of over 10 metres. It can be observed that the limb switching caused an incorrect rotation and scale factor to be calculated.	
2. Poor landmark detection	Neither of the participant's feet were estimated as making contact with the ground, despite the frame being a ground contact. This negatively impacted the homography transformation, leading to an incorrect last step length result of over five metres.	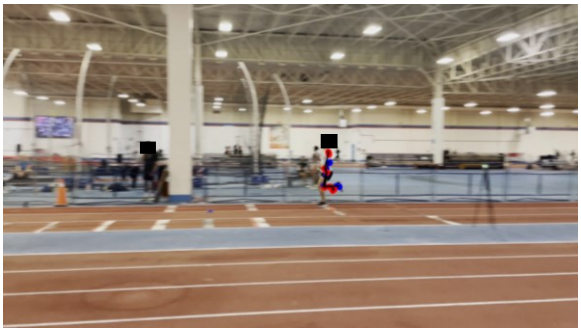

3. Presence of background people and objects	A person in the background was detected by GMP pose detection. Though in this example, the bounding box was manually corrected, some instances caused the GMP pose detections to be highly inaccurate.	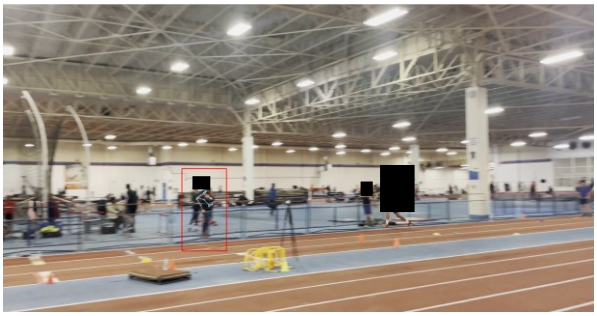

6.2.4 Methodology-Related

One of the most significant limitations present is the reliance on qualitative evaluation measures. Given the goal of the study was to propose and end-to-end framework for evaluating triple jump technique using markerless motion capture and a single camera, and not to optimize any individual step, the evaluation approach is acceptable. However, quantitative assessments for each step in the framework should be performed if the solution is to be utilized by coaches and athletes for performance evaluation. One critical aspect of this to validate the proposed methodology against the "gold standard" marker-based motion capture approach, discussed further in Section 7: Future Work.

Another key limitation in the proposed methodology is that all homography-based performance metrics are only applicable to ground contact frames. While this can provide valuable insights and aligned with many performance metrics included in the 2017 and 2018 World Athletics reports [6], [7], [8], [9], it does not encompass the triple jump movement in its entirety. Consequently, the analysis may miss critical aspects of the triple jump that occur during flight time.

Furthermore, another significant constraint in this study is the reliance on human intervention and the requirement to develop custom software for nearly all aspects of the methodology. Phase labels and homography key point labels were manually created with the aid of custom-developed software. Facility measurements were obtained manually, often under time constraints in each location. Start and end times for video trimming were identified manually and inputted into a Python script. The main Python processing script required frame-by-frame verification, including overriding incorrect bounding boxes and manually skipping inaccurate pose results to improve downstream processing. Validation of smoothing and homography results

were primarily done visually on a frame-by-frame basis, assisted by the custom visualization tool previously described. While these manual procedures were necessary in the current framework, they introduce the potential for human error, which cannot be easily quantified. Moreover, it makes the methodology difficult for other researchers to replicate consistently. Automation of these processes, as outlined in the Section 7: Future Work, would ideally minimize the impact of human error and improve the repeatability of the framework in different contexts.

Chapter 7: Future Work

Throughout the development of the study methodology, numerous areas for improvement and future work in the design and implementation of single-camera markerless motion capture studies were identified. The primary recommendations are to focus on improving pose detection results, developing new tools and standards for open-source HPE systems, validating the proposed framework against accepted standards, as well as introducing automated approaches to facilitate homography transformations in uncontrolled environments and extending the homography transformations beyond ground-contact frames.

Improving GMP pose landmark detection performance is a primary focus area within the current framework. Perhaps most importantly, the GMP pose landmark model – or an alternative pose model – should be improved by using triple jump-specific datasets. More generally, task-specific datasets would likely improve the pose detection results. Thanks to the open-source nature of GMP, the model and code are publicly available allowing the pose landmarker model to be retrained on task-specific data. For example, retraining the model with a prepared triple jump dataset using a tool like DeepLabCut may improve the pose detection performance [18]. Moreover, the GMP object detection task, which greatly improved pose detection results, could ideally be directly integrated within the GMP pose landmark model. This would reduce the need for future researchers to develop custom logic to incorporate the object detection step.

For use cases where identifying the correct foot position is critical, improving the pose detection performance for foot landmarks is essential. By re-training the GMP pose model with a prepared triple jump dataset, the foot landmark detection would likely improve as the dataset would contain scenes with footwear worn by athletes for triple jump. Alternatively, improving foot landmark detection could potentially be improved using the current GMP pose model and adding a post-processing step. The post-processing step would involve confirming the validity of the foot size and position at each frame, and making adjustments based on the knowledge that foot size should not change drastically between frames. These adjustments would ensure the homography transformation had more consistent inputs and should produce improved real-world coordinates. Improving the GMP pose model by re-training using a tailored dataset is recommended as the preferred method given the unknowns around adjusting foot size as a post-processing step. However, both techniques combined may produce the best results.

Another post-processing option for potentially improving GMP pose landmark detection is investigating the application of image enhancement techniques. Since the presence of background objects and people appeared to interfere with GMP pose landmark detection performance, investigating the impact of various image enhancement techniques would provide valuable insights. Future research could explore how background blurring or removal and contrast enhancement affect GMP pose landmark detection. Given the complexity of these techniques, which may need to be refined on a per-participant basis, starting with a small subset of data to observe whether there is an impact on GMP pose detection performance would be a prudent initial approach.

The *development and standardization of open-source software tools* designed to work with open-source HPE software solutions would accelerate the development of similar projects in the future. Throughout the development of the proposed framework, one of the greatest challenges was the reliance on creating custom software at nearly every step. This differs from the marker-based motion capture approach, where proprietary software is typically available for data storage, preprocessing, and exporting. Researchers should ideally agree on a standard method for managing open-source markerless software outputs. For example, the proposed framework leverages an SQLite database with table schemas that, if adopted by other researchers, would facilitate the reproducibility of methodologies. Of course, this standard should not be determined by a single researcher and requires a diverse set of inputs.

If researchers can agree on a standard approach to storing data produced from open-source HPE solutions such as GMP and OpenPose, this would enable the development of tooling to perform a variety of preprocessing and validation tasks. This includes standard tools for data labelling, visualization of pose detection results, applying smoothing and gap filling, and exporting results. Moreover, open-source software should be created to automatically or semi-automatically identify when open-source markerless motion capture solutions perform limb swapping, miss a pose detection completely, or detect landmarks that do not correspond to the actual pose, for example, landmarks that are unrealistically clustered together. This could involve the ability to observe the pose landmark trajectories across the video via time-series plots and quickly identify any discrepancies, as is common in marker-based motion capture data processing software. While the proposed framework introduced a variety of custom software to

achieve study goals, a standardized approach to open-source HPE software assessments would greatly facilitate reproducibility and collaboration in the research community.

The *proposed methodology should ideally be evaluated against a "gold standard" marker-based motion capture system* in a laboratory setting. The validation study should use a multi-camera marker-based motion capture setup in addition to a single smartphone camera to record the triple jump movement, if possible, in the laboratory. Alternatively, a movement such as running or jumping in place could be substituted based on the laboratory constraints. Within the validation study, the proposed methodology could also be validated against proprietary markerless motion capture solutions, such as Theia Markerless, and other open-source HPE solutions, such as OpenPose. This approach would enable a quantitative assessment to validate the performance of the proposed framework against widely accepted alternatives.

Automating components of the homography transformation process and extending the functionality beyond ground contact frames are both essential considerations for improving the proposed framework. It is recommended that the key points for homography are automatically detected using known reference objects, rather than requiring manual measurements of facility dimensions. For this study, key points for homography were manually measured and labelled and then mapped to the real-world environment using the 2D track templates. Popular feature-matching algorithms are not suitable for this task as they are unable to distinguish one line on the track or one take-off board from another. Known reference objects could be placed around the jumping area, ensuring a minimum of four objects are visible in all frames to meet the requirements for homography, and these objects could be detected automatically, similar to the methodology proposed by Pueo et al. [87]. Despite the challenges of introducing reference objects, such as potential obstructions and the risk of damage, it is worth further exploring as it would greatly reduce the amount of manual intervention required and improve the scalability of the proposed approach.

Moreover, performance metric calculations in this study were simplified by focusing only on video frames with ground contacts. Developing solutions to evaluate non-ground contact frames, perhaps informed by the knowledge of projectile motion, would enable more comprehensive triple jump analyses. It is recommended that semi-ground contact frames, where only the toe is on the ground, are incorporated into the current framework to more accurately

capture the individual's position and velocity at each take-off point. This information would enable an improved estimate for the COM trajectory after take-off, enabling the inclusion of additional triple jump performance metrics.

Once the methodology has been validated and the other recommendations are implemented, additional research projects incorporating machine learning could be undertaken. One idea is around activity recognition. Specifically, the highly debated single- versus double-arm technique in triple jump could be investigated. To facilitate analyses, automatically detecting whether a participant used single- or double-arm technique would be useful. This activity recognition task could be expanded to detect other aspects of the triple jump such as frames when the participant is on the ground or what jump phase they are in, which would enable more efficient downstream analyses to better understand the impact on jump performance. For example, automatically identifying the number of ground contact frames could enable the automatic calculation of flight time and ground contact time, among other performance metrics.

Another suggestion once the approach and data outputs are validated is to investigate the application of machine learning to understand triple jump performance patterns. The application of unsupervised ML techniques to perform triple jump technique evaluation could reveal previously unknown trends. For example, the application of unsupervised clustering algorithms, similar to the approach implemented by Ross et al. [117], could reveal jump phenotypes beyond single- and double-arm or find relationships between skill level and less established performance metrics like knee angles.

Finally, by selecting accessible, low-cost technology, the proposed methodology lays the foundation for potential future development of a mobile application enabling athletes and coaches to evaluate triple jump technique at their own track and field facility. The mobile application could be available for iOS and Android and enable near real-time quantitative triple jump technique from videos, using the previously presented performance metrics to provide feedback. Furthermore, the mobile application could allow athletes and coaches to collect these quantitative metrics over time and observe the performance trends. Though significant work is required before a mobile application could be developed, it is an exciting endeavour that would enable a data-driven approach for evaluating triple jump technique available to anyone with a smartphone and without requiring access to additional costly equipment.

Chapter 8: Conclusion

This study demonstrates that a single-camera markerless motion capture system can facilitate triple jump analysis in a real-world setting, albeit with limitations. Significant manual labelling was required to implement the proposed methodology, making it impractical for coaches and athletes to use. Future research should focus on automated approaches for determining real-world coordinate systems in uncontrolled environments; if successful, this would enhance the approach and increase the feasibility of developing a real-time mobile application for objective triple jump analysis. The current framework is best suited for assessing trends in triple jump techniques rather than accurately determining specific performance metric values. The approach could be extended to other applications in sports performance, including other track and field events such as the long jump.

The Google MediaPipe pose task was investigated and found to perform satisfactorily for HPE in a variety of indoor and outdoor settings. However, the foot detection often lacked precision, negatively impacting the accuracy of any subsequent metrics calculated from the pose data. Future studies should explore approaches for improving GMP pose results, especially the foot detection performance.

While single-camera markerless systems still require substantial improvements to be confidently used in uncontrolled settings, they hold incredible potential. Their cost-effectiveness and versatility are unparalleled, enabling the inclusion of a far greater number of participants in biomechanical studies. If future research addresses the current limitations and builds on the work outlined in this study, these techniques could achieve performance improvements and become ubiquitous. This study presents an example of an end-to-end framework for implementing such systems, with the hope of informing future research.

Chapter 9: References

[1] J. Hay, "Citius, Altius, Longius (Faster, Higher, Longer): The Biomechanics of Jumping for Distance," *Journal of Biomechanics,* vol. 26, no. 1, pp. 7-21, 1993.

[2] S. Allen, M. King and M. Yeadon, "Trade-offs between horizontal and vertical velocities during triple jumping and the effect on phase distances," *Journal of Biomechanics,* vol. 46, no. 5, pp. 979-983, 2013.

[3] A. Eissa, "Biomechanical Evaluation of the Phases of the Triple Jump Take-Off in a Top Female Athlete," *Journal of Human Kinetics,* vol. 40, pp. 29-35, 2014.

[4] J. Song and J. Ryu, "Biomechanical Analysis of the Techniques and Phase Ratios of Domestic Elite Triple Jumpers," *International Journal of Applied Sports Sciences,* vol. 23, no. 2, pp. 487-504, 2011.

[5] J. Hay, "The biomechanics of the triple jump: A review," *Journal of Sports Sciences,* vol. 10, pp. 343-478, 1992.

[6] C. Tucker, G. Nicholson, M. Cooke and A. Bissas, "Biomechanical Report for the IAAF World Indoor Championships 2017: Triple Jump Women," International Association of Athletics Federations, London, UK, 2018.

[7] C. Tucker, G. Nicholson, M. Cooke and A. Bissas, "Biomechanical Report for the IAAF World Indoor Championships 2017: Triple Jump Men," International Association of Athletics Federations, London, UK, 2018.

[8] C. Tucker, A. Bissas and S. Merlino, "Biomechanical Report for the IAAF World Indoor Championships 2018: Triple Jump Men," International Association of Athletics Federations, Birmingham, UK, 2019.

[9] C. Tucker, A. Bissas and S. Merlino, "Biomechanical Report for the IAAF World Indoor Championships 2018: Triple Jump Women," International Association of Athletics Federations, Birmingham, UK, 2019.

[10] L. Mündermann, S. Corazza and T. P. Andriacchi, "The evolution of methods for the capture of human movement leading to markerless motion capture for biomechanical applications," *J Neuroeng Rehabil,* vol. 3, no. 6, 2006.

[11] P. Nogueira, "Motion capture fundamentals: a critical and comparative analysis on real-world applications," *Doctoral Symposium in Informatics Engineering,* 2011.

[12] Z. Ripic, J. Signorile, C. Kuenze and M. Eltoukhy, "Concurrent validity of artificial intelligence-based markerless motion capture for over-ground gait analysis: A study of spatiotemporal parameters," *Journal of Biomechanics,* vol. 143, 2022.

[13] N. Ribeiro and C. Santos, "Inertial measurement units: A brief state of the art on gait analysis," in *2017 IEEE 5th Portuguese Meeting on Bioengineering*, Coimbra, Portugal, 2017.

[14] M. Rad, V. Gremeaux, F. Massé, F. Dadashi and K. Aminian, "Coaching Assistance by Phase-Based Performance Evaluation Feedback Obtained from a Single Sacrum IMU," in *40th International Society of Biomechanics in Sports Conference*, Liverpool, United Kingom, 2022.

[15] U. Jensen, M. Schmidt, M. Hennig, F. Dassler, T. Jaitner and B. Eskofier, "An IMU-based mobile system for golf putt analysis," *Sports Engineering,* vol. 18, pp. 123-133, 2015.

[16] K. Clément, F. Croteau, M. Gagnon and S. Cros, "Automatic detection of skate strokes in short-track speed skating using one single IMU: validation of a new method," *Sports Biomechanics,* p. 1–12, 2024.

[17] M. Moro, G. Marchesi, F. Hesse, F. Odone and M. Casadio, "Markerless vs. Marker-Based Gait Analysis: A Proof of Concept Study," *Sensors,* vol. 22, no. 5, 2022.

[18] J. Drazan, W. Phillips, N. Seethapathi, T. Hullfish and J. Baxter, "Moving outside the lab: Markerless motion capture accurately quantifies sagittal plane kinematics during the vertical jump," *Journal of Biomechanics,* vol. 125, 2021.

[19] T. Aderinola, H. Younesian, D. Whelan, B. Caulfield and G. Ifrim, "Quantifying Jump Height Using Markerless Motion Capture with a Single Smartphone," *IEEE Open Journal of Engineering in Medicine and Biology,* vol. 4, pp. 109-115, 2023.

[20] A. Gupta, P. Shrestha, B. Thapa, R. Silwal and R. Shrestha, "Knee Flexion/Extension Angle Measurement for Gait Analysis Using Machine Learning Solution “MediaPipe Pose” and Its Comparison with Kinovea," in *IOP Conference Series: Materials Science and Engineering*, Kathmandu, Nepal, 2023.

[21] A. Schmitz, M. Ye, R. Shapiro, R. Yang and B. Noehren, "Accuracy and repeatability of joint angles measured using a single camera markerless motion capture system," *Journal of Biomechanics,* vol. 47, no. 2, pp. 587-591, 2014.

[22] B. Scott, M. Seyres, F. Philip, E. Chadwick and D. Blana, "Healthcare applications of single camera markerless motion capture: a scoping review," *PeerJ,* vol. 10, 2022.

[23] N. Cronin, J. Walker, C. Tucker, N. G, M. Cooke, S. Merlino and A. Bissas, "Feasibility of OpenPose markerless motion analysis in a real athletics competition," *Frontiers in Sports and Active Living,* vol. 5, 2023.

[24] L. Wade, L. Needham, P. McGuidan and J. Bilzon, "Applications and limitations of current markerless motion capture methods for clinical gait biomechanics," *PeerJ,* vol. 10, 2022.

[25] Y. Hen and R. Paramesran, "Single camera 3D human pose estimation: A Review of current techniques," in *2009 International Conference for Technical Postgraduates (TECHPOS)*, Kuala Lumpur, Malaysia, 2009.

[26] M. Aqel, M. Marhaban, M. Iqbal Saripan and N. Ismail, "Review of visual odometry: types, approaches, challenges, and applications," *SpringerPlus,* vol. 5, 2016.

[27] T. Baumgartner, B. Paassen and S. Klatt, "Extracting spatial knowledge from track and field broadcasts for monocular 3D human pose estimation," *Scientific Reports,* vol. 13, no. 1, 2023.

[28] B. Bjering, "Estimations of 3D velocities from a single camera view in hockey," KTH Royal Institute of Technology, School of Engineering Sciences in Chemistry, Biotechnology and Health, Stockholm, Sweden, 2019.

[29] K. Yagi, K. Hasegawa, Y. Sugiura and H. Saito, "Estimating a runner's stride length and frequency from a race video by using ground stitching," in *36th Conference of the International Society of Biomechanics in Sports*, Auckland, New Zealand, 2018.

[30] J. Neves, J. Moreno, S. Barra, F. Narducci and H. Proença, "Chapter 1 - Unconstrained Data Acquisition Frameworks and Protocols," in *Human Recognition in Unconstrained Environments*, Academic Press, 2017, pp. 1-30.

[31] Encyclopaedia Britannica, "triple jump," 2 07 2024. [Online]. Available: https://www.britannica.com/sports/triple-jump. [Accessed 20 07 2024].

[32] Wikipedia, "Triple jump," [Online]. Available: https://en.wikipedia.org/wiki/Triple_jump. [Accessed 20 7 2024].

[33] World Athletics, "World Records," World Athletics, 2024. [Online]. Available: https://worldathletics.org/records/by-category/world-records. [Accessed 20 7 2024].

[34] Athletics Canada, "Canadian Records," [Online]. Available: https://athletics.ca/rankings-records/canadian-records/. [Accessed 20 7 2024].

[35] Canadian Olympic Committee, "Athletics," [Online]. Available: https://olympic.ca/sports/athletics/. [Accessed 20 7 2024].

[36] Canadian Olympic Committee, "Paris 2024 - Team Canada Medal Count," 2024. [Online]. Available: https://olympic.ca/games/paris-2024/. [Accessed 11 08 2024].

[37] Canadian Olympic Committee, "Related Posts For: Triple Jump," 2024. [Online]. Available: https://olympic.ca/tag/triple-jump/. [Accessed 11 08 2024].

[38] World Athletics, "Triple Jump," World Athletics, 2024. [Online]. Available: https://worldathletics.org/disciplines/jumps/triple-jump. [Accessed 29 05 2024].

[39] German Athletics Federation, "Biomechanical analyses of selected events at the 12th IAAF World Championships in Athletics, Berlin 15-23 August 2009," Deutscher Leichtathletik-Verband, Darmstadt, 2009.

[40] World Athletics, "World Athletics Technical Rules," World Athletics, 2019.

[41] S. J. Allen, M. A. King and M. R. Yeadon, "Is a single or double arm technique more advantageous in triple jumping?," *Journal of Biomechanics,* pp. 3156-3161, 2010.

[42] S. J. Allen, M. A. King and M. Yeadon, "Optimisation of phase ratio in the triple jump using computer simulation," *Human Movement Science,* vol. 46, pp. 167-176, 2016.

[43] M. Čoh and O. Kugovnik, "Variability of Biomechanical Parameters in the Triple Jump Technique - A Case Study," *SportLogia,* vol. 7, no. 2, pp. 113-121, 2011.

[44] B. Yu and J. Hay, "Optimum phase ratio in the triple jump," *Journal of Biomechanics,* vol. 29, no. 10, pp. 1283-89, 1996.

[45] J. Brimberg and H. B, "An operations research approach to triple jump," *International Journal of Sport Management and Marketing,* vol. 1, no. 3, pp. 208-214, 2006.

[46] J. Hay, J. Miller and R. Canterna, "The techniques of elite male long jumpers," *Journal of Biomechanics,* vol. 19, no. 10, pp. 855-866, 1986.

[47] S. Allen, M. Yeadon and M. King, "The effect of increasing strength and approach velocity on triple jump performance," *Journal of Biomechanics,* vol. 49, no. 16, pp. 3796-3802, 2016.

[48] J. Vaseekaran and A. Chandana, "Sagittal plane kinematics of triple jump: A review," *IOSR Journal of Sports and Physical Education,* vol. 8, no. 4, pp. 53-60, 2021.

[49] B. Yu, "Biomechanical Studies on Triple Jump Techniques: Theoretical Considerations and Applications," in *17th International Symposium on Biomechanics in Sports*, Perth, Australia, 1999.

[50] B. Yu, "Horizontal-to-vertical velocity conversion in the triple jump," *Journal of Sports Science,* vol. 17, no. 3, pp. 221-9, 1999.

[51] V. Panoutsakopoulos, A. Theodorou, D. Katsavelis and P. Roxanas, "Gender differences in triple jump phase ratios and arm swing motion of international level athletes," *Acta Gymnica,* vol. 46, no. 4, pp. 174-183, 2016.

[52] World Athletics, "Jonathan Edwards: Men's Triple Jump World Record," YouTube, [Online]. Available: https://www.youtube.com/watch?v=mi9KwAy5iQo. [Accessed 11 08 2024].

[53] World Athletics, "15.74m! WORLD TRIPLE JUMP RECORD FOR ROJAS | World Indoor Championships Belgrade 22," YouTube, [Online]. Available: https://www.youtube.com/watch?v=SkuROrHlBlQ. [Accessed 11 08 2024].

[54] T. Wren, P. Isakov and S. Rethlefsen, "Comparison of kinematics between Theia markerless and conventional marker-based gait analysis in clinical patients," *Gait & Posture,* vol. 104, pp. 9-14, 2023.

[55] B. Lahkar, A. Muller, R. Dumas, L. Reveret and T. Robert, "Accuracy of a markerless motion capture system in estimating upper extremity kinematics during boxing," *Front Sports Act Living,* 2022.

[56] G. Strutzenberger, R. Kanko, S. Selbie, H. Schwameder and K. Deluzio, "Assessment of Kinematic CMJ Data Using a Deep Learning Algorithm-Based Markerless Motion Capture System," *ISBS Proceedings,* vol. 39, no. 1, 2021.

[57] J. Outerleys, A. Mihic, V. Keller, E. Laende and K. Deluzio, "Markerless motion capture provides repeatable gait outcomes in patients," *Journal of Biomechanics,* vol. 168, no. 10.1016/j.jbiomech.2024.112115, pp. 112-115, 2024.

[58] Theia Markerless Inc., "Camera System Requirements," Theia Markerless Inc., [Online]. Available: https://www.theiamarkerless.ca/docs/cameras.html#:~:text=16.1.&text=Theia3D%20requires%20a%20minimum%20of,of%20people%20to%20be%20tracked.. [Accessed 11 08 2024].

[59] L. Needham, M. Evans, L. Wade, D. Cosker, M. B. J. McGuigan and S. Colyer, "The development and evaluation of a fully automated markerless motion," *Journal of Biomechanics,* vol. 144, 2022.

[60] N. Nakano, T. Sakura, K. Ueda, L. Omura, A. Kimura, Y. Iino and S. Y. S. Fukashiro, "Evaluation of 3D Markerless Motion Capture Accuracy Using OpenPose With Multiple Video Cameras," *Front Sports Act Living,* vol. 2, 2020.

[61] "Verification of reliability and validity of motion analysis systems during bilateral squat using human pose tracking algorithm," *Gait & Posture,* vol. 80, pp. 62-67, 2020.

[62] T. Fukushima, P. Blauberger, T. Russomanno and M. Lames, "The potential of human pose estimation for motion capture in sports: a validation study," *Sports Engineering,* vol. 27, 2024.

[63] S. Vafadar, W. Skalli, A. Bonnet-Lebrun, M. Khalifé, M. Renaudin, A. Hamza and L. Gajny, "A novel dataset and deep learning-based approach for marker-less motion capture during gait," *Gait Posture,* vol. 86, pp. 70-76, 2021.

[64] L. Sigal, "Computer Vision," in *Human Pose Estimation*, Boston, MA, Springer, 2016, pp. 362-370.

[65] A. Baca, P. Dabnichki, C. Hu, P. Kornfeind and J. Exel, "Ubiquitous Computing in Sports and Physical Activity—Recent Trends and Developments," *Sensors,* vol. 22, no. 21, 2022.

[66] T.-Y. Lin, M. Maire, S. Belongie, J. Hays, P. Perona, D. Ramanan, P. Dollár and Z. CL, "Microsoft COCO: Common Objects in Context," in *Computer Vision – ECCV 2014*, Zurich, Switzerland, 2014.

[67] CMU Perceptual Computing Lab, "keypoints_pose_25.png," [Online]. Available: https://github.com/CMU-Perceptual-Computing-Lab/openpose/blob/master/.github/media/keypoints_pose_25.png. [Accessed 21 07 2024].

[68] CMU Perceptual Computing Lab, "OpenPose Doc," [Online]. Available: https://cmu-perceptual-computing-lab.github.io/openpose/web/html/doc/md_doc_00_index.html. [Accessed 21 7 2024].

[69] Z. Cao, G. Hidalgo, T. Simon, S. Wei and Y. Sheikh, "OpenPose: Realtime Multi-Person 2D Pose Estimation Using Part Affinity Fields," *IEEE Transactions on Pattern Analysis and Machine Intelligence,* vol. 43, pp. 172-186, 2021.

[70] CMU Perceptual Computing Lab, "OpenPose License," [Online]. Available: https://github.com/CMU-Perceptual-Computing-Lab/openpose/blob/master/LICENSE.

[71] Google for Developers, "MediaPipe Solutions guide," [Online]. Available: https://developers.google.com/mediapipe/solutions/guide. [Accessed 12 04 2024].

[72] Google for Developers, "Pose landmark detection guide for Python," [Online]. Available: https://ai.google.dev/edge/mediapipe/solutions/vision/pose_landmarker/python. [Accessed 20 12 2023].

[73] V. Bazarevsky, I. Grishchenko, K. Raveendran, T. Zhu, F. Zhang and G. M, "BlazePose: On-device Real-time Body Pose tracking," *Google Research,* 2000.

[74] Google Research, "Model Card: MediaPipe BlazePose GHUM 3D," 16 04 2021. [Online]. Available: https://drive.google.com/file/d/10WlcTvrQnR_R2TdTmKw0nkyRLqrwNkWU/preview.

[75] H. Xu, E. Bazavan, A. Zanfir, W. Freeman, R. Sukthankar and C. Sminchisescu, "GHUM & GHUML: Generative 3D Human Shape and," in *Proceedings of the IEEE/CVF Conference on Computer Vision and Pattern Recognition*, Seattle, United States, 2020.

[76] K. Tanaka, "A Simple Method to Calculate Positions in Pose Tracking to Verify Work Procedures," *Engineering Science Letter,* vol. 2, no. 2, pp. 33-36, 2023.

[77] CMU Perceptual Computing Lab, "OpenPose Advanced Doc - 3-D Reconstruction Module and Demo," [Online]. Available: https://cmu-perceptual-computing-lab.github.io/openpose/web/html/doc/md_doc_advanced_3d_reconstruction_module.html. [Accessed 2024].

[78] M. Zhao, N. Lu and Y. Guan, "Classification of Pilates Using MediaPipe and Machine Learning," *IEEE Access,* vol. 12, 2024.

[79] F. Lawin, A. Byström, C. Roepstorff, M. Rhodin, M. Almlöf, M. Silva, P. Andersen, H. Kjellström and E. Hernlund, "Is Markerless More or Less? Comparing a Smartphone Computer Vision Method for Equine Lameness Assessment to Multi-Camera Motion Capture," *Animals,* vol. 13, no. 3, 2023.

[80] R. Hamilton, Z. Glavcheva-Lavela, M. Haque Milon, Y. Anil, J. Williams, B. P and C. Holt, "Comparison of computational pose estimation models for joint angles with 3D motion capture," *Journal of Bodywork and Movement Therapies,* vol. 40, pp. 315-319, 2024.

[81] J. Deng, W. Dong, R. Socher, L. Li and L. Fei-Fei, "ImageNet: A large-scale hierarchical image database," in *2009 IEEE Conference on Computer Vision and Pattern Recognition (CVPR)*, Miami, United States, 2009.

[82] C. Ionescu, D. Papava, V. Olaru and C. Sminchisescu, "Human3.6M: Large Scale Datasets and Predictive Methods for 3D Human Sensing in Natural Environments," *IEEE Transactions on Pattern Analysis and Machine Intelligence,* vol. 36, no. 7, pp. 1325-1339, 2014.

[83] L. Sigal, A. Balan and M. Black, "HumanEva: Synchronized video and motion capture dataset and baseline algorithm for evaluation of articulated human motion," *International Journal of Computer Vision,* vol. 87, no. 1, pp. 4-27, 2010.

[84] A. Mathis, P. Mamidanna, K. Cury, T. Abe, V. Murthy, M. Mathis and M. Bethge, "DeepLabCut: markerless pose estimation of user-defined body parts with deep learning," *Nature Neurosciences,* vol. 21, pp. 1281-1289, 2018.

[85] K. Yamamoto, Y. Hasegawa, T. Suzuki, H. Suzuki, H. Tanabe and K. Fujii, "Extracting proficiency differences and individual characteristics in golfers' swing using single-video markerless motion analysis," *Frontiers in Sports and Active Living,* vol. 5, 2023.

[86] Y. Luo, X. Wang, Y. Liao, Q. Fu, C. Shu, Y. Wu and Y. He, "A Review of Homography Estimation: Advances and Challenges," *Electronics,* vol. 12, no. 24, 2023.

[87] B. Pueo, J. Lopez, J. Mossi, A. Colomer and J. Jimenez-Olmedo, "Video-Based System for Automatic Measurement of Barbell Velocity in Back Squat," *Sensors,* vol. 21, no. 3, 2021.

[88] P. Walters, M. Fani, D. Clausi and A. Wong, "A tool for annotating homographies from hockey broadcast video," University of Waterloo, Waterloo, Canada, 2021.

[89] OpenCV, "Geometric Image Transformations," [Online]. Available: https://docs.opencv.org/4.x/da/d54/group__imgproc__transform.html. [Accessed 5 3 2024].

[90] OpenCV, "Camera Calibration and 3D Reconstruction," [Online]. Available: https://docs.opencv.org/4.x/d9/d0c/group__calib3d.html. [Accessed 05 03 2024].

[91] A. Krishna, P. Smith, M. Nicolescu and S. Hayes, "Vision-based Assessment of Instructional Content on Golf Performance," in *IPMV '22: Proceedings of the 4th International Conference on Image Processing and Machine Vision*, Hong Kong, China, 2022.

[92] K. Ka Sai, K. Kawakita, A. Kubota, H. Tsurusaki, R. Watanbe and M. Sugano, "Robust and Efficient Homography Estimation Using Directional Feature Matching of Court Points for Soccer Field Registration," *IEICE Transactions on Information and Systems,* vol. E104.D, no. 10, pp. 1563-1571, 2021.

[93] P. Glazier, "Beyond animated skeletons: How can biomechanical feedback be used to enhance sports performance?," *Journal of Biomechanics,* vol. 129, 2021.

[94] Athletics Canada, "Athletics Canada Technical Rules," 2021. [Online]. Available: https://athletics.ca/wp-content/uploads/2021/07/Athletics-Canada-Technical-Rules-June-2021.pdf. [Accessed 14 08 2024].

[95] MOVE 'N SEE, "PIXEM 2 | auto-follow camera for individual sports and stage," MOVE 'N SEE, [Online]. Available: https://shop.movensee.com/en/pixem-2-individual-sports-and-stage/368-pixem-2.html.

[96] MOVE 'N SEE, "PIXEM 2 Manuals," MOVE 'N SEE, [Online]. Available: https://shop.movensee.com/en/content/42-pixem-2-robot-cameraman-support.

[97] Software Freedom Conservancy, "git --everything-is-local," [Online]. Available: https://git-scm.com/.

[98] GitHub, Inc., "GitHub Docs," [Online]. Available: https://docs.github.com/en.

[99] Q. Li and Y. . Chen, "Entity-Relationship Diagram," in *Modeling and Analysis of Enterprise and Information Systems*, Berlin, Springer, 2009, pp. 125-139.

[100] IBM, "What is an entity relationship diagram?," [Online]. Available: https://www.ibm.com/think/topics/entity-relationship-diagram. [Accessed 11 04 2024].

[101] R. Hipp, "SQLite," [Online]. Available: https://www.sqlite.org/.

[102] Python Software Foundation, "moviepy 1.0.3," [Online]. Available: https://pypi.org/project/moviepy/. [Accessed 04 02 2024].

[103] Google for Developers, "Object detection guide for Python," [Online]. Available: https://ai.google.dev/edge/mediapipe/solutions/vision/object_detector/python.

[104] NumPy Developers, "numpy.polyval," [Online]. Available: https://numpy.org/doc/stable/reference/generated/numpy.polyval.html. [Accessed 22 03 2024].

[105] OpenCV, "OpenCV: Open Source Computer Vision Library," [Online]. Available: https://opencv.org/. [Accessed 17 12 2023].

[106] The SciPy Community, "scipy.interpolate - CubicSpline," 2024. [Online]. Available: https://docs.scipy.org/doc/scipy/reference/generated/scipy.interpolate.CubicSpline.html.

[107] D. Winter, "Anthropometry," in *Biomechanics and Motor Control of Human Movement, Fourth Edition*, Waterloo, Canada, John Wiley & Sons, Inc., 2009, pp. 86-90.

[108] J. Hunter, D. Dale, E. Firin and M. Droettboom, "matplotlib.pyplot," [Online]. Available: https://matplotlib.org/3.5.3/api/_as_gen/matplotlib.pyplot.html. [Accessed 09 10 2023].

[109] 1024jp, "LensCalibrator," 2022. [Online]. Available: https://github.com/1024jp/LensCalibrator. [Accessed 15 12 2023].

[110] Y.-B. Jia, "Homogeneous Transformations," 30 08 2022. [Online]. Available: https://faculty.sites.iastate.edu/jia/files/inline-files/homogeneous-transform.pdf.

[111] M. Duncan, "Homogeneous Coordinates and Transformations of Space," in *Applied Geometry for Computer Graphics and CAD*, London, United Kingdom, Springer, 2005, pp. 41-42.

[112] F. Magera, T. Hoyoux, O. Barnich and M. Van Droogenbroeck, "A Universal Protocol to Benchmark Camera Calibration for Sports," in *IEEE/CVF Conference on Computer Vision and Pattern Recognition 2024*, Seattle, United States, 2024.

[113] OpenCV, "Camera Calibration," OpenCV, [Online]. Available: https://docs.opencv.org/4.x/dc/dbb/tutorial_py_calibration.html. [Accessed 24 02 2024].

[114] NumPy Developers, "numpy.lib.format - NPY format," [Online]. Available: https://numpy.org/devdocs/reference/generated/numpy.lib.format.html.

[115] The SciPy Community, "scipy.optimize.minimize," 2024. [Online]. Available: https://docs.scipy.org/doc/scipy/reference/generated/scipy.optimize.minimize.html.

[116] I. Van Crombrugge, S. Sels, B. Ribbens, G. Steenackers, R. Penne and R. Vanlanduit, "Accuracy Assessment of Joint Angles Estimated from 2D and 3D Camera Measurements," *Sensors (Basel),* vol. 22, no. 5, 2022.

[117] G. Ross, B. Dowling, N. Troje, S. Fischer and R. Graham, "Classifying Elite From Novice Athletes Using Simulated Wearable Sensor Data," *Frontiers in Bioengineering and Biotechnology,* vol. 8, no. 814, 2020.

[118] Pallets, "click," [Online]. Available: https://click.palletsprojects.com/en/8.1.x/.

[119] DBeaver, "DBeaver Community: Free Universal Database Tool," [Online]. Available: https://dbeaver.io/.

[120] Microsoft, "Visual Studio Code," [Online]. Available: https://code.visualstudio.com/.

[121] Anaconda, Inc., "Miniconda," [Online]. Available: https://docs.anaconda.com/miniconda/.

[122] Anaconda, Inc., "Managing environments," [Online]. Available: https://conda.io/projects/conda/en/latest/user-guide/tasks/manage-environments.html.

Appendix A: Ethics Certificate and Research Consent Forms

21/06/2024

Université d'Ottawa
Bureau d'éthique et d'intégrité de la recherche

University of Ottawa
Office of Research Ethics and Integrity

CERTIFICAT D'APPROBATION ÉTHIQUE | CERTIFICATE OF ETHICS APPROVAL

Numéro du dossier / Ethics File Number	H-04-23-9061
Titre du projet / Project Title	Run Fast, Jump Far: Objectively Evaluating Triple Jump Technique Using Markerless Motion Capture
Type de projet / Project Type	Thèse de maîtrise / Master's thesis
Statut du projet / Project Status	Renouvelé / Renewed
Date d'approbation (jj/mm/aaaa) / Approval Date (dd/mm/yyyy)	15/06/2023
Date d'expiration (jj/mm/aaaa) / Expiry Date (dd/mm/yyyy)	14/06/2025

Équipe de recherche / Research Team

Chercheur / Researcher	Affiliation	Role
Heather GRANDY	Département de génie mécanique / Department of Mechanical Engineering	Chercheur Principal / Principal Investigator
Ryan GRAHAM	École des sciences de l'activité physique / School of Human Kinetics	Superviseur / Supervisor
Annabelle MANY	Département de génie mécanique / Department of Mechanical Engineering	Assistant de recherche / Research Assistant

Conditions spéciales ou commentaires / Special conditions or comments

550, rue Cumberland, pièce 154
Ottawa (Ontario) K1N 6N5 Canada

550 Cumberland Street, Room 154
Ottawa, Ontario K1N 6N5 Canada

613-562-5387 • 613-562-5338 • ethique@uOttawa.ca / ethics@uOttawa.ca
www.recherche.uottawa.ca/deontologie | www.recherche.uottawa.ca/ethics

Université d'Ottawa
Bureau d'éthique et d'intégrité de la recherche

University of Ottawa
Office of Research Ethics and Integrity

Le Comité d'éthique de la recherche (CÉR) de l'Université d'Ottawa, opérant conformément à l'*Énoncé de politique des Trois conseils* (2014) et toutes autres lois et tous règlements applicables, a examiné et approuvé la demande d'éthique du projet de recherche ci-nommé.

L'approbation est valide pour la durée indiquée plus haut et est sujette aux conditions énumérées dans la section intitulée "Conditions Spéciales ou Commentaires". Le formulaire « Renouvellement ou Fermeture de Projet » doit être complété quatre semaines avant la date d'échéance indiquée ci-haut afin de demander un renouvellement de cette approbation éthique ou afin de fermer le dossier.

Toutes modifications apportées au projet doivent être approuvées par le CÉR avant leur mise en place, sauf si le participant doit être retiré en raison d'un danger immédiat ou s'il s'agit d'un changement ayant trait à des éléments administratifs ou logistiques du projet. Les chercheurs doivent aviser le CÉR dans les plus brefs délais de tout changement pouvant augmenter le niveau de risque aux participants ou pouvant affecter considérablement le déroulement du projet, rapporter tout évènement imprévu ou indésirable et soumettre toute nouvelle information pouvant nuire à la conduite du projet ou à la sécurité des participants.

The University of Ottawa Research Ethics Board, which operates in accordance with the *Tri-Council Policy Statement* (2014) and other applicable laws and regulations, has examined and approved the ethics application for the above-named research project.

Ethics approval is valid for the period indicated above and is subject to the conditions listed in the section entitled "Special Conditions or Comments". The "Renewal/Project Closure" form must be completedfour weeks before the above-referenced expiry date to request a renewal of this ethics approval or closure of the file.

Any changes made to the project must be approved by the REB before being implemented, except when necessary to remove participants from immediate endangerment or when the modification(s) only pertain to administrative or logistical components of the project. Investigators must also promptly alert the REB of any changes that increase the risk to participant(s), any changes that considerably affect the conduct of the project, all unanticipated and harmful events that occur, and new information that may negatively affect the conduct of the project or the safety of the participant(s).

Coordonateur / COORDINATOR
Coordonnateur de l'éthique / Ethics Coordinator
Pour/For **Daniel LAGAREC** Président(e) du/ Chair of the **Comité d'éthique de la recherche en sciences de la santé et sciences / Health Sciences and Sciences Research Ethics Board**

550, rue Cumberland, pièce 154
Ottawa (Ontario) K1N 6N5 Canada

550 Cumberland Street, Room 154
Ottawa, Ontario K1N 6N5 Canada

613-562-5387 • 613-562-5338 • ethique@uOttawa.ca / ethics@uOttawa.ca
www.recherche.uottawa.ca/deontologie | www.recherche.uottawa.ca/ethics

English and French consent forms and questionnaires were available to all participants. Only the English versions were included in this Appendix.

uOttawa

Université d'Ottawa
Faculté des sciences de la santé

École des sciences de l'activité physique

University of Ottawa
Faculty of Health Sciences

School of Human Kinetics

☎ 613-562-5853
🖷 613-562-5149

125 University Private
Ottawa ON K1N 6N5 Canada

www.uOttawa.ca

Research Consent Form

Research Project Title: **Run Fast, Jump Far: Objectively evaluating triple jump technique using markerless motion capture**

Principal Investigator: **Heather Grandy[1]**
Supervisor: **Dr. Ryan Graham[2]**

Funding Agency: **N/A**

[1]University of Ottawa, Faculty of Engineering, Department of Mechanical Engineering, 800 King Edward Avenue, Ottawa, ON K1N 6N5

[2]University of Ottawa, Faculty of Health Sciences, Department of Human Kinetics, 200 Lees Ave (E020), Ottawa, ON K1N6N5

COVID-19 Precautions:
For the safety of both you and the researchers, precautions have been put in place to try and prevent the spread of COVID-19. Researchers and participants will perform a self-assessment for COVID-19 symptoms before arriving at their local track and field facility. If any symptoms are present, the researcher(s) and participant(s) are asked to stay home. Masks are recommended for data collection occurring indoors but are not required. Further, given the markerless modality of data collection, limited contact is needed between researchers and participants, therefore reducing the probability of spreading COVID-19.

Background and Purpose of the Study:
Triple jump is a highly complex track and field event that demands exceptional acceleration, preservation of velocity, and timing as athletes execute the hop, step, and jump phases. Due to the complexities of the event, identifying specific movement patterns required to improve performance can be challenging for coaches and athletes. Moreover, while experienced coaches can provide useful feedback to their athletes based on visual observation alone, more quantitative methods may offer additional information that can enhance a coach's recommendations and training programs.

Advancements in the areas of computer vision and machine learning have enabled improved pose estimation algorithms, accelerating the use of markerless motion capture for biomechanical applications. With these innovations, it is feasible to use markerless motion capture technology to evaluate triple jump technique outside of a lab setting. While various methods to evaluate triple jump technique have been discussed in the literature, few, if any, have employed markerless motion capture which enables data collection in a real-life setting.

Using a portable camera system to capture full approach triple jumps at approved track and field facilities, markerless motion capture will be used to identify key biomechanics metrics as well as to determine which movement patterns (features) are the most significant predictors of performance. This information will be encapsulated into a mobile application that can be used by athletes and coaches to obtain objective feedback on their triple jump technique. Equipped with this knowledge, coaches and athletes can create effective, data-driven training programs.

Description of Study Procedures:
You are invited to participate in a motion analysis study being conducted by Heather Grandy, a master's student at the University of Ottawa for her master's thesis project, who is part of Dr. Ryan Graham's Movement Biomechanics and Analytics Laboratory (200 Lees Avenue, E020). This study aims to objectively evaluate triple jump technique using markerless motion capture for data collection. It is anticipated that the data collection will take 60-90 minutes, depending on the time taken for warm-up and the amount of rest you wish to take between jumps.

Upon arrival, your name, email, age, and sex will be recorded. Further, your height and weight will be measured, and you will be asked to answer the following four questions: (1) How many times per week do you train for triple jump? (2) How long have you been training for triple jump? (3) What is your dominant leg for jumping? (4) Do you have any neurological, cardiovascular, or muscular disorders that may impact your triple jump performance? The last question requires only a yes or no response, no details are required.

After this, you will be given sufficient time to warm-up as you normally would for a track and field practice; you are permitted to warm-up however you'd like. Following your warm-up, you will be asked to perform six triple jumps which will be measured by the research team. The researchers will record each jump distance, and can announce the results after each jump, if desired. The jump distances will not be announced if you would prefer not to know. Each jump will be recorded by either by eight cameras positioned on each side of the runway (four on each side), or by an iPhone video camera. The camera(s) will record your movements during each of your attempts; the research team will show you where the camera(s) is (are) positioned for your awareness. If the iPhone video camera is used, you may be asked to wear a silicon wristband. This wristband is paired with a smartphone app and three small beacons to facilitate accurate video tracking. By using this setup, the research team can ensure high-quality video recordings are captured for each jump. The wristband, app, and beacons work together to reduce variation in video capture and eliminate or reduce the need for the student researcher to manually position the iPhone video camera. The research team will show you the position of the beacons, if used.

You do not have to change anything about your approach run or jump technique to participate. You are not required to jump from a full approach and can shorten your approach run as needed per your training program and competition schedule. You will also be permitted a minimum rest period of five minutes, which can be extended as needed. Further, while the protocol specifies six jumps, you are permitted to stop jumping at any time and for any reason. Please note that while tight-fitting clothing is best for markerless motion capture accuracy, you are encouraged to wear clothing that you are comfortable jumping in, being aware that baggy clothing may impact the accuracy of your results.

Possible Risks and Discomforts:
The primary risks associated with participating in this study are related the pre-existing risks of training for triple jump. This includes both the risk of physical harm due to fatigue or injury as well as exposure to stress and anxiety. As a study participant, you are familiar with the proper technique and can stop jumping at any time if you become injured, if you experience any discomfort, and/or if you wish to stop for any other reason. If worn, you may experience minor irritation from the silicon wristband.

If you become injured, the student researcher will assess the severity of the injury and provide appropriate first aid measures within their capabilities. The student researcher will bring a first aid kit to all data collection sessions. If necessary, the student researcher will contact emergency services by calling 911 to ensure you receive prompt medical attention. Further, an emergency contact field is included in this consent form, and the emergency contact will be called as soon as possible in the event of an injury. The student researcher will be responsible for informing the emergency contact in this scenario.

If the injury is minor, you may be able to continue with the study after receiving appropriate first aid. However, if the injury is severe, you will not be able to continue with the study and will be referred for further medical treatment. Importantly, even if the injury is minor, you can choose to stop jumping and/or to withdraw from the study. In addition to these actions, it is important to ensure that steps are taken to prevent injuries from occurring in the first place. During the study, the student researcher will closely monitor for any signs of discomfort or injury, and you are encouraged to immediately inform the researcher if you experience any pain or discomfort during the study. If you become injured or experience any discomfort, please inform the student researcher, and seek primary care from a medical professional at the University of Ottawa (100 Marie Curie, Ottawa, Tel.: 613-564-3950), or a medical professional of your choosing. The student researcher can assist you in doing this.

Possible Benefits:
As a benefit for participating, you will receive a personalized biomechanics report presenting key metrics related to your jumping technique upon completion of the study. If you chose to withdraw from the study for any reason but would still like a report on your biomechanics metrics, please inform the researchers as soon as possible. Please note that depending on when you chose to withdraw from the study, there may be insufficient data to complete the report. In this scenario, we will inform you that insufficient data were collected, and nothing will be provided to you. Further, the information learned from this study will be used to develop a mobile application that can provide objective feedback on triple jump technique. You may be chosen as one of the first users of this application, if desired.

Please note that the information provided in the biomechanics report is intended to be descriptive rather than prescriptive. We do not intend to provide you with specific training recommendations based on our findings.

Voluntary Participation:
You are not obliged to participate in this study; your participation is completely voluntary. You may withdraw from the study at any time with no penalty or coercion. This includes withdrawal after the data collection period as well as at any point in the future. You may ask to no longer have your jumps recorded at any time during the data collection period, at which time the cameras will be turned off and the data collection session will end. If you choose to withdraw after the study has been published, your data will be destroyed to prevent use in other projects. If you do choose to withdraw for any reason and at any time, any data collected about you will be deleted unless you specify via email to the student researcher, Heather Grandy, that they are permitted to use your data.

There are no social obligations to participating nor will there be any social or academic penalties that will prevent you from withdrawing from the study at any point.

Confidentiality:
All personal information is kept confidential. Information gained from this study will be stored electronically and will need a password to access, which will only be known to Dr. Ryan Graham, and Heather Grandy. Paper study records are stored in a locked cabinet; electronic records will be deleted, and paper records will be shredded ten years after the study ends. To maintain anonymity, you will not be identified by name

in any reports of the completed study, and the use of quasi-identifiers will be minimized. You will be identified instead by a unique participant number, and privacy-enhancing techniques to preserve anonymity will be implemented where possible.

Compensation:
You will not receive any compensation for participating in this study.

Questions about the Study:
You are free to ask questions at any time during and after the protocol and by contacting the principal investigator by email: Heather Grandy . The ethical components of this research project have been approved by the University of Ottawa research ethics board. If you have any questions regarding the ethical conduct of this study, you may contact the Protocol Officer for Ethics in Research, University of Ottawa, Tabaret Hall, 550 Cumberland Street, Room 154, Ottawa ON, K1N 6N5. Tel.: (613) 562-5387 Email: ethics@uottawa.ca. There are two copies of the consent form, one of which is yours to keep.

Research Project Title: **Run Fast, Jump Far: Objectively evaluating triple jump technique using markerless motion capture**

Consent:
I have read this consent form, and I agree to participate in the procedures of this study.

_____
Printed Name of Participant

_____ _____
Signature of Participant Date

Investigator Statement (or Person Explaining the Consent):
I have carefully explained to the research participant the nature of the above research study. To the best of my knowledge, the research participant signing this consent form understands the nature, demands, risks and benefits involved in participating in this study. I acknowledge my responsibility for the care and well-being of the above research participant, to respect the rights and wishes of the research participant, and to conduct the study according to applicable Good Clinical Practice guidelines and regulations.

_____
Name of Investigator/Delegate (printed)

_____ _____
Signature of Investigator/Delegate Date

Informed Consent to have Pictures and Videos Taken:
I consent to have videos taken of myself while performing triple jumps and understand that no footage will be taken at any point without my knowledge. Video recordings will be used to track my movement patterns using *Theia3D* or *OpenPose* software. I also understand that if any of these videos are used in a subsequent presentation or publication, they will be anonymized by only using the resulting skeleton/skeleton video overlay. If any photos are extracted from the video recordings to be used in a presentation or publication, I understand that my face and any other identifiers will be blurred. *You cannot participate in the research study without consenting to have pictures and videos taken.*

_____ _____
Printed Name of Participant Date

_____
Signature of Participant

_____ _____
Witness Name Witness Signature

Future Participation:
- ☐ I am interested in being contacted to participate in future research performed by this laboratory (your email information will be saved in a password protected file).

Emergency Contact Information
This individual will be contacted in the event of an injury.

_____ _____
Emergency Contact Name Emergency Contact Phone Number

_____
Emergency Contact Relationship to Participant

uOttawa

Université d'Ottawa
Faculté des sciences de la santé

École des sciences de l'activité physique

University of Ottawa
Faculty of Health Sciences

School of Human Kinetics

Research Parental Consent Form

Research Project Title: **Run Fast, Jump Far: Objectively evaluating triple jump technique using markerless motion capture**

Principal Investigator: **Heather Grandy[1]**
Supervisor: **Dr. Ryan Graham[2]**

Funding Agency: **N/A**

[1]University of Ottawa, Faculty of Engineering, Department of Mechanical Engineering, 800 King Edward Avenue, Ottawa, ON K1N 6N5

[2]University of Ottawa, Faculty of Health Sciences, Department of Human Kinetics, 200 Lees Ave (E020), Ottawa, ON K1N6N5

As a Substitute Decision Maker, you are being asked to provide informed consent on behalf of your child who is unable to provide consent for him/herself because they are under 14 years of age. If the participant gains the capacity to consent for him/herself, your consent for them will end. Throughout this form, "the participant" means your child who you are representing.

COVID-19 Precautions:
For the safety of both your child and the researchers, precautions have been put in place to try and prevent the spread of COVID-19. Researchers and participants will perform a self-assessment for COVID-19 symptoms before arriving at their local track and field facility. If any symptoms are present, the researcher(s) and participant(s) are asked to stay home. Masks are recommended for data collection occurring indoors but are not required. Further, given the markerless modality of data collection, limited contact is needed between researchers and participants, therefore reducing the probability of spreading COVID-19.

Background and Purpose of the Study:
Triple jump is a highly complex track and field event that demands exceptional acceleration, preservation of velocity, and timing as athletes execute the hop, step, and jump phases. Due to the complexities of the event, identifying specific movement patterns required to improve performance can be challenging for coaches and athletes. Moreover, while experienced coaches can provide useful feedback to their athletes based on visual observation alone, more quantitative methods may offer additional information that can enhance a coach's recommendations and training programs.

☎ 613-562-5853
613-562-5149

125 University Private
Ottawa ON K1N 6N5 Canada

www.uOttawa.ca

Advancements in the areas of computer vision and machine learning have enabled improved pose estimation algorithms, accelerating the use of markerless motion capture for biomechanical applications. With these innovations, it is feasible to use markerless motion capture technology to evaluate triple jump technique outside of a lab setting. While various methods to evaluate triple jump technique have been discussed in the literature, few, if any, have employed markerless motion capture which enables data collection in a real competition setting.

Using a portable camera system to capture full approach triple jumps at approved track and field facilities, markerless motion capture will be used to identify key biomechanics metrics as well as to determine which movement patterns (features) are the most significant predictors of performance. This information will be encapsulated into a mobile application that can be used by athletes and coaches to obtain objective feedback on their triple jump technique. Equipped with this knowledge, coaches and athletes can create effective, data-driven training programs.

Description of Study Procedures:

Your child is invited to participate in a motion analysis study being conducted by Heather Grandy, a master's student at the University of Ottawa for her master's thesis project, who is part of Dr. Ryan Graham's Movement Biomechanics and Analytics Laboratory (200 Lees Avenue, E020). This study aims to objectively evaluate triple jump technique using markerless motion capture for data collection. It is anticipated that the data collection will take 60-90 minutes, depending on the time taken for warm-up and the amount of rest your child wishes to take between jumps.

Upon arrival, your child's name, email, age, and sex will be recorded. Further, their height and weight will be measured, and they will be asked to answer the following four questions: (1) How many times per week do you train for triple jump? (2) How long have you been training for triple jump? (3) What is your dominant leg for jumping? (4) Do you have any neurological, cardiovascular, or muscular disorders that may impact your triple jump performance? The last question requires only a yes or no response, no details are required. You may assist them in answering these questions.

After this, they will be given sufficient time to warm-up as they normally would for a track and field practice; they are permitted to warm-up however they would like. Following their warm-up, they will be asked to perform six triple jumps which will be measured by the research team. The researchers will record each jump distance, and can announce the results after each jump, if desired. The jump distances will not be announced if your child would prefer not to know. Each jump will be recorded either by eight cameras positioned on each side of the runway (four on each side), or by an iPhone video camera. The camera(s) will record their movements during each of their attempts; the research team will show your child where the camera(s) is (are) positioned for their awareness. If the iPhone video camera is used, your child may be asked to wear a silicon wristband. This wristband is paired with a smartphone app and three small beacons to facilitate accurate video tracking. By using this setup, the research team can ensure high-quality video recordings are captured for each jump. The wristband, app, and beacons work together to reduce variation in video capture and eliminate or reduce the need for the student researcher to manually position the iPhone video camera. The research team will show your child the position of the beacons, if used.

Your child does not have to change anything about their approach run or jump technique to participate. They are not required to jump from a full approach and can shorten their approach run as needed per their training program and competition schedule. They will also be permitted a minimum rest period of five minutes, which can be extended as needed. Further, while the protocol specifies six jumps, they are permitted to stop jumping at any time and for any reason. Please note that while tight-fitting clothing is best for markerless motion capture accuracy, your child is encouraged to wear clothing that they are comfortable jumping in, being aware that baggy clothing may impact the accuracy of their results.

Possible Risks and Discomforts:
The primary risks associated with participating in this study are related the pre-existing risks of training for triple jump. This includes both the risk of physical harm due to fatigue or injury as well as exposure to stress and anxiety. As a study participant, your child is familiar with the proper technique and can stop jumping at any time if they become injured, if they experience any discomfort, and/or if they wish to stop for any other reason. If worn, your child may experience minor irritation from the silicon wristband.

If your child becomes injured, the student researcher will assess the severity of the injury and provide appropriate first aid measures within their capabilities. The student researcher will bring a first aid kit to all data collection sessions. If necessary, the student researcher will contact emergency services by calling 911 to ensure the participant receives prompt medical attention. Further, an emergency contact field is included in this consent form, and they will be contacted as soon as possible in the event of an injury. The student researcher will be responsible for informing the emergency contact in case of injury.

If the injury is minor, your child may be able to continue with the study after receiving appropriate first aid. However, if the injury is severe, they will not be able to continue with the study and will be referred for further medical treatment. Importantly, even if the injury is minor, they can choose to stop jumping and/or to withdraw from the study. In addition to these actions, it is important to ensure that steps are taken to prevent injuries from occurring in the first place. During the study, the student researcher will closely monitor for any signs of discomfort or injury, and your child is encouraged to immediately inform the researcher if they experience any pain or discomfort during the study. If they become injured or experience any discomfort, they should inform the student researcher, and seek primary care from a medical professional at the University of Ottawa (100 Marie Curie, Ottawa, Tel.: 613-564-3950), or a medical professional of your choosing. The student researcher can assist you and your child in doing this.

Possible Benefits:
As a benefit for participating, your child will receive a personalized biomechanics report presenting key metrics related to their jumping technique upon completion of the study. If they chose to withdraw from the study for any reason but would still like a report on their biomechanics metrics, please inform the researchers as soon as possible. Please note that depending on when they chose to withdraw from the study, there may be insufficient data to complete the report. In this scenario, we will inform you and your child that insufficient data were collected, and nothing will be provided. Further, the information learned from this study will be used to develop a mobile application that can provide objective feedback on triple jump technique. Your child may be chosen as one of the first users of this application, if desired. Please note that the information provided in the biomechanics report is intended to be descriptive rather than prescriptive. We do not intend to provide your child with specific training recommendations based on our findings.

Voluntary Participation:
Your child is not obliged to participate in this study; their participation is completely voluntary. Your child may withdraw from the study at any time with no penalty or coercion. This includes withdrawal after the data collection period as well as at any point in the future. Your child may ask to no longer have their jumps recorded at any time during the data collection period, at which time the cameras will be turned off and data collection session will end. If your child chooses to withdraw after the study has been published, their data will be destroyed to prevent use in other projects. If your child chooses to withdraw for any reason and at any time, any data collected about them will be deleted unless you specify via email to the student researcher, Heather Grandy, that she is permitted to use your child's data.

There are no social obligations to participating nor will there be any social or academic penalties that will prevent your child from withdrawing from the study at any point.

Confidentiality:
All personal information is kept confidential. Information gained from this study will be stored electronically and will need a password to access, which will only be known to Dr. Ryan Graham, and Heather Grandy. Paper study records are stored in a locked cabinet; electronic records will be deleted, and paper records will be shredded ten years after the study ends. To maintain anonymity, your child will not be identified by name in any reports of the completed study, and the use of quasi-identifiers will be minimized. They will be identified instead by a unique participant number, and privacy-enhancing techniques to preserve anonymity will be implemented where possible.

Compensation and Benefits:
Your child will not receive any compensation for participating in this study.

Questions about the Study:
You and your child are free to ask questions at any time during and after the protocol and by contacting the principal investigator by email: Heather Grandy . The ethical components of this research project have been approved by the University of Ottawa research ethics board. If you or your child have any questions regarding the ethical conduct of this study, you may contact the Protocol Officer for Ethics in Research, University of Ottawa, Tabaret Hall, 550 Cumberland Street, Room 154, Ottawa ON, K1N 6N5. Tel.: (613) 562-5387 Email: ethics@uottawa.ca. There are two copies of the consent form, one of which is yours to keep.

Research Project Title: **Run Fast, Jump Far: Objectively evaluating triple jump technique using markerless motion capture**

Consent:
I have read this consent form, and I provide consent for my child to take part in this study.

_____
Printed Name of Parent/Guardian
(Substitute Decision Maker)

_____ _____
Signature of Parent/Guardian (Substitute Decision Maker) Date

Printed Name of Person Who Conducted Consent Discussion	Signature of Person Who Conducted Consent Discussion	Date

Investigator Statement (or Person Explaining the Consent):
I have carefully explained to the research participant and their Substitute Decision Maker (parent or guardian) the nature of the above research study. To the best of my knowledge, the Substitute Decision Maker (parent or guardian) signing this consent form understands the nature, demands, risks and benefits involved in participating in this study. I acknowledge my responsibility for the care and well-being of the research participant, to respect the rights and wishes of the research participant and their Substitute Decision Maker (parent or guardian), and to conduct the study according to applicable Good Clinical Practice guidelines and regulations.

_____
Name of Investigator/Delegate (printed)

_____ _____
Signature of Investigator/Delegate Date

Informed Consent to have Pictures and Videos Taken:
I consent to have videos taken of my child while performing triple jumps and understand that no footage will be taken at any point without their knowledge. Video recordings will be used to track their movement patterns using *Theia3D* or *OpenPose* software. I also understand that if any of these videos are used in a subsequent presentation or publication, they will be anonymized by only using the resulting skeleton/skeleton video overlay. If any photos are extracted from the video recordings to be used in a presentation or publication, I understand that my child's face and any other identifiers will be blurred. *Your child cannot participate in the research study without consenting to have pictures and videos taken.*

_____
Printed Name of Parent/Guardian
(Substitute Decision Maker)

_____ _____
Signature of Parent/Guardian (Substitute Decision Maker) Date

_____	_____	_____
Printed Name of Person Who Conducted Consent Discussion	Signature of Person Who Conducted Consent Discussion	Date

Future Participation:

- ☐ I am interested in being contacted to participate in future research performed by this laboratory (your email information will be saved in a password protected file).

Emergency Contact Information

This individual will be contacted in the event of an injury.

_____ _____

Emergency Contact Name Emergency Contact Phone Number

_____

Emergency Contact Relationship to Participant

uOttawa

Université d'Ottawa
Faculté des sciences de la santé

École des sciences de l'activité physique

University of Ottawa
Faculty of Health Sciences

School of Human Kinetics

- 613-562-5853
- 613-562-5149

125 University Private
Ottawa ON K1N 6N5 Canada

www.uOttawa.ca

Research Assent Form

Research Project Title: **Run Fast, Jump Far: Objectively evaluating triple jump technique using markerless motion capture**

Principal Investigator: **Heather Grandy[1]**
Supervisor: **Dr. Ryan Graham[2]**

Funding Agency: **N/A**

[1]University of Ottawa, Faculty of Engineering, Department of Mechanical Engineering, 800 King Edward Avenue, Ottawa, ON K1N 6N5

[2]University of Ottawa, Faculty of Health Sciences, Department of Human Kinetics, 200 Lees Ave (E020), Ottawa, ON K1N6N5

COVID-19 Precautions:
For the safety of both you and the researchers, precautions have been put in place to try and prevent the spread of COVID-19. Researchers and participants will perform a self-assessment for COVID-19 symptoms before arriving before arriving at their local track and field facility. If any symptoms are present, the researcher(s) and participant(s) are asked to stay home. Masks are recommended for data collection occurring indoors but are not required. Further, given the markerless modality of data collection, limited contact is needed between researchers and participants, therefore reducing the probability of spreading COVID-19.

Why is this study being done?
We would like to invite you to be part of a research study. Research is a way to test new ideas to see if we can do things better.

In this study, we want use new technology to learn more about triple jump performance. We want to know what makes some individuals better at triple jump than others and create a tool that can help both coaches and athletes learn about their technique.

Who will take part?
People who have previous experience in triple jump are being asked to join this study. The people must train approximately twice per week in triple jump and must not have any health issues that impact their brain, heart, or muscles. The student researcher aims to have 15 female and 15 male triple jumpers involved in the study, for a total of 30 participants.

What will happen during the study?
When you arrive to participate in the study, your name, email, age, and sex will be written down. Next, your height and weight will be measured, and you will be asked the following four questions: (1) How many times per week do you train for triple jump? (2) How long have you been training for triple jump? (3) What is your dominant leg for jumping? (4) Do you have any neurological, cardiovascular, or muscular disorders that may impact your triple jump performance? The last question requires only a yes or no response, no details are required. You are encouraged to wear clothing that you are comfortable jumping in for this study.

Next, you will be given time to warmup as you normally would at a track and field practice or competition. You are allowed to warmup however you'd like. Afterwards, you will be asked to perform six triple jumps which will be measured by the research team. The researchers can tell you how far you jumped after each attempt but will only tell you if you'd like to know. All of your jumps will be recorded either by eight video cameras placed on either side of the jumps runway or with one iPhone video camera placed on a tripod on one side of the jumps runway. The research team can show you the location of camera(s). If an iPhone video camera is used, you may be asked to wear a silicon wristband. This wristband works together with other technologies to help capture accurate videos of your jumps.

You do not have to change anything about your approach run or jump technique to be in this study. You are not required to jump from a full approach and can shorten your approach run if you'd like. You will also be given a minimum rest period of five minutes between jumps, which can be longer if you need more rest. which can be extended as needed. In addition, you do not need to complete all six jumps if you don't want to and are allowed to stop at any time. The total time for the study will be about 60-90 minutes depending on how long you warmup for and how much rest you would like to take between jumps.

Are there good things that can happen from this study?
Sometimes good things can happen to people when they are in a study. These good things are called "benefits." This study will help us better understand the track and field event of triple jump using new technologies. We will give you unique information about your triple jump technique when you participate in the study which you can share with your coach. This may help you learn more about your triple jump performance. Also, a mobile application to help coaches and athletes learn about their triple jump technique will be developed through this study. You may be chosen as one of the first users of this application if you wish. There are no other benefits that the researchers can think of if you decide to join this study.

Are there bad things that can happen from this study?
Since you will be doing triple jump, there is a chance that you may become injured. This chance isn't bigger than the chance of you becoming injured at a practice. You will only be allowed to participate if your parent or guardian and doctor say it is ok. There is a chance you may get tired when doing your jumps. This is why you can choose to participate. If you do not want to, you do not have to.

What if something bad happens?
If something does go wrong, the researchers will help you as best as they can. Your parent or guardian will also be around to help you, and we can call your doctor if needed.

Is this private?
We will keep your information private whether you decide to join this study or not.

Will I be paid to participate?
No, you will not be paid to participate.

Can I say no?
You can choose to be a part of this study or not. You can also decide to stop being in this study at any time once you start. Talk to your parents or guardian and/or your doctor if you want to stop being in the study, and they will tell the researchers. No one will be mad at you if you choose not to take part.

What if I have questions?
Please ask us and we will do anything we can to answer your questions.

Assent form Signatures
If you agree to participate in this research study, please sign the form.

I understand the information that was explained to me, and I can ask any question that I like about the study.

Signature of Participant	Name of Participant	Date

Printed Name of Person Who Conducted Assent Discussion	Signature of Person Who Conducted Assent Discussion	Date

Appendix B: Software Architecture

This Appendix presents the software architecture implemented for the proposed end-to-end triple jump technique evaluation framework. The diagram in Figure B.1 provides an overview of the key Python and SQL scripts used, and how they interact with one another. The remainder of Appendix B provides a more detailed explanation of each script, with a particular emphasis on the most significant ones.

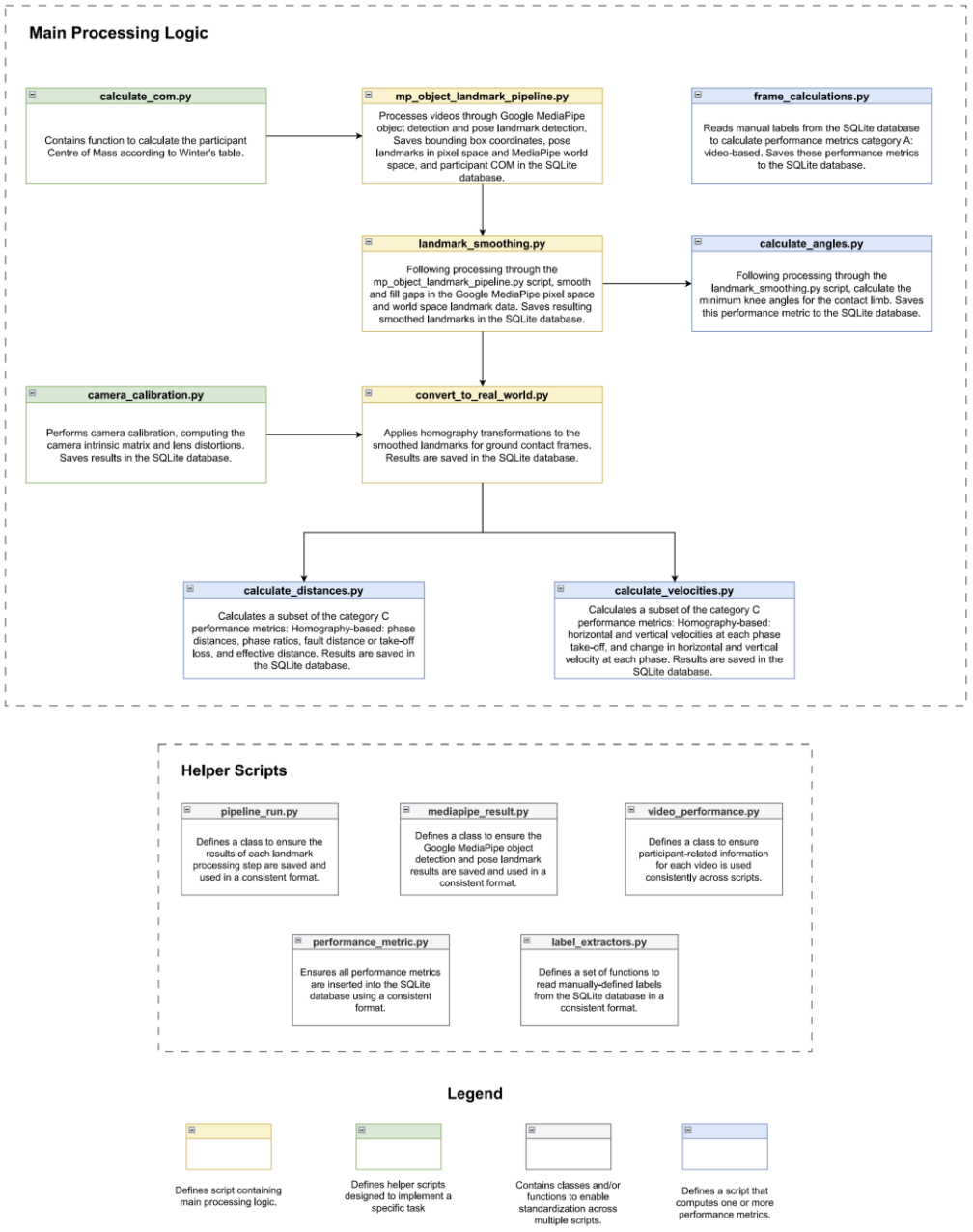

Figure B.1: High-level software architecture diagram, highlighting dependencies between scripts.

Note that for all scripts, the Click Python package was used to facilitate passing in command line arguments [118].

The **pipeline_run.py** script defines a PipelineRun class with the methods described in Table B.1.

Table B.1: Methods in the PipelineRun class. The asterisk indicates a class method, intended to work on the whole class and not on a particular instance of the class. All other methods are designed to work on a class instance.

Method Name	Description
start	Gets the current time. Intended use is to get the time at the start of a pipeline execution.
stop	Gets the current time. Intended use is to get the time at the end of a pipeline execution.
save_to_db	Saves pipeline run information to the PipelineRuns table given a database connection.
save_to_dict	Saves pipeline run information to a Python dictionary (can be used to save to a JSON file).
read_from_db*	Gets pipeline information from the PipelineRuns table given a database connection and video ID.

The **pipeline_run.py** script is not intended to be executed directly by a user, but instead contains functionality that is used by other scripts to facilitate consistency. As an example, in the **mp_object_landmark_pipeline.py** script, described later in this Appendix, the PipelineRun class is used:

- To obtain pipeline results from the function containing the majority of script logic, run().
    - The PipelineRun object is instantiated at the beginning of the run() function.
    - The start() method is used on the object, named pipeline_run, to get the current time when the pipeline was initially executed.
    - Similarly, the end() method is used on the object at pipeline completion.
- Within the detect_landmarks() function:
    - The save_to_dict() method is used if the output_json flag is set to True. This saves the pipeline run information (ID, pipeline name, start time, end time) to a JSON file. It is saved along with the GMP pose results.
    - The video_id attribute of the object is used to set the correct video ID before saving the pipeline information to the SQLite database.
    - The save_to_db() method is used to save the pipeline run information (ID, videoID, pipeline name, start time, end time) to the database table, PipelineRuns.

The **mediapipe_result.py** script defines several classes related to MediaPipe results: BoundingBox (Table B.2), Landmark (Table B.3), FrameResult (Table B.4), MediapipeResult (Table B.5), as well as a function read_labels_from_db(), which does not belong to any class. Methods in each class are described in their respective tables below.

Table B.2: Methods in the BoundingBox class, defined in the mediapipe_result.py Python script. The asterisk indicates a class method, intended to work on the whole class and not on a particular instance of the class. All other methods are designed to work on a class instance.

Method Name	Description
from_mediapipe*	Gets the bounding box coordinates in MediaPipe's format, and returns them in a non-MediaPipe format, providing more control over how the bounding box coordinates are used.
save_to_dict	Saves bounding box coordinates to a Python dictionary (can be used to save to a JSON file).

Table B.3: Methods in the Landmark class, defined in the mediapipe_result.py Python script. The asterisk indicates a class method, intended to work on the whole class and not on a particular instance of the class. All other methods are designed to work on a class instance.

Method Name	Description
world_landmarks_from_mediapipe*	Gets the world landmarks in MediaPipe's format, and returns them in a non-MediaPipe format, providing more control over how the world landmarks are used.
normalized_landmarks_from_mediapipe*	Gets the normalized pixel landmarks in MediaPipe's format, and returns them in a non-MediaPipe format, providing more control over how the normalized pixel landmarks are used.
save_to_dict	Saves landmark coordinates to a Python dictionary (can be used to save to a JSON file).

Table B.4: Methods in the FrameResult class, defined in the mediapipe_result.py Python script. The asterisk indicates a class method, intended to work on the whole class and not on a particular instance of the class. All other methods are designed to work on a class instance.

Method Name	Description
from_mediapipe_result*	Gets the world landmarks in MediaPipe's format, and returns them in a non-MediaPipe format, providing more control over how the world landmarks are used.
world_landmarks_array	Gets theMediaPipe world landmarks (x, y, z coordinates) into an array.
compute_com	Uses the world_landmarks_array method to get world landmarks in a format that can be passed into a function that computes the centre of mass (this function is in another script called calc_com.py).
save_to_dict	Saves relevant metrics for a frame - frame number, bounding box coordinates, world landmarks, normalized landmarks, bounding box overridden flag, and centre of mass coordinates - to a Python dictionary (can be used to save to a JSON file).
save_to_db	Saves MediaPipe results from a pipeline run to a database, given the database connection and pipeline run information. This updates the MediapipeOutput and Landmarks tables.
read_from_db*	Read MediaPipe landmark results from a database, given the database connection, and mediapipeOutputID. Returns the frame number, bounding box coordinates, world landmarks, normalized landmarks, bounding box overridden flag, and centre of mass coordinates for a given mediapipeOutputID.

Table B.5: Methods in the MediapipeResult class, defined in the mediapipe_result.py Python script. The asterisk indicates a class method, intended to work on the whole class and not on a particular instance of the class. All other methods are designed to work on a class instance.

Method Name	Description
add_frame_results	Appends a frame result instance to a list of frame results.
save_to_dict	Saves landmark results to a Python dictionary (can be used to save to a JSON file).
save_to_db	Saves the frame results list to a database, given a database connection and pipeline ID.
read_from_db*	Reads MediaPipe results saved in the MediapipeOutput table given a database connection and pipeline run ID. Uses the FrameResult.save_to_db method to do this.
read_from_dict*	Reads from a Python dictionary (JSON file), and extracts the MediaPipe results - frame number, bounding box coordinates, landmark information, and overridden flag using the FrameResult, BoundingBox, and Landmark classes.

The **mediapipe_result.py** script is not intended to be executed directly by a user, but instead contains functionality that is used by other scripts to facilitate consistency. As an example, in the **mp_object_landmark_pipeline.py script**, described later in this Appendix, the MediapipeResult class is used:

- To obtain MediaPipe results computed within the run() function, which contains the majority of the script logic:
    - An object of the MediapipeResult class called mediapipe_result is instantiated at the start of the run() function.
    - The add_frame_result() method is used to add MediaPipe data for a particular frame to the mediapipe_result object (frame number, bounding box coordinates, pose landmark coordinates, and bounding box overridden flag).
    - After iterating through all frames, the resulting mediapipe_result object is returned.

- Within the detect_landmarks() function:
    - The save_to_dict() method is used to save MediaPipe results to a JSON file, if the output_json flag is set to True.
    - The save_to_db method is used to save the MediaPipe results to a table in the SQLite database, given a database connection, and pipeline run information. The PipelineRuns, MediapipeOutput, and Landmarks tables are updated accordingly.

The FrameResult class is also used in in the **mp_object_landmark_pipeline.py** script:

- To get MediaPipe results for a specific frame within the run() function:
    - The from_mediapipe_result method is used to initialize a frame result object which contains the frame number, bounding box coordinates, pose landmark coordinates, and bounding box overridden flag.
    - The compute_com() method is used to compute the centre of mass for the current frame.
    - The resulting frame_result object is saved to a MediapipeResult object.

The **camera_calibration.py** Python script performs camera calibration and outputs the camera intrinsic matrix and distortion coefficients used in the homography transformation. The script accepts the file path to a video of a checkerboard of known dimensions, recorded using an iPhone 12 camera at 30 Hz, to reflect the settings used for data collection. The camera calibration steps were implemented by adapting an OpenCV tutorial [113]. The resulting camera calibration outputs are saved as NPY files and loaded into the SQLite database as blobs using a SQL script.

The **video_performance.py** Python script defines a VideoPerformance class which contains information related to a specific video, including the participant ID, location ID, jump distance, and jump attempt number, among other attributes. This script also contains one function, to be used within other scripts, to read the camera calibration outputs (the camera intrinsic matrix and distortion coefficients) from the SQLite database and return the values as NumPy arrays. The VideoPerformance class contains two class methods, described in Table B.6. The class is used across several scripts to extract video-related attributes in a consistent manner, either by specifying a video ID, or a participant ID and jump attempt number.

Table B.6: Class methods in the VideoPerformance class, defined in the video_performance.py Python script.

Method Name	Description
read_from_db	Reads video attributes saved in the VideoPerformances table given a database connection and video ID.
read_from_db_by_participant	Reads video attributes saved in the VideoPerformances table given a database connection, participant ID, and jump attempt number.

The **mp_object_landmark_pipeline.py** Python script is the main processing script for the project. This script opens an OpenCV window that allows the user to move frame-by-frame through a specified video, view the GMP object detection and pose detection results, and override the bounding box if necessary. The **mp_object_landmark_pipeline.py** script implements the steps described below and the functions in Table B.7 to generate initial GMP pose detection results.

- Uses GMP object detection to identify the bounding box of the subject in each frame.
    - Enables the user to overwrite the bounding box if detected incorrectly.
    - Requires the object detection model path to be specified.

- Uses GMP pose to identify the pose landmarks of the subject in each frame.
    - The bounding box is used as input to the GMP pose model to ensure the participant is found in the frame.
    - Requires the pose landmarker model path to be specified.

- Saves the results to the SQLite database and/or JSON file, depending on arguments passed in by the user. Within the proposed framework, the SQLite database was primarily used, with the JSON file option maintained for initial testing purposes.

Table B.7: Functions in the mp_object_landmark_pipeline.py Python script, the main processing script. Note: GMP is an acronym for Google MediaPipe.

Functions Name	**Description**
build_object_detector	Builds and returns a GMP object detector using the GMP light object detection model.
build_pose_landmarker	Builds and returns a GMP pose landmarker object using the GMP heavy pose landmarker model.
crop_to_bounding_box	Crops an image based on the specified bounding box dimensions.
detect_landmarks	Detects pose landmarks in a video by running and object detection and pose landmark pipeline, with options to save the results to a JSON file or an SQLite database (main function).
draw_bounding_box	Draws a bounding box on an image based on inputted coordinates.
expand_bounding_box	Expands a bounding box by a specified ratio, ensuring it stays within the image boundaries.
manually_draw_bounding_box	Allows the user to manually draw a bounding box on a video frame by interacting with the video display.
overlay_image	Overlays one video frame onto another based on the specified bounding box area. This function enables the frame to be cropped to a bounding box area for pose detection purposes, and subsequently overlay the pose detection results on the full-size video.
percent_overlap	Calculates the percentage overlap between two bounding boxes.
predict_next_bbox	Predicts the next bounding box position based on previous bounding boxes using polynomial fitting.
run	Runs the main video processing pipeline, applying object detection and pose detections on each video frame, and visualizing the results for validation.
visualize_detection_result	Draws bounding boxes on an image based on GMP object detection results, used in conjunction with the run function.
visualize_pose_landmark_result	Draws pose landmarks on a video frame based on GMP pose landmark detection results.

The **mp_object_landmark_pipeline.py** script accepts the following arguments:

- **--database**: Specify the full file system path to the SQLite database. The example below will open the first jump attempt for participant 1 (default values) and will write results to the SQLite database location specified after the --database parameter.

  ```
  python code/mp_object_landmark_pipeline.py --database
  'C:/myfolder/thesis-triplejump.db'
  ```

- **--participant**: The participant ID, valid values are from 1 through 30. If not specified, the default value is 1. The example below will open the first jump for participant 5 and will write results to the default SQLite database.

  ```
  python code/mp_object_landmark_pipeline.py --participant 5
  ```

- **--attempt_num**: The jump attempt number. For most participants, there will be six attempts. If not specified, the default value is 1. The example below will open the fourth jump for participant 5 and will write results to the default SQLite database.

  ```
  python code/mp_object_landmark_pipeline.py --participant 5
  --attempt_num 4
  ```

- **--output_json**: Using this option will save the label results in a JSON file in the working directory. This is optional but may be used to verify results if desired. If not specified, no JSON file is generated. The example below will open the first jump for participant 1 and will save the labels to an output JSON in the working directory as well as to the default SQLite database. Note that the JSON filename is automatically generated in the script and does not need to be specified.

  ```
  python code/mp_object_landmark_pipeline.py --output_json
  ```

- **--output_db/--no_output_db**: Specify whether labels should be saved to the SQLite database. The default behaviour is to write results to the SQLite database. However, for testing scenarios --no_output_db can be used to ensure results are not saved. The example below will open the first jump for participant 1 and allow navigation through each frame but will not save any results to the SQLite database nor to a JSON file.

  ```
  python code/mp_object_landmark_pipeline.py --no_output_db
  ```

  The example below will open the second jump for participant 6 and will save the results in the default SQLite database.

  ```
  python code/mp_object_landmark_pipeline.py --participant 6
  --attempt_num 2
  ```

- **--video_path_override**: If not looking up the video in the database by specifying the participant and attempt number, the path to the video file can be provided instead. The example below will open the sixth jump attempt for participant 1.

  ```
  python code/mp_object_landmark_pipeline.py --
  video_path_override
  "C:/myvideos/Participants/P01/videos/trimmed/P01_6.MOV"
  ```

- **--video_directory**: Specify the directory containing the jumps videos. The script expects the videos to be stored in a parent directory called "Participants." The example below will open the first jump for participant 1 per the specified video directory, and the labels will be saved in the default SQLite database.

  ```
  python code/mp_object_landmark_pipeline.py --
  video_directory "C:/myvideos/Participants"
  ```

The **label_extractors.py** Python script contains functions to enable data to be read from the SQLite database in consistent formats to facilitate data processing in other scripts. The functions in this script are summarized in Table B.8.

Table B.8: Functions in the label_extractors.py Python script.

Function Name	Description
read_loc_from_db	Reads point IDs and corresponding x and y coordinates from the LocationCoordinates table into a Pandas DataFrame, given a database connection and location ID.
read_labels_from_db	Reads point IDs and corresponding frame numbers, x and y coordinates from the LocationKeypointLabels table into a Pandas DataFrame, given a database connection and video ID.
read_labels_from_db_dict	Reads point IDs and corresponding frame numbers, x and y coordinates from the LocationKeypointLabels table into a Python dictionary, given a database connection and video ID.
read_manual_phase_labels_df	Reads the frame number, foot, phase, contact type, and switch (erroneous swap of left and right limb landmarks), which were labelled manually, from the ManualPhaseLabels table into a Pandas DataFrame, given a database connection and video ID.

The **landmark_smoothing.py** Python script is intended to be used after videos have been processed by the **mp_object_landmark_pipeline.py** script. This script leverages functions from the **label_extractors.py** script, as well as the MediapipeResult, PipelineRun, and VideoPerformance classes. The pose landmarks, generated by the **mp_object_landmark_pipeline.py** script, are read from the SQLite database and are interpolated to fill any gaps or smooth out noisy data. Cubic spline interpolation is used to smooth the GMP pose 3D world and 2D pixel landmark coordinates for each video frame [106].

The **performance_metric.py** Python script contains a single function to be used within other scripts to write performance metric results to the appropriate table in the SQLite database with all required information. This ensures that no required data attributes are missing when writing performance metrics to the SQLite database.

The **convert_to_real_world.py** Python script, also referred to as the homography script, contains the homography transformation logic, an essential component of the data processing tasks. This script leverages functions from the **label_extractors.py** and **performance_metric.py** scripts, the MediapipeResult, PipelineRun, and VideoPerformance classes, as well as the camera intrinsic matrix and distortion coefficients generated from the **camera_calibration.py** script. The homography script was adapted to process homography transformations for a single video or

for all participants based on the arguments passed in by the user. The **convert_to_real_world.py** script implements the steps described below and the functions in Table B.9 to perform the homography transformations:

- Extracts GMP 3D world landmarks for the participant.
- Reads the manually labelled participant-related and video-related data from the SQLite database. The participant-related data is used to determine ground contact frames, and the video-related data contains the key point labels that enable the mapping between the video frames and 2D track templates.
- Applies a homography transformation to convert the GMP 3D world landmarks into 3D real-world coordinates for the contact foot landmarks.
- Optimizes the homography transformation by minimizing the reprojection error. This enables the remaining GMP 3D world landmarks to be converted into 3D real-world coordinates.
- Saves transformed coordinates in the SQLite database for downstream performance metric calculations.
- Optionally, plots the real-world foot position after applying homography as a preliminary validation step.

Table B.9: Functions in convert_to_real_world.py Python script. Note: GMP is an acronym for Google MediaPipe.

Function Name	**Description**
compute_optimized_transform	Optimizes the transformation between the GMP pose 3D world landmarks and 3D real-world foot position by minimizing reprojection error.
compute_transformation	Computes the homography transformation matrix using the key point labels and facility coordinates to obtain the 3D real-world foot position.
convert_to_real_world	Processes participant data, extracts GMP pose landmarks, orchestrates the computation of 3D real-world coordinates (main function).
find_real_world_feet	Finds the 3D real-world position of the ground contact frame as part of the homography transformation process.
objective_function	Calculates the mean squared error between 2D pixel landmarks obtained from GMP pose and 2D reprojected pixel landmarks after applying the real-world transformation. Used in conjunction with the compute_optimized_transform function.
transform_points	Applies a 4x4 transformation matrix to a set of 3D points, used in conjunction with the objective_function function.

The **convert_to_real_world.py** script accepts the following arguments:

- **--database**: Specify the full file system path to the SQLite database. The example below will obtain 3D real-world pose landmarks for the most recent pipeline run for each participant, as this is the default script behaviour, and will write results to the SQLite database location specified after the --database parameter.

```
python code/convert_to_real_world.py --database
'C:/myfolder/thesis-triplejump.db'
```

- **--participant**: Optionally specify the participant ID, valid values are from 1 through 30. If not specified, all participant data will be processed. If specified, an attempt number must also be specified. The example below will obtain the 3D real-world pose landmarks for participant 5, attempt 4.

  ```
  python code/convert_to_real_world.py --participant 5
  --attempt_num 4
  ```

- **--attempt_num**: Optionally specify the jump attempt number. If not specified, all participant data will be processed. If specified, a participant ID must also be specified (refer to previous example).

- **--pipeline_run_id**: Optionally specify a specific pipeline run ID, which can be looked up in the database. If specified, 3D real-world pose landmarks will be computed for the participant attempt associated with the pipeline run ID. Assuming the desired pipeline run ID was looked up in the SQLite database and found to be 256, the example below will obtain the 3D real-world pose landmarks for the corresponding participant data.

  ```
  python code/convert_to_real_world.py --pipeline_run_id 256
  ```

- **--display/--no-display**: Optional flag to specify whether the Matplotlib plots of the 3D real-world foot coordinates will be displayed, alongside the trimmed participant video. The default behaviour is to not display the plots. The example below will process data for participant 5, attempt 4 and display the aforementioned plots.

  ```
  python code/convert_to_real_world.py --participant 5
  --attempt_num 4 --display
  ```

- **--video_directory**: Specify the directory containing the jumps videos. This option is only required when the display flag, described above, is enabled, ensuring the correct participant video is displayed.

  ```
  python code/convert_to_real_world.py --video_directory
  "C:/myvideos/Participants"
  ```

- **--output_landmarks_to_db/--no_output_landmarks_to_db**: Specify whether the resulting 3D real-world landmarks should be saved to the SQLite database. The default behaviour is to write results to the SQLite database. However, for testing scenarios, --no_output_landmarks_to_db flag can be used to ensure results are not saved. The example below will open the fourth jump for participant 5 and display the 3D real-world foot coordinates plots but will not save any results to the SQLite database.

  ```
  python code/convert_to_real_world.py --participant 5
  --attempt_num 4 –display --no_output_landmarks_to_db
  ```

The **frame_calculations.py** Python script takes the manual phase label data as input and computes Category A performance metrics (video-based). This script leverages functions from the **label_extractors.py** and **performance_metric.py** scripts, as well as the MediapipeResult and PipelineRun classes. The resulting ground contact time and flight time for the specified participant and attempt number, are computed and saved to the SQLite database.

The **calculate_angles.py** Python script computes joint angles based on the GMP pose landmark IDs inputted by the user and saves the results to the SQLite database. This script was used to calculate Category B performance metrics (MediaPipe-based), knee angles. This script leverages functions from the **label_extractors.py** and **performance_metric.py** scripts, as well as the MediapipeResult and PipelineRun classes. The minimum knee angle for the contact limb was identified in another post-processing script. A set of joint angles that can be calculated were defined, referring to landmark IDs in the GMP pose landmarker model, allowing the script to be used to calculate additional angles if required in the future: right knee, left knee, right hip, and left hip. The script was adapted to compute angles for a single video or for all participants based on the arguments passed in by the user. The knee angles presented in the proposed framework are later filtered to select the correct limb and minimum angle per jump phase using a separate Python script.

The **calculate_distances.py** and **calculate_velocities.py** Python scripts were used to compute Category C performance metrics (homography-based). These scripts both leverage functions from the **label_extractors.py** and **performance_metric.py** scripts, as well as the MediapipeResult, PipelineRun, and VideoPerformance classes. Moreover, both scripts require the manual phase labels to determine ground contact frames and jump phases. They are both capable of computing distance/velocity metrics for a single video or for all participants. The resulting metrics are saved in the SQLite database and are later aggregated using a separate Python script.

Appendix C: Visual Validation Tool

This Appendix describes the visual validation tool used to visually assess the initial GMP pose detections, the landmark results after applying gap filling and smoothing, COM calculations, homography key point labels, and finally, the GMP pose landmarks after applying the homography transformation to ground contact frames. To accomplish this, a Python script, **plot_normalized_and_world.py**, was developed. This script enables the display of the GMP pixel landmarks overlaid on the video, and the world landmarks as a "skeleton" on a 3D plot. Matplotlib was leveraged to generate the plot and the Python implementation of OpenCV enabled video display and frame-by-frame navigation [108]. Note that the pose landmarks 0-10, representing the head and features on the face, were not included in these displays since they were not used in the downstream analyses. Figure C.1 presents a specific frame for a participant, with the GMP pose 3D world landmarks on the left, and the GMP pixel landmarks overlaid on the video on the right.

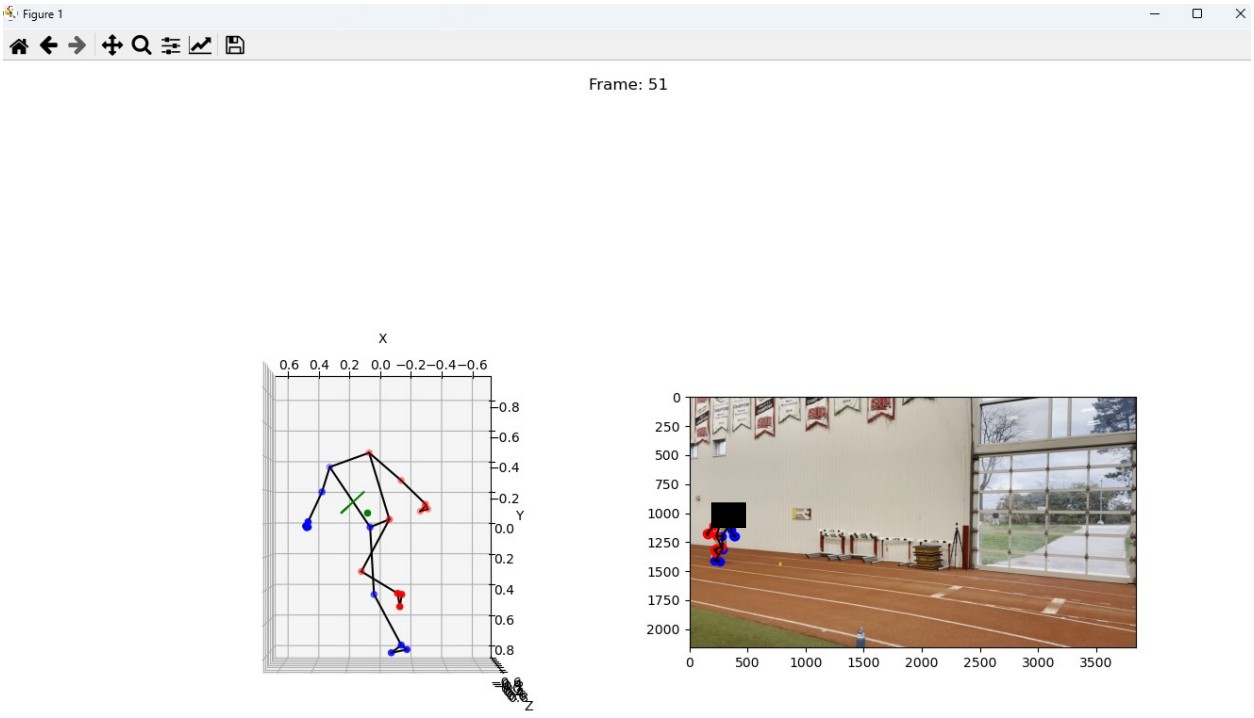

Figure C.1: Example of plot_normalized_and_world.py display window. The 3D plot shows the direction of travel (green line) and centre of mass (green dot). Both the 3D plot and video show the MediaPipe pose landmarker model results (right landmarks are red, and left landmarks are blue). Landmarks are intentionally enlarged to preserve participant privacy.

The **plot_normalized_and_world.py** script does not write any information to the SQLite database. It only reads and displays data from the SQLite database. The **plot_normalized_and_world.py** script accepts the following arguments:

- **--database:** Specify the full file system path to the SQLite database. The example below will open the first jump attempt for participant 1 (default values) and will read results from the SQLite database location specified after the --database parameter.

  ```
  python plot_normalized_and_world.py --database
  'C:/myfolder/thesis-triplejump.db'
  ```

- **--participant**: The participant ID, valid values are from 1 through 30. If not specified, the default value is 1. The example below will open the first jump for participant 5 and will read results from the default SQLite database.

  ```
  python plot_normalized_and_world.py --participant 5
  ```

- **--attempt_num**: The jump attempt number. If not specified, the default value is 1. The example below will open the fourth jump for participant 5 and will read results from the default SQLite database.

  ```
  python plot_normalized_and_world.py --participant 5
  --attempt_num 4
  ```

- **--pipeline_run_id:** Optionally, specify a pipeline run ID which can be looked up in the SQLite database. The example below will display results for participant 1, attempt 1, with the pipeline run ID 10. If there is no pipeline run ID with these attributes, the pop-up window will display a blank plot and blank rectangle in place of loading the video.

  ```
  python plot_normalized_and_world.py --pipeline_run_id 10
  ```

- **--input_json**: Using this option allows for plotting MediaPipe results stored in a JSON file. The file path to the JSON file must be specified when this option is used.

  ```
  python plot_normalized_and_world.py --input_json
  "C:/data/mediapipe_results.json"
  ```

- **--display_labels**: This flag enables manually labelled key points to be overlaid on the specified video. Enabling this flag will load coordinates from the LocationKeypointLabels table in the SQLite database and display the points on applicable frames. Since only ground contact frames were labelled, labels will only be displayed for those frames. An example of the displayed labels is provided in Figure C.2.

  ```
  python plot_normalized_and_world.py --display_labels
  ```

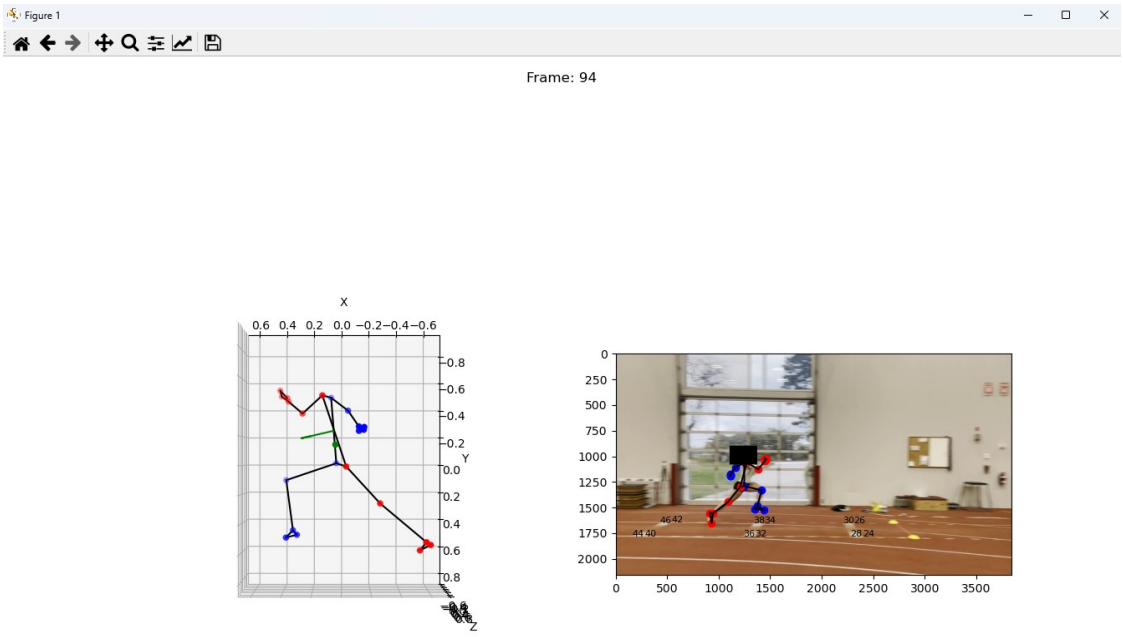

Figure C.2: Example of plot_normalized_and_world.py display window with key point labels for homography shown. The 3D plot shows the direction of travel (green line) and centre of mass (green dot). Both the 3D plot and video show the MediaPipe pose landmarker model results (right landmarks are red, and left landmarks are blue). Landmarks are intentionally enlarged to preserve participant privacy.

- **--video_directory**: Specify the directory containing the jumps videos. The script expects the videos to be stored in a parent directory called "Participants." The example below will open the first jump for participant 1 per the specified video directory, and the labels will be saved in the default SQLite database.

  ```
  python plot_normalized_and_world.py --video_directory
  "C:/myvideos/Participants"
  ```

Appendix D: Relational Data Model

To standardize data reading and writing, a relational data model was created. This section provides an overview of the data model, as well as information about the database tables and their intended purpose. The final Entity-Relationship diagram implemented in the SQLite database is shown in Figure D.1

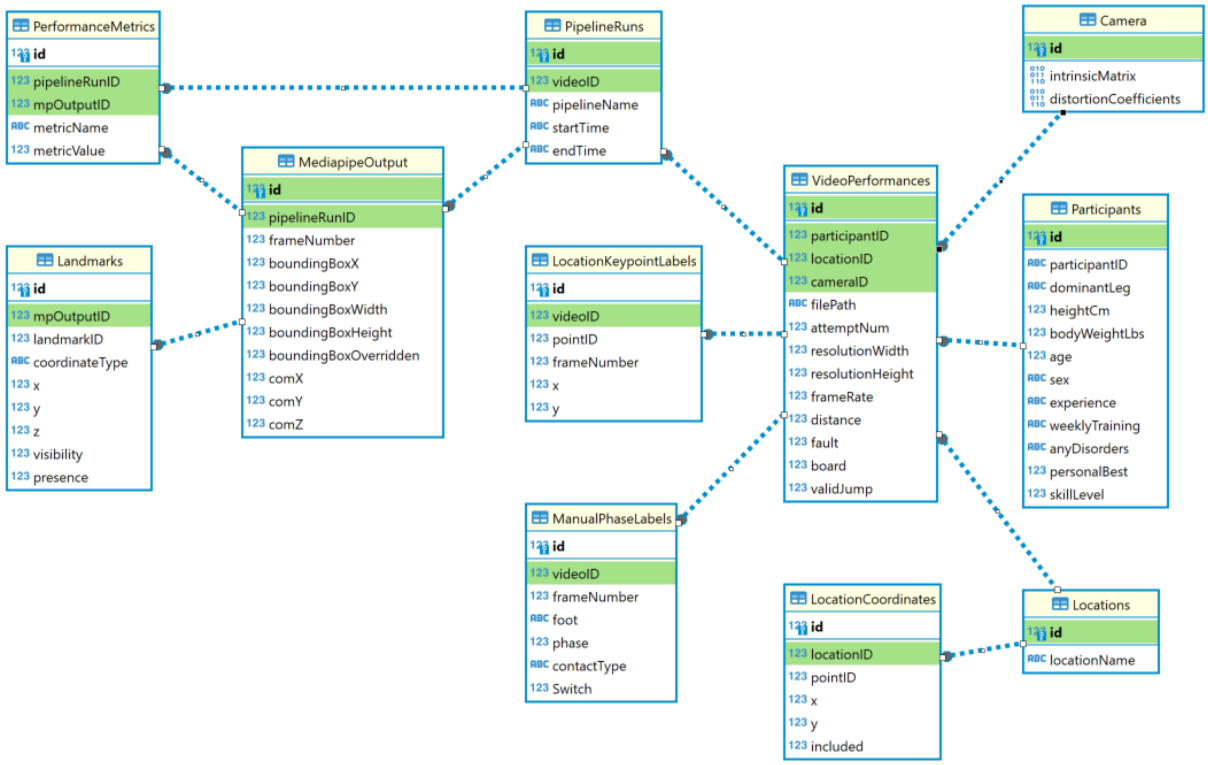

Figure D.1: Entity-Relationship diagram for the SQLite database implemented to facilitate data management and data analysis. Each rectangle represents a table, and the first row of each table represents the primary key column. The dotted lines between tables represent relationships, and the rows highlighted in green indicate columns that are used as foreign keys.

Camera Table: Stores the intrinsic matrix and distortion coefficients for the iPhone 12 camera used in data collection. The *primary key*, id, is a *foreign key*, cameraID in the VideoPerformances table.

Landmarks Table: For each frame, GMP pose returns 33 normalized pixel pose landmarks and 33 world landmarks, as well as visibility and presence scores for each landmark. Storing these values in the MediapipeOutput table would result in significant data duplication, so the Landmarks table was introduced. MediapipeOutput and Landmarks have a one-to-many relationship where id, the *primary key* for the MediapipeOutput table is a *foreign key*, mpOutputID, in the Landmarks table. This data model design minimizes data duplication while

enabling the creation of queries to extract all relevant GMP pose output information for a given video.

Locations Table: Contains the name and unique ID assigned to each data collection location. The *primary key*, id, is a *foreign key*, locationID, in the LocationCoordinates and VideoPerformances tables.

LocationCoordinates Table: Stores the x and y coordinates for each data collection location, used to create the 2D track templates and subsequently leveraged in the homography transformation. The *foreign key*, locationID from the Locations table is saved in this table to facilitate establishing a relationship to the VideoPerformances table.

LocationKeypointLabels Table: Stores the manual key point labels for each ground contact frame to be used in the homography transformation, along with the corresponding point ID. The videoID *foreign key* from the VideoPerformances table allows key point labels to be mapped to a specific video.

ManualPhaseLabels Table: Stores the manual labels for ground contact frames, based on videos. This includes the frame number, the ground contact limb (left or right), triple jump phase (approach run, hop, step, jump, landing), whether there was a switch (right landmarks erroneously swapped to the left side of the body, or vice versa), and whether the jump attempt was a foul. The videoID *foreign key* from the VideoPerformances table allows manual phase labels (participant-related labels) to be mapped to a specific video.

MediapipeOutput Table: Contains the pipelineRunID as a *foreign key* and associated results including the frame number, bounding box coordinates, and centre of mass. This represents partial information from the main MediaPipe processing script, with the remaining output stored in the Landmarks table. The *primary key*, id, is a *foreign key*, mpOutputID, in the PerformanceMetrics and Landmarks tables.

Participants Table: Contains the participant information collected during the informed consent process, as well as their assigned skill level. The *primary key*, id, is a *foreign key*, participantID in the VideoPerformances table to map video attributes to a participant.

PerformanceMetrics Table: The PerformanceMetrics table is used to store final metrics results and has a one-to-many relationship with the MediapipeOutput and PipelineRuns tables. Contains *foreign keys* mpOutputID and pipelineRunID from these tables to obtain the correct pipeline run ID and corresponding MediaPipe output results.

PipelineRuns Table: The PipelineRuns table was created to enable multiple runs of the same script without overwriting any table entries. For example, the main Python processing script is executed to obtain the landmark information for each of participant 5's videos. Then, a minor change is made to the main processing script which impacts the bounding box coordinates, requiring all of participant 5's videos to be processed again. Using the PipelineRuns table, no information is lost; the landmarks with the old and new bounding box coordinates are both stored. A timestamp is included in this table to determine which run was more recent. The

primary key, id, is a *foreign key*, pipelineRunID in the PerformanceMetrics and MediapipeOutput tables. Contains a *foreign key*, videoID, from the VideoPerformances table to associate a pipeline run with a specific video.

VideoPerformances Table: The VideoPerformances table contains important information about each video, including jump distances, camera properties, and a participant ID to relate the video to a participant. This table is connected to another table, PipelineRuns, by the id column. The id column is the *primary key* of the VideoPerformances table, and is a *foreign key*, videoID, in the PipelineRuns table via one-to-many relationship.

Appendix E: Folder Structure for Data Storage

Figure E.1 visually depicts the folder structure implemented to manage the 192 videos obtained during data collection. The original videos were stored in folder named “raw” and the trimmed videos, used for downstream processing, in a folder named “trimmed.”

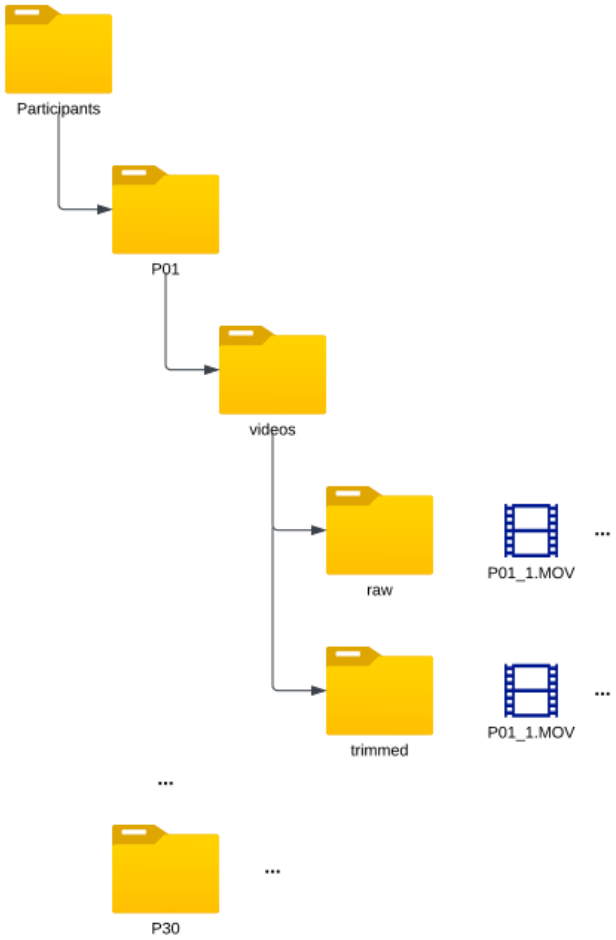

Figure E.1: Folder structure for storing participant videos.

Appendix F: Manual Override Guide

When navigating frame-by-frame through a video in the window opened with the **mp_object_landmark_pipeline.py** script, an incorrect bounding box may be observed, where the bounding box fails to accurately capture the participant. Additionally, pose detection errors might occur for a given frame, even after adjusting the bounding box. This behaviour can be manually corrected or flagged by following the steps outlined below:

1. With the OpenCV window open, a frame that did not detect the subject accurately is observed.
2. Click the “A” key. This opens a new window with no bounding box nor pose landmarks.
3. In this window, draw a new bounding box by clicking and dragging. The new bounding box will appear in green in this window. The box can be redrawn as many times as needed before confirming.
4. When satisfied with the new bounding box, click the “Q” key to exit the window. The other OpenCV window will still be open. Click the right arrow key to see the new bounding box, and the resulting GMP pose detections.
5. Most of the time, the GMP pose landmark detections are corrected after overriding the bounding box. In some cases, an improved bounding box will not fix the pose detections, in which case these frames should be marked as erroneous using the “X” key. Continue navigating through the video as before, continuing to override incorrect bounding boxes if applicable.

Note: The **mp_object_landmark_pipeline.py** script keeps track of any overridden bounding boxes, and the resulting data is saved in the SQLite database.

A screenshot of the tool is not included to preserve participant privacy, since the GMP pose landmarks are not overlaid at the object detection stage in the processing pipeline.

Appendix G: MediaPipe Pose Landmark Mapping to Dempster's Table

To calculate the participant COM at each frame, the COM was estimated using the Dempster's anthropometric table and the calculations described by Winter [107]. The body segments from Dempster's anthropometric table were mapped to the GMP pose landmarks; the mappings are shown in Table G.1.

Table G.1: Anthropometric segment mappings to Google MediaPipe (GMP) pose landmarks, used to calculate participant centre of ass. Anthropometric table was created by Dempster and obtained from [107].

Dempster's Segment	Dempster's Definition	GMP pose Landmark 1	GMP pose Landmark 2
Hand Left	Wrist axis/knuckle 2 middle finger	15	19
Hand Right	Wrist axis/knuckle 2 middle finger	16	20
Forearm Left	Elbow axis/ulnar styloid	13	15
Forearm Right	Elbow axis/ulnar styloid	14	16
Upper Arm Left	Glenohumeral axis/elbow axis	11	13
Upper Arm Right	Glenohumeral axis/elbow axis	12	14
Foot Left	Lateral malleolus/head metatarsal 2	27	31
Foot Right	Lateral malleolus/head metatarsal 2	28	32
Leg Left	Femoral condyles/medial malleolus	25	27
Leg Right	Femoral condyles/medial malleolus	26	28
Thigh Left	Greater trochanter/femoral condyles	23	25
Thigh Right	Greater trochanter/femoral condyles	24	26
Head and Neck	C7-T1 and 1st rib/ear canal	7	8
Trunk Left	Greater trochanter/glenohumeral joint	11	23
Trunk Right	Greater trochanter/glenohumeral joint	12	24

Appendix H: 2D Track Templates and Facility Measurements

This Appendix provides partial 2D track templates and facility measurements for all four locations included in the study. For each facility, both the Python-generated plot with point IDs and the hand-drawn plot with corresponding IDs are presented; the original hand-drawn diagrams and CSV files containing point IDs and x-y coordinates are not included. The coordinate values were stored in the LocationCoordinates SQLite table, as described in Appendix D. The Terry Fox Athletic Facility, Toronto Track and Field Facility, Gryphon Fieldhouse, and Pavillon d' Éducation Physique et Sport are shown in Figures H.1, H.2, H.3, and H.4, respectively.

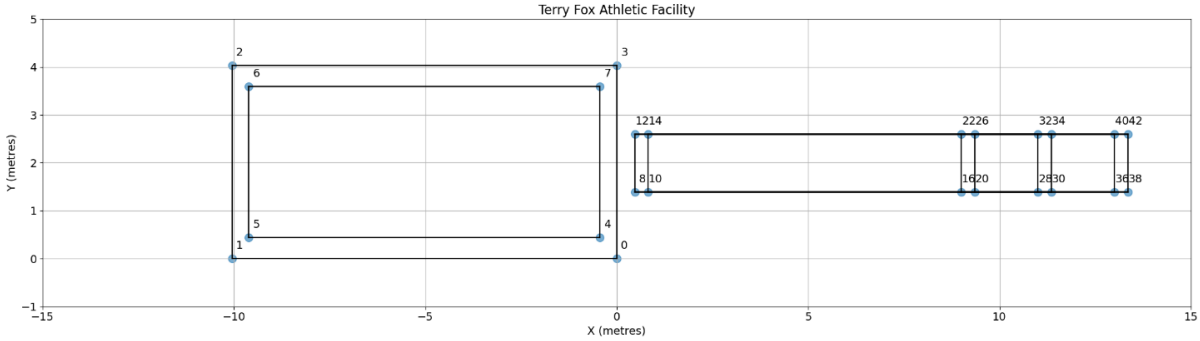

(a) Python-generated facility coordinates

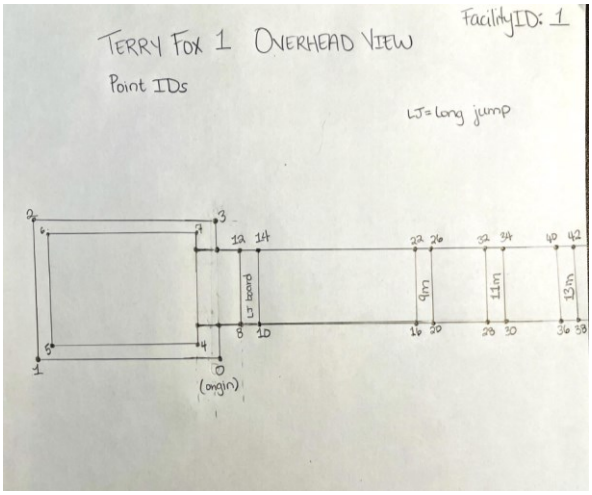

(b) Improved hand-drawn facility coordinates

Figure H.1:Terry Fox Athletic Facility in Ottawa, Ontario, (a) Python-generated facility coordinates, and (b) improved hand-drawn facility coordinates with point IDs.

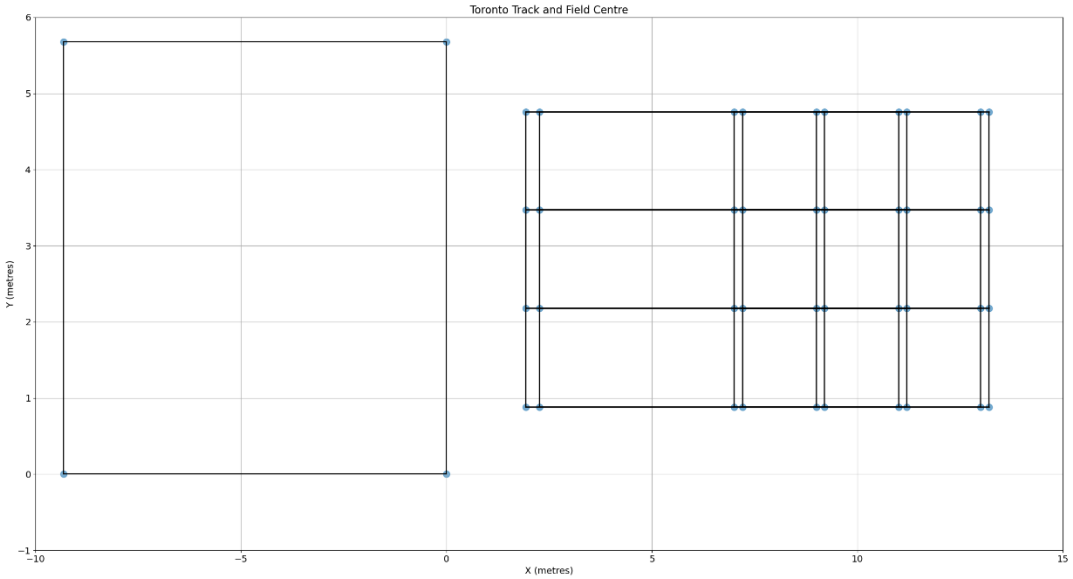

(a) Python-generated facility coordinates

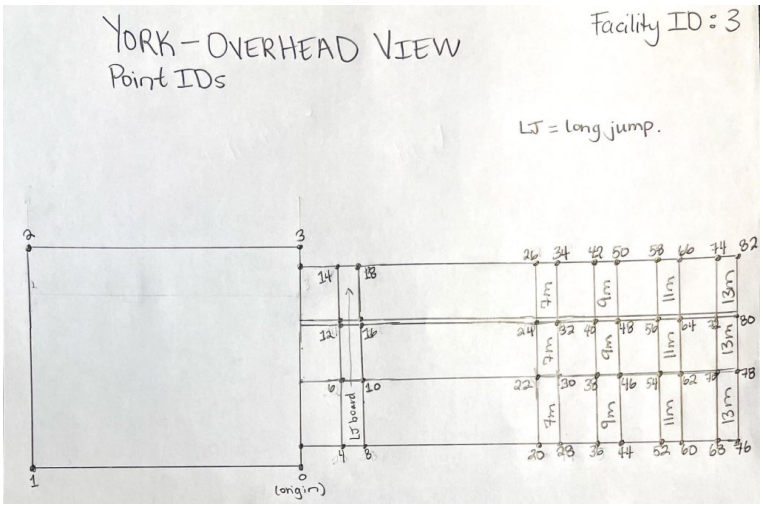

(b) Improved hand-drawn facility coordinates

Figure H.2: Toronto Track and Field Centre in North York, Ontario, (a) Python-generated facility coordinates, and (b) improved hand-drawn facility coordinates with point IDs. Point ID labels were omitted from (a) to avoid overcrowding the plot, as the points were validated in smaller sets.

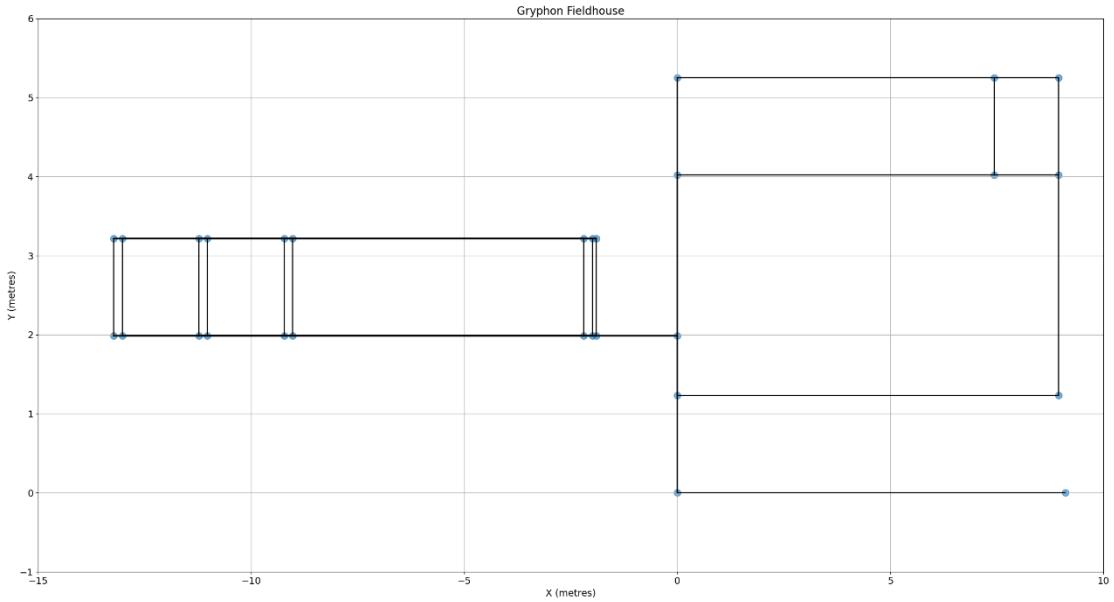

(a) Python-generated facility coordinates

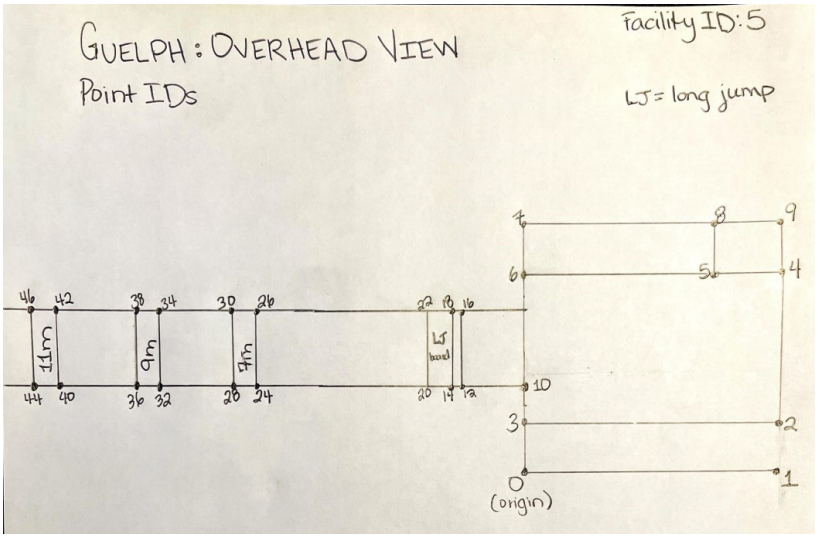

(b) Improved hand-drawn facility coordinates

Figure H.3: Gryphon Fieldhouse in Guelph, Ontario, (a) Python-generated facility coordinates, and (b) improved hand-drawn facility coordinates with point IDs. Point ID labels were omitted from (a) to avoid overcrowding the plot, as the points were validated in smaller sets.

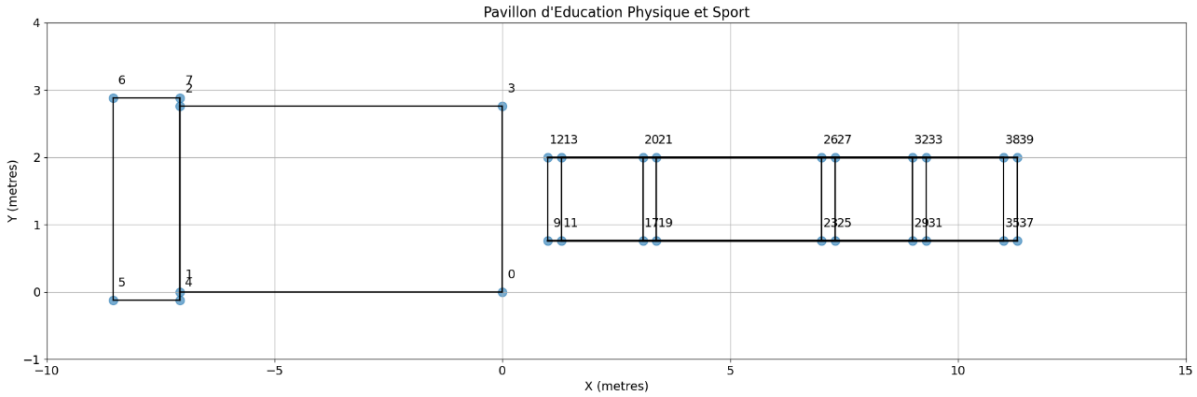

(a) Python-generated facility coordinates

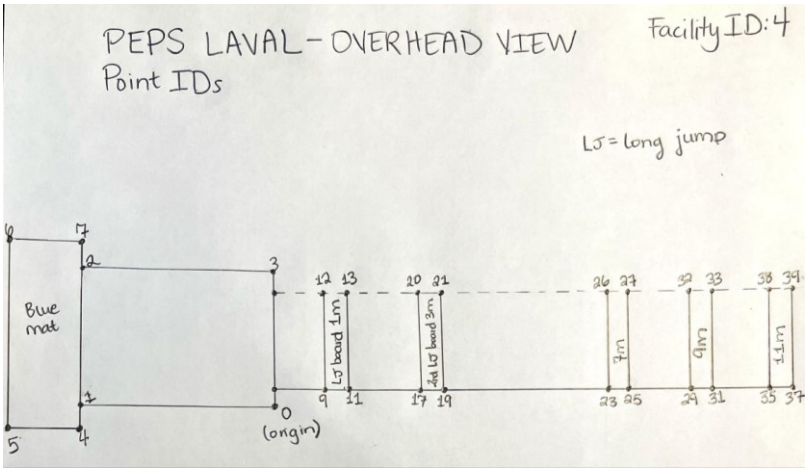

(b) Improved hand-drawn facility coordinates

Figure H.4: Pavillon d' Éducation Physique et Sport in Quebec City, Quebec, (a) Python-generated facility coordinates, and (b) improved hand-drawn facility coordinates with point IDs.

Appendix I: Key Point Labelling Tool User Guide

The Python script, **label_keypoints.py**, was created to manually label key points for homography in video frames. This script takes a participant ID and attempt number via command-line input, opens the appropriate video in a new window, and allows the user to navigate frame-by-frame to select point IDs corresponding to the 2D track templates. The resulting key point labels are saved in the SQLite database for downstream processing. The steps below detail the setup and usage of this tool.

Prepare SQLite database: An SQLite database named thesis-triplejump.db was used to manage all study-related data. Storing data in this database facilitated the automation of repetitive processing tasks and allowed data retrieval with SQL queries and Python scripts. SQLite can be installed for free on any device, and a variety of tools are available to view, manage, and query the database. The open-source tool used for database management purposes in the study is DBeaver, Community edition [119].

Set up Python environment: Python must be installed and up to date on the development device. Additionally, an integrated development environment (IDE) is required; Visual Studio Code (VS Code), a widely used open-source IDE, was used in the study [120]. It is also highly recommended to use a package manager, with Miniconda being used in the study [121]. Without a package manager, Python packages are installed directly into the main Python environment, making it challenging to track which packages belong to specific projects.

After the pre-requisites of preparing an SQLite database and setting up a Python environment are completed, the steps below can be followed to begin labelling key points.

1. Create an environment using the Anaconda command line prompt, which is part of the Miniconda installation, and install the appropriate libraries using a provided environment.yml file [121]. The environment file can be extracted from a VS Code project using Miniconda [122].

   ```
   conda env create -f environment.yml
   ```

   Note: To activate the environment in the Anaconda command prompt, use the following command:

   ```
   conda activate triple-jump
   ```

2. Open the **label_keypoints.py** file in VS Code and select the Python environment created in the previous step.
    a. In VS Code, after opening the file, press Ctrl + Shift + P to open the command palette. Figure I.1 displays an example of the menu options that will appear:

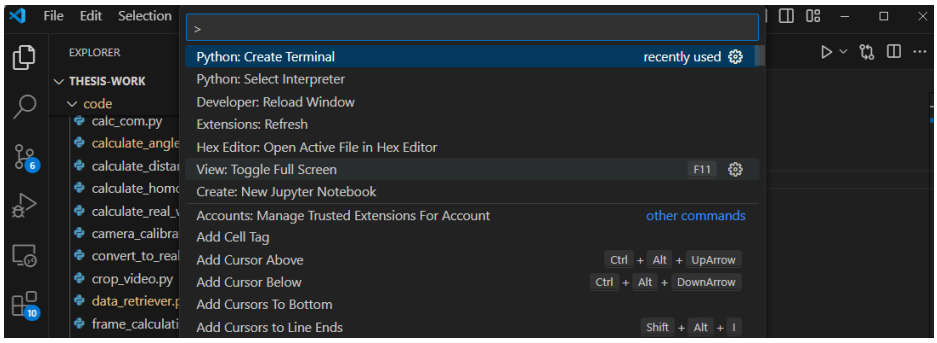

Figure I.1: Open the command palette in Visual Studio Code.

    b. In Figure I.1, the menu option Python: Select Interpreter, will allow the environment created in step 1 to be applied. If this item does not appear on the menu, begin typing Python: Select Interpreter. Click on this menu option.
    c. A list of environments should then appear as options. Choose the environment named “triple-jump” and click on it, as shown in Figure I.2:

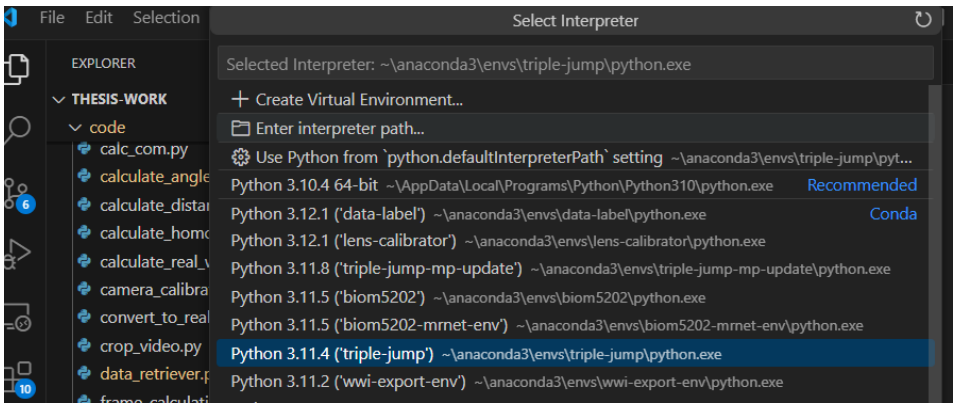

Figure I.2: Select the appropriate Python environment in Visual Studio Code.

    d. The correct environment should now be loaded in VS Code and the **label_keypoints.py** script can be executed. In the bottom right-hand corner of the VS Code window, it should indicate that the “triple-jump” environment is active.

Running the labelling script

1. Copy the Participants folder, which contains trimmed videos for all jump attempts, to the local development device. This will ensure there are no OneDrive-related issues when applying video labels.
2. To open a terminal in VS Code and run commands, click on Terminal and then New Terminal in the top menu as shown in Figure I.3:

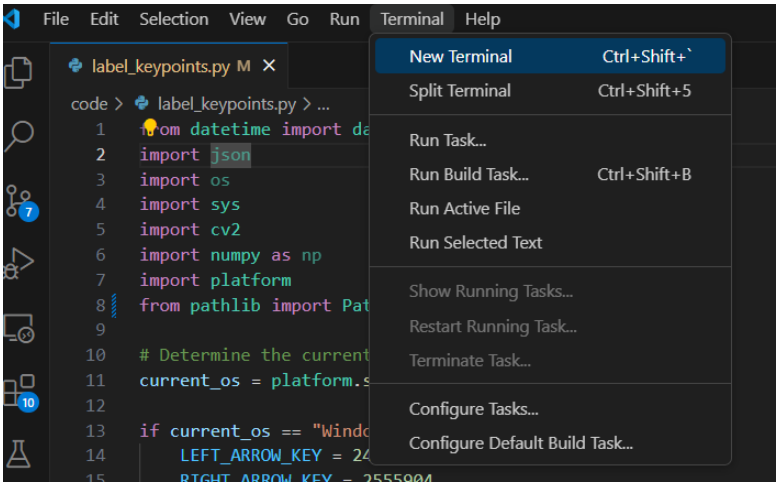

Figure I.3: Open a terminal in Visual Studio Code.

A terminal will appear at the bottom of the window. The size can be adjusted as desired.

3. It is essential that the terminal is in the correct directory. To change the directory via the terminal, use the cd command: `cd code`. A full file path can be specified after the `cd` command. To go back in a directory, use `cd ..` as shown in Figure I.4.

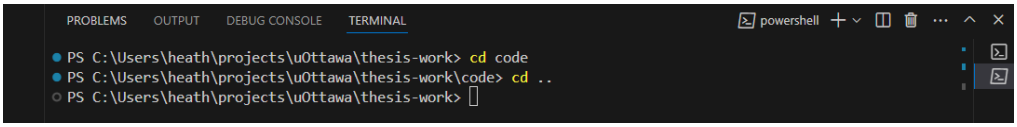

Figure I.4: Go back in the working directory in the Visual Studio Code terminal.

To view a list of the items in the current directory, use the `dir` command. Note that the `ls` command will also work. An example using the `dir` command is presented in Figure I.5.

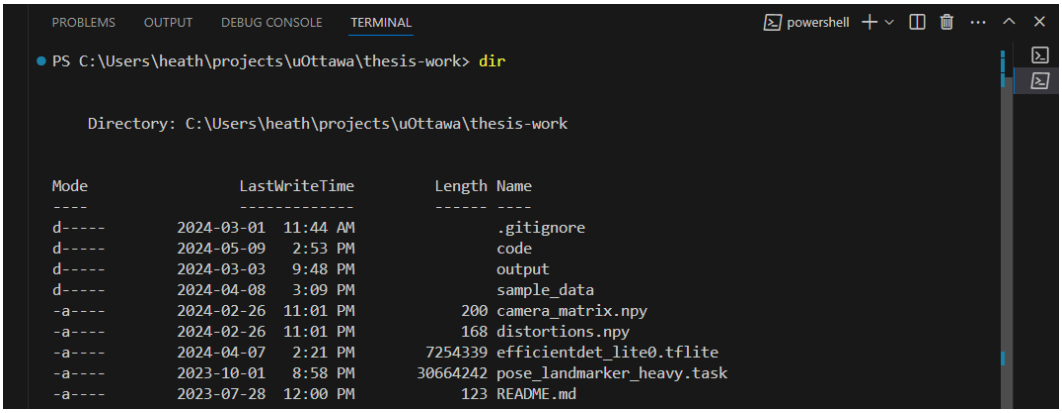

Figure I.5: Use the "dir" command in the Visual Studio Code terminal to obtain a list of the contents in the current directory.

4. The **label_keypoints.py** script accepts the following command line arguments. The Click Python package is leveraged to simplify passing in command line arguments [118]. Example usage for each argument is also included; these commands can be executed in the VS Code terminal.

    - **--database**: Specify the full file system path to the SQLite database. Ensure to either update the script directly, setting the default to the database location on the development device, or pass in this argument on every execution with the correct path. The example below will open the first jump attempt for participant 1 (default values) and will write results to the SQLite database location specified after the --database parameter.

      ```
      python label_keypoints.py --database
      'C:/myfolder/thesis-triplejump.db'
      ```

    - **--participant**: The participant ID, valid values are from 1 through 30. If not specified, the default value is 1. The example below will open the first jump for participant 5 and will write results to the default SQLite database.

      ```
      python label_keypoints.py --participant 5
      ```

    - **--attempt_num**: The jump attempt number. If not specified, the default value is 1. The example below will open the fourth jump for participant 5 and will write results to the default SQLite database.

```
python label_keypoints.py --participant 5 --
attempt_num 4
```

- **--output_csv**: Using this option will save the label results in a CSV file in the working directory. This is an optional feature to be used for testing purposes. If not specified, no CSV file is generated. The example below will open the first jump for participant 1 and will save the labels to an output CSV in the working directory as well as to the default SQLite database. Note that the CSV filename is automatically generated in the script and does not need to be specified.

  ```
  python label_keypoints.py --output_csv
  ```

- **--output_db/--no_output_db**: Specify whether to save the labels to the SQLite database. By default, the results are saved to the LocationKeypointLabels table, as all labels should be stored there. However, for testing purposes, if saving the results is not required, use the --no_output_db argument. The example below will open the first jump for participant 1 and save the labels to the default SQLite database.

  ```
  python label_keypoints.py
  ```

  The example below will open the second jump for participant 6 and will not save the labels anywhere.

  ```
  python label_keypoints.py --participant 6
  --attempt_num 2 --no_output_db
  ```

- **--video_directory**: Specify the directory containing the jumps videos. The script expects the videos to be stored in a parent directory called “Participants.” A default path to the Participants directory on the development device can be specified, or it can be passed in on every execution. The example below will open the first jump for participant 1 per the specified video directory, and the labels will be saved in the default SQLite database.

  ```
  python label_keypoints.py --video_directory
  “C:/myvideos/Participants”
  ```

5. After executing any valid command, the specified video will open in a separate window, as in Figure I.6, and can be manually resized as desired. The participant is redacted to preserve their privacy.

Figure I.6 The window pop-up generated from the label_keypoints.py script to facilitate key point labelling for homography. The participant is redacted to preserve their privacy.

Labelling the videos

With the video open, points can be labelled frame-by-frame by using keyboard commands as follows:

- *Up/down arrow keys*: Use to select the correct point ID. The up arrow increments the point ID number, and the down arrow decreases the point ID number.
- *Right/left arrow key*s: Move forward or backward through frames. It is not possible to move backward from the first frame or forward from the last frame.
- *C key*: Clears all labelled points for the current frame.
- *Q key*: Exits the program without saving any labels. If errors are made during labelling and a restart is necessary, the "Q" key should be used to ensure no labels are saved. Upon pressing "Q", a prompt will appear in the VS Code terminal confirming whether to exit. To exit without saving, enter "Y," otherwise, enter "N" to continue.

- *Esc key*: Exits the OpenCV window, respecting any arguments passed into the command line argument. For example, when using the default option of saving to the SQLite database, the labels will be saved in the database, even if the labels for the entire video were incomplete. Use the Escape key to exit when finished with labelling a video.

The most labour-intensive aspect of the labelling process is accurately mapping the correct point ID from the 2D track templates to the corresponding real-world point. As familiarity with the point IDs for each facility increases, the process becomes more manageable.

Appendix J: Minimum Knee Angle Calculation

This section details the steps required to compute the minimum knee angle calculation, including the inputs, steps, and final equation, adapted from [116]. The knee angle is defined as the angle between the thigh and lower leg, considered to be 180° in the anatomical standing position per the World Athletics reports definition [6], [7], [8], [9].

Inputs:

$$coordinates1 = (x_1, y_1, z_1)$$
$$coordinates2 = (x_2, y_2, z_2)$$
$$coordinates3 = (x_3, y_3, z_3)$$

Steps:

1. Compute vectors

$$\overrightarrow{v_1} = (x_1 - x_2, y_1 - y_2, z_1 - z_2)$$
$$\overrightarrow{v_2} = (x_3 - x_2, y_3 - y_2, z_3 - z_2)$$

2. Compute dot product

$$\overrightarrow{v_1} \cdot \overrightarrow{v_2} = (x_1 - x_2)(x_3 - x_2) + (y_1 - y_2)(y_3 - y_2) + (z_1 - z_2)(z_3 - z_2)$$

3. Compute magnitudes

$$|\overrightarrow{v_1}| = \sqrt{(x_1 - x_2)^2 + (y_1 - y_2)^2 + (z_1 - z_2)^2}$$
$$|\overrightarrow{v_2}| = \sqrt{(x_3 - x_2)^2 + (y_3 - y_2)^2 + (z_3 - z_2)^2}$$

4. Calculate cosine of the angle

$$\cos(\theta) = \frac{\overrightarrow{v_1} \cdot \overrightarrow{v_2}}{|\overrightarrow{v_1}||\overrightarrow{v_2}|}$$

5. Convert angle from radians to degrees

$$\theta = \arccos(\cos(\theta))$$
$$angle\ in\ degrees = \theta \times \left(\frac{180}{\pi}\right)$$

Final Equation:

$$knee\ angle = arccos\left(\frac{(x_1 - x_2)(x_3 - x_2) + (y_1 - y_2)(y_3 - y_2) + (z_1 - z_2)(z_3 - z_2)}{\sqrt{(x_1 - x_2)^2 + (y_1 - y_2)^2 + (z_1 - z_2)^2} \cdot \sqrt{(x_3 - x_2)^2 + (y_3 - y_2)^2 + (z_3 - z_2)^2}}\right) \times \left(\frac{180}{\pi}\right)$$